

DOCTORAL THESIS

---

**LEARNING TO LEARN FROM SIMULATION  
USING SIMULATIONS TO LEARN FASTER ON ROBOTS**

---

Akshara Rai

*Thesis Committee:*  
Christopher G. Atkeson, Chair  
Hartmut Geyer  
Oliver Kroemer  
Stefan Schaal, USC

*A thesis submitted in fulfillment of the requirements  
for the degree of Doctor of Philosophy*

*in the*

Robotics Institute, School of Computer Science  
Carnegie Mellon University

October 12, 2018



## *Abstract*

Robot controllers, including locomotion controllers, often consist of expert-designed heuristics. It is typical to use simulation to tune or learn these heuristics, and test on hardware. However, controllers learned in simulation often don't transfer to hardware due to modelling errors. One way to overcome this is to optimize controller directly on hardware, which can be expensive, due to the time involved and fear of damage to the robot. This has led to an interest in using data-efficient learning techniques like Bayesian Optimization. But the performance of Bayesian Optimization typically degrades in higher dimensions, including dimensions of the scale seen in bipedal locomotion. We aim to overcome this problem by incorporating prior knowledge from simulation to reduce the dimensionality of the problem, with a focus on bipedal locomotion. We propose two ways of doing this, hand-designed features based on knowledge of human walking and using neural networks to extract this information automatically. Our hardware experiments on the ATRIAS robot, and simulation experiments on two robots - ATRIAS and a 7-link biped model, show that these feature transforms capture important aspects of walking and accelerate learning on hardware and perturbed simulation, as compared to traditional Bayesian Optimization and other optimization methods. Another question arises: What if the simulation significantly differs from hardware? To answer this, we create increasingly approximate simulators and study the effect of increasing simulation-hardware mismatch on the performance of Bayesian optimization. We also compare our approach to other approaches from literature, and find it to be more reliable, especially in cases of high mismatch.

An alternative to directly optimizing policies on hardware is to learn robust policies in simulation that can directly be implemented on hardware. We study the effect of structure on the robustness of very high-dimensional neural network policies. Our experiments on the ATRIAS robot show that structured neural network policies have a higher rate of transfer between simulation and hardware than unstructured policies.



*Acknowledgements*



# Contents

<b>Abstract</b>	<b>iii</b>
<b>Acknowledgements</b>	<b>v</b>
<b>1 Introduction</b>	<b>1</b>
1.1 Adding prior knowledge to optimization . . . . .	2
1.1.1 Expert-designed feature transforms . . . . .	2
1.1.2 Data-driven feature transforms . . . . .	2
1.2 Accounting for mismatch between hardware and simulation . . . . .	3
1.3 Using neural networks to learn walking policies . . . . .	3
1.4 Summary of completed goals and contributions . . . . .	4
<b>2 Background</b>	<b>7</b>
2.1 Dynamic Programming and Reinforcement Learning . . . . .	7
2.2 Bayesian Optimization for Robotics . . . . .	9
2.2.1 Bayesian Optimization and Gaussian Processes . . . . .	9
2.2.2 Bayesian optimization for policy search . . . . .	11
2.2.3 Bayesian optimization for legged robots . . . . .	12
2.2.4 Incorporating behavior information in Bayesian Optimization .	13
2.3 Reinforcement learning for bipedal robots . . . . .	15
2.3.1 Learning with neural networks in robotics . . . . .	16
<b>3 Learning to learn</b>	<b>19</b>
3.1 Distance metrics from simulation . . . . .	19
3.1.1 A bipedal locomotion specific transform . . . . .	19
3.1.2 A feature transform from data . . . . .	22
3.2 Modelling mismatch between simulation and hardware . . . . .	26
3.2.1 Interpretation of Kernel with Mismatch Modeling . . . . .	28
3.3 Transfer learning with contextual Bayesian optimization . . . . .	30
<b>4 Robots and controllers evaluated</b>	<b>33</b>
4.1 Robot morphologies tested . . . . .	33
4.1.1 The ATRIAS Robot . . . . .	33
4.1.2 A 7-link biped model . . . . .	33
4.2 Controllers tested . . . . .	34
4.2.1 Neuromuscular model for humanoid robots . . . . .	34
4.2.2 Feedback based reactive stepping policy . . . . .	36
4.2.3 Virtual Neuromuscular Controller for ATRIAS . . . . .	38
4.3 Inaccurate simulations for constructing kernels . . . . .	39
4.3.1 Incorrect dynamics parameters . . . . .	39
4.3.2 Incorrect dynamics models . . . . .	40
4.4 Neural network policies on the ATRIAS biped . . . . .	41
4.4.1 Neural Network Policy . . . . .	42

4.4.2 Neural Network in the Heuristic Policy . . . . .	42
<b>5 Results and evaluation</b>	<b>45</b>
5.1 Completed Experiments . . . . .	45
5.2 Experiments with the DoG Transform . . . . .	45
5.2.1 Hardware experiments with the 5-dimensional controller . . . . .	45
5.2.2 Hardware experiments with the 9 dimensional controller . . . . .	46
5.2.3 Simulation experiments with the 9-dimensional controller . . . . .	47
5.2.4 Simulation experiments with the 50-dimensional controller . . . . .	49
5.2.5 Simulation experiments on a 16-dimensional controller . . . . .	50
5.2.6 Summary of experiments with the DoG transform . . . . .	54
5.3 Experiments with the NN transform . . . . .	54
5.3.1 Hardware experiments with a 5-dimensional controller . . . . .	55
5.3.2 Hardware experiments with a 9-dimensional controller . . . . .	56
5.3.3 Simulation experiments with the 16-dimensional controller . . . . .	57
5.3.4 Simulation experiments with 50-dimensional controller . . . . .	59
5.4 Effect of inaccurate simulations on the performance . . . . .	60
5.4.1 Incorrect dynamics models . . . . .	60
5.4.2 Incorrect dynamics parameters . . . . .	64
5.5 Deep reinforcement learning for learning high level policies . . . . .	65
5.5.1 Simulation Experiments . . . . .	65
5.5.2 Hardware Experiments . . . . .	67
<b>6 Conclusion</b>	<b>71</b>
6.1 Discussion . . . . .	71
6.1.1 Feature transforms from simulation in hardware experiments .	72
6.1.2 Accounting for simulation inaccuracies . . . . .	72
6.1.3 Effect of structure on high-dimensional neural network policies	74
6.2 Future work and open questions . . . . .	74
6.2.1 Learning general features from data . . . . .	74
6.2.2 Safe exploration and learning . . . . .	75
6.2.3 Transfer learning between controllers and robots . . . . .	75
6.3 Closing remarks . . . . .	76
<b>Bibliography</b>	<b>77</b>

## Chapter 1

# Introduction

Robot controllers, and locomotion controllers in particular, can consist of many expert designed heuristics, for example feedback control of the Center of Mass (CoM) position and velocity, feedback control of robot joints, and designing reference trajectories and desired position. State of the art works in walking robots featuring such heuristics include Feng et al., 2015, Kuindersma et al., 2016 and Hubicki et al., 2016b. These heuristics consist of sets of inter-dependent parameters, which can be hard to tune, especially in higher dimensions. In such cases, it is an art, rather than a science, to tune these parameters. This complexity motivates methods for learning parameters automatically. A simple approach is to learn in simulation and deploy on hardware. However, due to commonly encountered differences between simulation and hardware, such as modelling errors, performance in simulation often does not transfer to hardware. On the other hand, directly learning on hardware can require a prohibitively large number of experiments, making it nearly impossible to learn these controllers using traditional methods. This has led to a surge in interest in data-efficient learning techniques for robotics.

One popular data-efficient method for learning controller parameters is Bayesian Optimization (BO). BO is a sample-efficient gradient-free black-box optimization method that has been applied to a wide range of robotics problems. For example, Calandra et al., 2016a, Marco et al., 2017b, Cully et al., 2015 try to learn parameters directly on hardware using BO. However, the performance of BO degrades in high dimensions (see Akroun et al., 2017 for a related discussion), even for dimensionalities commonly encountered in locomotion controllers. We aim to overcome this problem by incorporating domain knowledge into BO.

One way of incorporating domain knowledge could be to learn approximate models of the system from simulation, before moving to hardware. The idea of using simulation performance to speed up optimization on hardware has been explored before. A common approach is to learn controllers in simulation, and use this as a starting point on hardware. A domain expert would then typically have to



FIGURE 1.1: Our testbed is CMU’s ATRIAS robot.

fine-tune parameters on hardware. Mordatch, Lowrey, and Todorov, 2015 learn parameters using a collection of simulations that help account for model uncertainty. Ha and Yamane, 2015 iteratively learns both the model and controller parameters using the differences between simulated behaviors and observed hardware experiments. Marco et al., 2017b uses evaluations from simulation as a noisy prior for the optimization on hardware. Cully et al., 2015 pre-selects high performing controllers from simulation and search among them on hardware.

## 1.1 Adding prior knowledge to optimization

**We propose incorporating domain knowledge by building informed feature transforms that project the higher dimensional controller parameter space to an easy to optimize lower dimensional space of features.** These can be expert-designed or learned from data, as described below:

### 1.1.1 Expert-designed feature transforms

We use human-walking inspired features to develop a feature transform for bipedal walking that roughly groups controllers based on their walking features in short simulations. The objective of such a transformation is that some behavioural cues have a higher probability of transferring between simulation and hardware than exact cost or controller performance. For example, a controller that falls instantly in simulation by tilting its torso, would have a small chance of walking on hardware. On the other hand, a controller that walks efficiently in simulation might have a higher chance of walking on hardware, albeit with a different cost. Hence, it seems reasonable to roughly group parameters based on the behaviour they produce in simulation, and use this as a distance metric to distinguish between them. Despite being motivated by human walking features, these features also generalize to other robot morphologies and controllers, like the ATRIAS biped.

### 1.1.2 Data-driven feature transforms

Using extensive expert knowledge, as suggested above, has several advantages. It helps us learn and design features fast as well as provides transparency as to what the learning approach is prioritizing. However, it does raise concerns about problems for which such knowledge might not be available or as easily implementable. With this in mind, **we also develop a method to construct an informed metric automatically, without relying heavily on domain experts.** We propose to learn a distance metric with a neural network, utilizing data obtained from a high-fidelity simulator. This involves first running short simulations of a locomotion controller on a large grid of control parameters and recording the behavior of each set of parameters. The neural network then learns a mapping between input controller parameters and simulation output/behavior. We propose two ways of defining the target to be learned by the network. The first approach is based on the cost function that is to be optimized with BO on hardware, or a perturbed simulator. The second is cost-agnostic: learning to reconstruct a summary of robot trajectories obtained from simulation. This provides a useful re-parameterization: controller parameters that produce similar walking trajectory summaries are closer in this re-parameterized space.

## 1.2 Accounting for mismatch between hardware and simulation

An important question that arises when using simulation to guide hardware searches is: how can we learn and take into account the differences between simulation and hardware? For example MacAlpine, Liebman, and Stone, 2016 adapts the target task based on the mismatch between the expected and actual performance. Marco et al., 2017b develops an automatic way of transitioning between simulation and hardware based on data collected so far.

We propose to learn a mismatch-map that represents the mismatch between behaviour encountered in simulation and hardware. This allows us to build an error map over our parameter space, based on data. We start by trusting all simulation points with predicted mismatch of 0, and as we sample points on hardware, we update our estimate of error on each simulation sample. The advantage of this is that we can have different error values for different regions of parameter space, as some parts of the parameter space might transfer well between hardware and simulation, while others might not. To study the efficacy of this approach, we create a series of increasingly approximate simulators and use features from approximate simulators to optimize controllers on the original simulator. This allows us to empirically examine the deterioration of sample-efficiency as the simulator becomes more and more inaccurate, as well as the advantage of building a mismatch-map to close the loop between simulation and hardware. Our experiments show that this approach can learn controllers when simulation dynamics are perturbed by up to 60% of their “true” value. In addition, it is also robust to systematic under-modelling errors, such as unmodelled joint friction, actuator dynamics and other robot components. In comparison, other approaches from the literature that use simulation to speed up hardware experiments, such as Cully et al., 2015, suffer when simulation is significantly different from hardware.

A: TODO : Implement 50d with mismatch on hardware

## 1.3 Using neural networks to learn walking policies

While expert-designed policies are extremely powerful tools for sample-efficiency as well as safety of the robot, it can be challenging to design them in some situations. In such cases, high-dimensional policies like neural networks can be very useful. Typically, these are trained in simulation with deep reinforcement learning, and are shown to be capable of generating very diverse sets of behaviours. For example, Silver et al., 2016 use deep reinforcement learning to solve complex long horizon games like AlphaGo, starting with no human input. Similar progress has been achieved in the domain of continuous control, dealing with very high dimensional state and action spaces. For example, Deep Deterministic Policy Gradients (DDPG) Lillicrap et al., 2015 and Trust Region Policy Optimization (TRPO) Schulman et al., 2015 can solve several control challenges in the Mujoco simulation environment Todorov, Erez, and Tassa, 2012.

While simulation results for deep RL are very impressive, the simulation-hardware gap makes most controllers learned in simulation unsuitable to be implemented on hardware. This is partly because simulations are not perfect representations of real

systems, but also because learning approaches often tend to exploit simulation inaccuracies to achieve better performance. One approach to learn policies in simulation and deploy on hardware is domain randomization Mordatch, Lowrey, and Todorov, 2015. It can be used to learn robust neural network policies in simulation by applying random perturbations to the dynamics and other properties of the simulator. This approach has been applied to manipulation problems Peng et al., 2017, as well as quadrupedal locomotion problems Tan et al., 2018. However, typical domain randomization can lead to controllers that perform worse than controllers trained without randomization (Tan et al., 2018), as well as make the learning problem much harder (OpenAI et al., 2018) taking over 100 years of simulation time to learn successful policies.

Domain randomization from scratch is especially challenging for under-actuated bipedal robots, as the basin of stability around a controller is typically very small. As a result, it is very difficult to randomly explore the space of controllers to find successful controllers that stabilize a wide range of dynamic models, and other disturbances. Moreover, the learned controllers would typically be quasi-static in nature, similar to Mordatch, Lowrey, and Todorov, 2015 in behavior, which is not very impressive in performance.

We experiment with classical deep reinforcement learning techniques to learn robust controllers in simulation and test them on hardware. Instead of using domain randomization, we create disturbances in simulation by simulating ground height disturbances and study the effect of policy structure on the rate of transfer. Starting with a high-fidelity simulator (Martin, Wu, and Geyer, 2015), we experiment with different controller structures, and study their effect on transfer from simulation to hardware, without any domain randomization. The first neural network policy is a general policy that directly outputs the desired actions of the robot, while the second has the structure of an expert-designed policy and predicts the desired states for this policy. We find that structured neural network controllers have a fast training rate in simulation as well as higher rate of transfer to hardware. The structure also gives the user the power to modify the controller, if required, without having to re-train the neural network from scratch.

## 1.4 Summary of completed goals and contributions

In work done, we present evaluations of our proposed methods on the ATRIAS biped robot (Figure 1.1), ATRIAS simulation, and a 7-link biped simulation.

First, we use expert designed controllers and optimize their parameters using BO. We evaluate different feature transforms on three controllers of increasing dimensionality. We start with a 5 dimensional feedback-based reactively stepping controller, and increase its dimensionality to 9. Then we take a 50-dimensional highly non-linear neuromuscular controller and optimize its parameters. We successfully optimize parameters for a 5-dimensional and 9-dimensional controller on the ATRIAS hardware in less than 10 trials, which proves to be challenging for traditional BO. Our results show that these feature transforms - hand-designed and data-driven, extract useful information from simulations, and leads to an effective transfer of knowledge to hardware.

While, Bayesian Optimization benefits from feature transforms and informed distance metrics, we also explore if simulation can be useful in learning other walking policies which might be much higher dimensional. We train two neural network policies - with and without structure and study their rate of transfer to hardware.

Our studies show that structured neural network policies have a higher rate of transfer between simulation and hardware as compared to unstructured neural network policies.

The main contributions of this thesis are as below:

- A simulation-based feature transform that enables faster optimization of bipedal walking controllers on hardware.
- A hybrid optimization approach that integrates model-based information from simulation into a model-free global search framework like Bayesian Optimization
- A novel way of updating models from hardware data using feature transforms evaluated on simulation and hardware
- A study of the effect of structure on neural network policies trained in simulation and their rate of transfer to hardware



## Chapter 2

# Background

In this Chapter, we will cover some literature on Bayesian Optimization for robotics, using simulation information to learn faster on hardware and learning the mismatch between the dynamics in simulation and hardware. We also give a short introduction of other policy search methods in literature, which might benefit from simulation information.

## 2.1 Dynamic Programming and Reinforcement Learning

Let us consider a controller (agent) interacts with a process (environment) through a action, which changes the state of the process and generates a reward (feedback from the environment) (Figure 2.1). The controller receives the new state and the reward, and the whole process repeats. The behaviour of the controller is determined by a policy that maps the process state to an action. The process follows a stochastic or deterministic dynamics model which determines how the state changes as a result of actions.

The goal of reinforcement learning is to find an optimal policy that maximizes the (expected) return, consisting of the (expected) cumulative reward over the course of this interaction, called the value function. This framework can be used to address problems from a variety of fields, e.g., automatic control, artificial intelligence, operations research, and economics.

We assume a discrete-time process and denote the current time step by  $k$ . The transition model  $p$  is given by a probability distribution conditioned on the current state and current action. We assume a Markov decision process, where the distribution over the next state only depends on the previous state and actions.

$$s_{k+1} \sim p(s_{k+1}|s_k, u_k) \quad (2.1)$$

where  $u_k \in \mathbb{R}^M$  denotes the current action, and  $s_k, s_{k+1} \in \mathbb{R}^N$  denote the current and the next state respectively. We furthermore assume that actions are generated by a policy

$$u_k \sim \pi_\theta(u_k|s_k) \quad (2.2)$$

which is modeled as a probability distribution conditioned on the current state. This lets us naturally include exploratory actions in the policy. The policy is parameterized by some policy parameters  $\theta \in \mathbb{R}^K$ . Over one episode, the sequence of states and actions forms a trajectory, denoted by  $\xi = [s_{0:H}, u_{0:H}]$  where  $H$  denotes the length of the episode. At each instant of time, the learning system receives a reward (or cost for minimization) denoted by  $r(s_k, u_k) \in \mathbb{R}$ .

The objective of policy search algorithms is to maximize the expected return of a trajectory, as a function of the policy parameters  $\theta$ . We assume no-discounting in

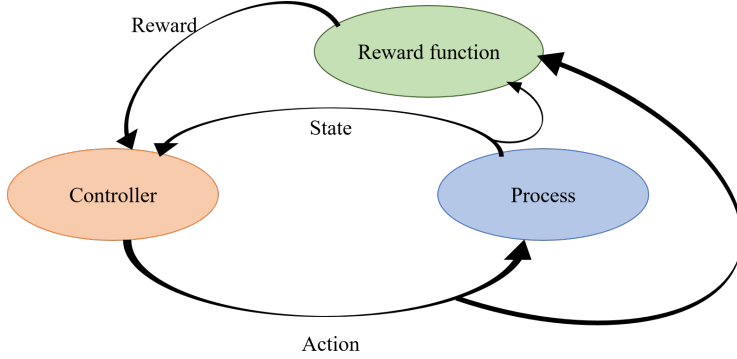


FIGURE 2.1: The interaction between the controller, process and reward function in dynamic programming and reinforcement learning.

all our formulations, but discounting factors that weigh future costs lower than the current cost could be added.

$$J(\theta) = \mathbb{E} \left[ \sum_{k=0}^H r_k \right] \quad (2.3)$$

In general, for each considered policy  $\pi_\theta$ , a state-value function  $V_\pi(s)$ , and a state-action value function (Q-function)  $Q_\pi(s, u)$  can be defined as

$$V_\pi(s) = \mathbb{E} \left[ \sum_{i=k}^H r_i | s_k = s \right] \quad (2.4)$$

$$Q_\pi(s, u) = \mathbb{E} \left[ \sum_{i=k}^H r_i | s_k = s, u_k = u \right] \quad (2.5)$$

Note, that we can define the expected return in terms of the state-value function by

$$J(\theta) = \int_s p(s_0) V_\pi(s_0) ds_0 \quad (2.6)$$

where  $p(s_0)$  is the probability of  $s_0$  being the initial state of an episode.

In the presence of a model, one of the widely used optimal control methods in robotics are dynamic programming algorithms, which can be considered a part of reinforcement learning. Popular dynamic programming methods include value iteration or policy iteration, which are iterative methods that are guaranteed to converge to the global optimum (Bertsekas and Tsitsiklis, 1995). However, dynamic programming methods do not scale to higher dimensional problems, leading to a "curse of dimensionality". For example, value iteration converges to the true value function in polynomial time in the number of states and actions (Sutton and Barto, 1998). This raises concerns about generalizing to higher dimensions, and especially for continuous action and states. To deal with this, approximate dynamic programming approaches have been suggested, for example, Atkeson, 2007 randomly sample over actions in a continuous space to avoid discretizing actions. Whitman and Atkeson, 2009 break down the problem of controlling a 5-link biped into 4 simpler, lower-dimensional problems and solve each separately.

Alternatively, in the absence of a model, function approximators can be used to learn the value function and Q-function, resulting in feasible methods even for higher dimensions and continuous action states, example SARSA and Q-learning

(Busoniu et al., 2010). However, this can result in biases in the estimate of the value function, especially with limited data. Unfortunately, in the general case, since these methods depend on their previous estimate of the target to generate the next solutions, they have an inherent bias based on their initial estimate. Coming up with an appropriate function approximator is a non-trivial problem and can involve using prior knowledge that might not be available, especially for model-free RL. Despite its short-comings, function approximators like deep neural networks have been shown to produce very impressive results in high dimensional control problems. We will talk more about these in Section 2.3.1

Policy search methods avoid the problem of approximating the value function or the Q-function by directly searching for an optimal control policy that maximizes the expected return. For a general problem, the optimization criterion may be a non-differentiable function, with multiple local optima. This means that global, gradient-free optimization techniques are more appropriate than local, gradient-based techniques. Some successful techniques include covariance-matrix adaptation Hansen, 2006, Bayesian optimization Shahriari et al., 2016 and cross-entropy optimization Rubinstein, 1999. We primarily use Bayesian optimization in this work, and we describe that next.

A: Mention a few more policy search works like PILCO, reinforce, etc.

## 2.2 Bayesian Optimization for Robotics

In this section, we will provide a basic introduction of Bayesian optimization (BO) and Gaussian processes. This will be followed by a survey of BO for policy search in robotics and in particular, using BO with trajectory information.

### 2.2.1 Bayesian Optimization and Gaussian Processes

Bayesian optimization (BO) is a framework for sample-efficient black-box and gradient free global search. It was introduced by Jones, Schonlau, and Welch, 1998 and originally was referred to as Efficient Global Optimization. Recent tutorials like Shahriari et al., 2016 and Brochu, Cora, and De Freitas, 2010 provide a comprehensive overview. Here, we will summarize the basic background for Bayesian optimization to establish notation that will be used in the following sections.

The goal of BO is to find  $\mathbf{x}^*$  that optimizes an objective function  $f(\mathbf{x})$ , while executing as few evaluations of  $f$  as possible. The class of functions is not restricted to continuous or smooth functions and hence BO can optimize non-differentiable functions. Little or no a-priori knowledge about  $f$  is necessary, but if available, prior knowledge can be incorporated (as we will discuss shortly).

The optimization starts with a prior roughly capturing the prior uncertainty over the value of  $f(\mathbf{x})$  for each  $\mathbf{x}$  in the domain. If no prior knowledge is available, this prior can be uninformed and updated with data. As points are sampled, these are included into the estimate of  $f(\mathbf{x})$ , giving an approximate model based on data seen so far. An auxiliary optimization function, called the *acquisition function*, is used to sequentially select points  $\mathbf{x}_n$  to sample next, based on the current model of  $f(\mathbf{x})$ .  $f(\mathbf{x}_n)$  is then evaluated and added to the sampled points. The aim of the acquisition function is to automatically balance exploration and exploitation: select points for which the posterior estimate of the objective  $f$  is promising, while also decreasing the uncertainty about  $f$ . An example of BO is shown in Figure 2.2.

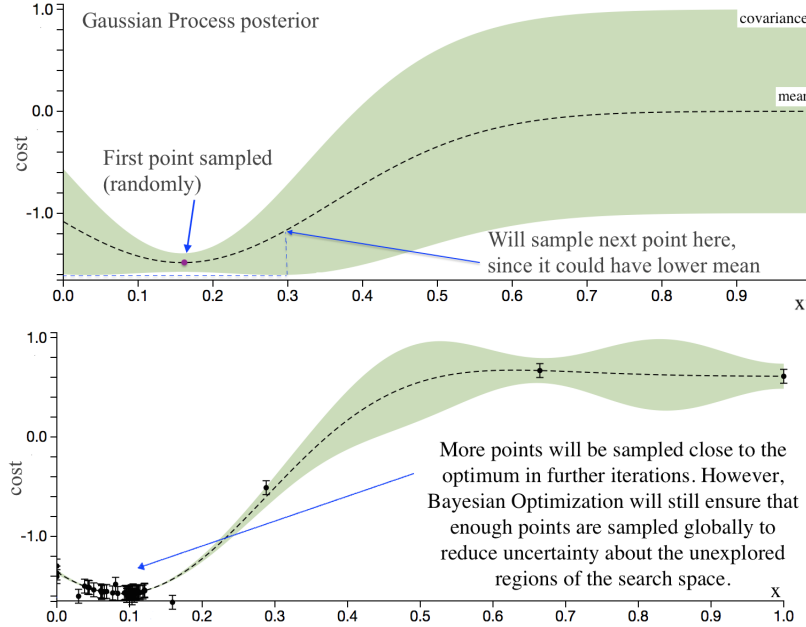


FIGURE 2.2: Bayesian Optimization posterior for a 1D function. Acquisition function computes the location of points to sample, taking into account both estimated mean and variance (uncertainty).

Expected Improvement (EI) function is commonly used as an acquisition function. EI selects  $\mathbf{x}$  to maximize expected improvement over the value of the best result obtained so far (Mockus, Tiesis, and Zilinskas, 1978). For maximization problems:

$$EI(\mathbf{x}) = \begin{cases} [f(\mathbf{x}^+) - \mu(\mathbf{x})]\Phi(Z) + \sigma(\mathbf{x})\phi(Z) & \text{if } \sigma(\mathbf{x}) > 0 \\ 0 & \text{otherwise} \end{cases} \quad (2.7)$$

where  $\mathbf{x}^+ = \arg \max_{x_i \in x_{1:t}} f(\mathbf{x}_i)$ ,  $Z = (f(\mathbf{x}^+) - \mu(\mathbf{x})) / \sigma(\mathbf{x})$ .

$\mathbf{x}_i$  are points for which objective  $f$  has been evaluated so far,  $\mu, \sigma$  are posterior mean, variance;  $\phi, \Phi$  are PDF and CDF of standard normal distribution. In all our experiments, we use EI as the acquisition function, as it doesn't have any hyperparameters to tune.

Another frequently used acquisition function is Upper Confidence Bound (UCB) or, for minimization problems, Lower Confidence Bound (LCB) (Srinivas et al., 2009). LCB balances the mean  $\mu$  and variance  $\sigma$  of the posterior by selecting points which minimize

$$LCB(\mathbf{x}) = \mu(\mathbf{x}) - \alpha\sigma(\mathbf{x}) \quad (2.8)$$

While there can be many ways of modelling  $f(\mathbf{x})$ , we describe a specific non-parametric way of describing  $f(\mathbf{x})$  using a Gaussian Process (GP). A Gaussian Process is defined by a set of random variables that are jointly Gaussian. It can be completely specified by its mean function and covariance function.

$$f(\mathbf{x}) \sim \mathcal{GP}(\mu(\mathbf{x}), k(\mathbf{x}_i, \mathbf{x}_j)), \quad (2.9)$$

with mean function  $\mu(\mathbf{x})$  and kernel  $k(\mathbf{x}_i, \mathbf{x}_j)$ .

$$\mu(\mathbf{x}) = \mathbb{E}[\mathbf{x}] \quad (2.10)$$

$$k(\mathbf{x}_i, \mathbf{x}_j) = \mathbb{E}[(f(\mathbf{x}_i) - \mu(\mathbf{x}_i))(f(\mathbf{x}_j) - \mu(\mathbf{x}_j))] \quad (2.11)$$

Assuming Gaussian noise with variance  $\sigma_{noise}^2$  on our measurements  $y_i$ ,

$$\mathbf{y}_i = f(\mathbf{x}_i) + \epsilon_{\mathcal{N}(0, \sigma_{noise}^2)} \quad (2.12)$$

Gaussian Process conditioned on sampled points represents a posterior distribution for  $f$ . After evaluating  $f$  at points  $x_1, \dots, x_t$  the predictive posterior  $P(f_{t+1} | \mathbf{x}_{1:t}, \mathbf{y}, \mathbf{x}_{t+1}) \sim \mathcal{N}(\mu_t(\mathbf{x}_{t+1}), cov_t(\mathbf{x}_{t+1}))$  can be computed in closed form with mean and covariance:

$$\mu_t(\mathbf{x}_{t+1}) = \mathbf{k}^T [\mathbf{K} + \sigma_{noise}^2 \mathbf{I}]^{-1} \mathbf{y} \quad (2.13)$$

$$cov_t(\mathbf{x}_{t+1}) = k(\mathbf{x}_{t+1}, \mathbf{x}_{t+1}) - \mathbf{k}^T [\mathbf{K} + \sigma_{noise}^2 \mathbf{I}]^{-1} \mathbf{k}, \quad (2.14)$$

where  $\mathbf{k} \in \mathbb{R}^t$ , with  $k_i = k(\mathbf{x}_{t+1}, \mathbf{x}_i)$ ;  $\mathbf{K} \in \mathbb{R}^{t \times t}$  with  $K_{ij} = k(\mathbf{x}_i, \mathbf{x}_j)$ ;  $\mathbf{I}$  is an identity  $\in \mathbb{R}^{t \times t}$ , and  $\mathbf{y}$  is a vector of values obtained after evaluating  $f(\mathbf{x}_1), \dots, f(\mathbf{x}_t)$ . More details can be found in Rasmussen and Williams, 2005.

The prior mean function  $\mu(\mathbf{x})$  can be set to 0 if no relevant domain-specific information is available. The kernel  $k(\mathbf{x}_i, \mathbf{x}_j)$  encodes how similar  $f$  is expected to be for two inputs  $\mathbf{x}_i, \mathbf{x}_j$ . The value of  $f(\mathbf{x}_i)$  has a significant influence on the posterior value of  $f(\mathbf{x}_j)$ , if  $k(\mathbf{x}_i, \mathbf{x}_j)$  is large. The Squared Exponential (SE) kernel is a commonly used similarity metric:

$$k_{SE}(\mathbf{x}_i, \mathbf{x}_j) = \sigma_k^2 \exp\left(-\frac{1}{2l^2} \|\mathbf{x}_i - \mathbf{x}_j\|^2\right), \quad (2.15)$$

where  $\sigma_k^2, l^2$  denote signal variance and a vector of length scales respectively;  $\sigma_k^2, l^2$  are called ‘hyperparameters’ in BO literature. It is possible to adjust these automatically during optimization to learn the overall signal variance and how quickly  $f$  varies in each input dimension. Squared Exponential kernel is a special case of a more general class of Matérn kernels (Stein, 1999).

### 2.2.2 Bayesian optimization for policy search

As described in Section 2.1 policy search circumvents the need to approximate value functions by directly searching for policies that maximize the expected return  $J(\theta)$ .

$$J(\theta) = \mathbb{E}\left[\sum_{k=0}^H r_k\right] \quad (2.16)$$

The optimal policy parameters  $\theta^*$  are defined as

$$\theta^* = \arg \max J(\theta) \quad (2.17)$$

This optimization can be solved sample-efficiently using Bayesian optimization. In this setting, the parameters  $\mathbf{x} = \theta$  and the reward/cost function  $f = J$ . BO samples different policy parameters, rolls out the policy, and obtains the reward of the episode. This is then used to update the model of  $f$  and used to choose the next policy to sample using the acquisition function. It is worth noting that while usual function approximators in reinforcement learning are over states, approximating the value function as a function of state for a given policy, BO is building an approximation over policies. This way, it is directly searching for the optimal policy that leads to the maximum reward with a fixed initial state distribution. This circumvents building a model over the whole state space, but depends on a specific initial condition distribution. However, as explained before, such assumptions are common in policy search literature.

### 2.2.3 Bayesian optimization for legged robots

Bayesian optimization has been used in robotics, usually to tune parameters of controllers, cost functions or planners. The advantage of using a global search framework like BO is that globally optimal policies can be discovered. These may perform better than human hand-designed policies as well as locally optimal solutions. As shown in Englert and Toussaint, 2016, the alternative of using Reinforcement Learning (RL) algorithms for policy search might not discover global optima reliably. Frean and Boyle, 2008 use BO to optimize parameters of a neural network controller for a two-link pendulum on a cart. Marco et al., 2017b solve the problem of balancing a pole on a real inverted pendulum, by optimizing the cost function for a LQR controller. Authors also propose a way of trading-off simulation and hardware experiments to optimally switch between hardware and simulation for experiments. Martinez-Cantin et al., 2007 learn the policy for planning the path of a simulated robot that minimizes the uncertainty in its environment.

The most prominent works using Bayesian Optimization for locomotion controllers include Lizotte et al., 2007, Tesch, Schneider, and Choset, 2011, Cully et al., 2015 and Calandra, 2017. These works typically involve simpler to control robots or smaller bipeds. Lizotte et al., 2007 use AIBO quadrupeds, Tesch, Schneider, and Choset, 2011 use snake robots, Cully et al., 2015 use hexapods and Calandra et al., 2016b use a small biped. Tesch, Schneider, and Choset, 2011 optimize 3 parameters for a open-loop parametric controller that generates trajectories for a 16 degree of freedom snake robot. The generated solutions find fast moving gaits of about  $0.13m/s$  in about 10-40 trials, depending on the difficulty of the task. Such performance was hard to achieve with hand-tuned parameters. Lizotte et al., 2007 use BO to optimize open-loop gait parameters for a AIBO robot to maximize velocity and smoothness of movement. Authors find that the Bayesian optimization approach not only outperformed previous techniques, but used drastically fewer evaluations.

Calandra et al., 2016b use BO for optimizing gaits of a 4 dimensional controller on a small biped on a boom. Authors report needing 30-40 samples for finding walking gaits for a finite-state-machine based controller. This controller consists of 4 threshold parameters that switch the states of a finite-state-machine cycling between stance and swing for each leg. Optimizing a higher-dimensional controller, which is needed for more complex robots and tasks, might prove to be even more challenging. The learning could be especially difficult if a significant number of the points/parameters sampled would lead to unstable gaits and falls. Such samples might result in eventual wear and breakage of the robot hardware (even if care is taken to prevent actual falls). Hence, there is a need to either limit search spaces to "safe" points, or bias the search towards such points.

Cully et al., 2015 tabulate best performing points in simulation versus their average score on a behavioural metric for a hexapod robot. This metric then guides BO to quickly find behaviours that can compensate for damage of the robot. The search on hardware is conducted in behaviour space, and limited to pre-selected "successful" points from simulation. This helps make their search faster and safer on hardware. However, if an optimal point was not pre-selected, BO cannot sample it during optimization, losing global optimality guarantees. "Best points" are cost-specific, so the map needs to be re-generated for each cost.

Our proposed method generalizes to highly dynamic behaviours and discontinuous cost functions, while maintaining the global guarantees of BO. We also bias our search towards sampling points successful in simulation (but not exclusively), leading to a sample-efficient and safer search.

### 2.2.4 Incorporating behavior information in Bayesian Optimization

Adding prior knowledge based on behavior of controllers is a promising avenue to speed up optimization. In higher dimensions, the performance of BO typically degrades, as discussed in Akrou et al., 2017. Incorporating domain knowledge, in the form of behavior might speed up optimization in such cases.

Domain knowledge can be incorporated in the form of trajectory information. If we could query the resultant trajectory of each controller, the problem of optimizing the cost would be trivial, as can be expected. To elaborate, consider a Markov Decision Process starting from a state  $s_0$ , consisting of states  $s$  and actions  $u$ , that follow a transition function  $p(s_{k+1}|s, u)$  at time step  $k$ . Here  $p$  defines the probability of transitioning to state  $s_{k+1}$  given current state  $s$  and taking action  $u$ . Bayesian Optimization, in the classic setting, studies episodic RL which looks at rewards at the end of the execution, or the value of a trajectory. Consider a trajectory  $\xi = (s_0, u_0, \dots, s_H, u_H)$ . The probability of sampling this trajectory is

$$P(\xi|\theta) = P(s_0) \prod_{k=0}^H P(s_{k+1}|s_k, u_k) P(u_k|x_k, \theta) \quad (2.18)$$

The cumulative reward of a trajectory is given as

$$R(\xi) = \sum_{k=0}^{H-1} R(s_{k+1}, u_k, x_k) \quad (2.19)$$

The expected return of a parameter set  $\theta$  then becomes

$$J(\theta) = \int R(\xi) P(\xi|\theta) d\xi \quad (2.20)$$

If we can query each trajectory  $\xi$  for every controller  $\theta$ , the cost  $J(\theta)$  is perfectly known and the uncertainty  $\sigma$  is 0.

$$f(\theta) = J(\theta)^T w \quad (2.21)$$

where  $w \sim \mathcal{N}(0, \Sigma_p)$ .

$$E[f(\theta)] = J(\theta) \quad (2.22)$$

$$E[f(\theta), f(\theta')] = J(\theta)^T \Sigma_p J(\theta') \quad (2.23)$$

The UCB acquisition for the posterior (similar to Equation 2.8) is

$$\begin{aligned} \mu(\theta) &= J(\theta) \\ \sigma(\theta) &= k(x_2, x_2) - k(x_2, x_1)k(x_1, x_1)^{-1}k(x_1, x_2) = 0 \\ UCB(\theta) &= \mu(\theta) + \alpha\sigma(\theta) = J(\theta)^T w \\ \theta_{next} &= \arg \max_{\theta} UCB(\theta) = \arg \max_{\theta} J(\theta) \end{aligned}$$

$\sigma(\theta) = 0$  is an intuitive result, as for a deterministic setting, there is no uncertainty about the posterior mean of any policy  $\theta$ . It is exactly equal to  $J(\theta)$ . Optimizing the acquisition function is equivalent to optimizing the cost. Although it can be difficult to optimize such a function globally, there is no real advantage to using Bayesian optimization anymore. Optimizing the acquisition function can typically need a very

large number of samples, which are assumed to be much cheaper than evaluating a policy in BO. However, in the current case, sampling policies for optimizing the acquisition function is just as costly as sampling the actual cost. However, this is impossible for a system without unrolling every possible  $\theta$  for a controller, which can be prohibitively large number of points. To overcome this, several alternative solutions to evaluating  $J(\theta)$  for each point exist in literature.

Wilson, Fern, and Tadepalli, 2014 prove an upper bound on the expected improvement of polices as a function of trajectories induced by these policies.

$$|J(\theta_i) - J(\theta_j)| = \left| \int R(\xi)P(\xi|\theta_i)d\xi - \int R(\xi)P(\xi|\theta_j)d\xi \right| \quad (2.24)$$

$$= \left| \int R(\xi)(P(\xi|\theta_i) - P(\xi|\theta_j))d\xi \right| \quad (2.25)$$

$$\leq \int |R(\xi)(P(\xi|\theta_i) - P(\xi|\theta_j))|d\xi \quad (2.26)$$

$$\leq R_{max} \int |P(\xi|\theta_i) - P(\xi|\theta_j)|d\xi \quad (2.27)$$

The difference between expected returns is now represented in terms of the maximum reward per trajectory  $R_{max}$ , and the variational difference in trajectories induced by each policy. Using Pinsker's inequality, and using the fact that  $|J(\theta_i) - J(\theta_j)| = |J(\theta_j) - J(\theta_i)|$  this can be written as

$$|J(\theta_i) - J(\theta_j)| = R_{max}\sqrt{2}(\sqrt{KL(P(\xi|\theta_i)||P(\xi||\theta_j))} + \sqrt{KL(P(\xi|\theta_j)||P(\xi||\theta_i))}) \quad (2.28)$$

The authors use this symmetric positive definite result to construct a kernel defined as:

$$D_{ij} = \sqrt{KL(P(\xi|\theta_i)||P(\xi||\theta_j))} + \sqrt{KL(P(\xi|\theta_j)||P(\xi||\theta_i))} \quad (2.29)$$

$$K(\theta_i, \theta_j) = \exp(-\alpha * D_{ij}) \quad (2.30)$$

This new Behavior Based Kernel (BBK) uses the KL distance of trajectories induced by the evaluated policies to calculate kernel distances. A kernel constructed to use behavior-based similarity offered an improvement over a standard SE kernel. However, BBK required obtaining trajectory data every time kernel values  $k(\mathbf{x}_i, \mathbf{x}_j)$  were evaluated. This would not be tractable when optimizing locomotion controllers, as it would need a full evaluation to determine the kernel distance (similar to the problem we described above). The authors suggest combining BBK with a model-based approach to overcome this difficulty by learning a transition model for the problem. But building a reliable model might need several data points, and building good models with few data points is an interesting research question in itself.

Cully et al., 2015 build a behavior map based on the simulation of controllers. Thus, they overcome the problem of building models of the robot from hardware data, but rely on behavior transfer between simulation and hardware. However, rather than using behavior as part of the kernel, like in Wilson, Fern, and Tadepalli, 2014, they build a look-up map between behavior and "successful" controllers. They then search in the low-dimensional behavior space, among the pre-selected controllers from simulation. Though this leads to a highly sample-efficient search and potentially safe samples, this method cannot search beyond the pre-selected

points, and hence loses the global guarantees of BO.

Marco et al., 2017a design a kernel for LQR assuming a quadratic cost and a one-dimensional linear system model. For such a problem, they show improvements in cost within 3 trials. It is unclear how this approach would scale to higher dimensional problems and non-LQR controllers.

Our approach constructs an informed kernel that incorporates behavior-based similarity, in a manner that ensures  $k(\mathbf{x}_i, \mathbf{x}_j)$  can be obtained efficiently when running BO. We pre-calculate locomotion-specific features on a high-fidelity simulator by running short simulations, enabling us to efficiently calculate the kernel distances during optimization. Our feature transform also biases the search towards high performing points in simulation, which have a higher chance of being stable on hardware than randomly selected points. In this manner, we try to incorporate behavior information from simulation, as also was proposed in Cully et al., 2015, but maintain global guarantees of BO.

## 2.3 Reinforcement learning for bipedal robots

Reinforcement learning (RL) has been widely applied to robotics problems, including simulations and hardware of manipulation, locomotion, perception problems. The widespread use of RL makes it hard to review all works in robotics, hence we will focus largely on RL for bipedal locomotion.

Some of the applications of RL on bipedal robots include, Tedrake, Zhang, and Seung, 2004, Morimoto et al., 2005, Benbrahim and Franklin, 1997 and Nakanishi et al., 2004. Tedrake, Zhang, and Seung, 2004 started with a passively stable 3d biped and added ankle actuation. With simplifications, like decoupling the roll and sagittal degrees of freedom, they approximate a value function and the control policy using linear function approximators. This system was shown to learn to walk in a very short time. Morimoto et al., 2005 modulate the via-points of reference trajectories of hip and knee joints of a 5-link biped, by learning a value function, control policy and a Poincaré section of the robot. The policy-gradient method, aided by the Poincaré model, found robust walking solutions in 100 trials on a complex robot hardware. Benbrahim and Franklin, 1997 use a central-pattern generator (CPG) based controller, whose parameters are tuned online using an actor critic method. However, the robot had to be externally supported with a "walker" to aid stability. Nakanishi et al., 2004 use a rhythmic dynamic movement primitive to learn an initial gait from locomotion and adapt the frequency of oscillation using RL on a 5-link biped.

Another popular approach employing RL or DP in robotics is using it to learn the Center of Mass (CoM) trajectory, and follow it using optimization based Inverse Dynamics. Kormushev et al., 2011 use RL to reduce the energy consumption by learning a variable-height CoM trajectory, with a evolving policy parametrization of their policy. The learned CoM trajectory exploits the passive dynamics of the COMAN robot and reduces the overall energy of walking better than the fixed policy parametrizations. Feng et al., 2015 use an approximation of dynamic programming, called Differential Dynamic Programming to optimize the CoM trajectory using an inverted pendulum model with ankle torques. Combining this with reactive foot placement in Feng et al., 2016 results in very a robust walking controller on the ATLAS humanoid robot. An application of approximate dynamic programming for whole-body control of bipedal robots was described in Whitman and Atkeson, 2009. Whitman and Atkeson, 2009 break down the problem of controlling a 5-link biped

into 4 simpler, lower-dimensional problems - sagittal stance, sagittal swing, coronal stance and yaw control. The coupled dynamics of the simpler models are considered as disturbances. The control policy generated by dynamic programming is robust to perturbations in forward and lateral directions, as well as generalize to different speeds. This was also implemented on the Sarcos humanoid and shown to reject small unknown disturbances while walking.

### 2.3.1 Learning with neural networks in robotics

Recently, there has been a surge in work using neural networks to control robots, though hardware results on locomotion robots are few. Techniques like deep reinforcement learning however have shown tremendous progress at solving complex manipulation and locomotion tasks in simulation. Recently deep reinforcement learning (DRL) has shown beyond human performance on complex long-horizon games such as AlphaGo Silver et al., 2016, even when starting with no human input. Similar progress has been achieved in the domain of continuous control too, dealing with very high dimensional state and action spaces. For example, Deep Deterministic Policy Gradients (DDPG) Lillicrap et al., 2015 and Trust Region Policy Optimization (TRPO) Schulman et al., 2015 can solve several control challenges in the Mujoco simulation environment Todorov, Erez, and Tassa, 2012. Heess et al., 2017 show that a variant of the Proximal Policy Optimization (PPO) Schulman et al., 2017 can learn to control a very high degree of freedom humanoid robot in Mujoco, even in very challenging environments. Similarly, Rajeswaran et al., 2017b use a variant of DDPG to learn to do dexterous manipulation with a high degree of freedom hand in simulation.

While simulation results for deep RL are very impressive, the simulation-hardware gap makes most controllers learned in simulation unsuitable to be implemented on hardware. This is partly because simulations are not perfect representations of real systems, but also because learning approaches often tend to exploit simulation inaccuracies to achieve better performance. High-dimensional neural network policies can approximate arbitrarily complex controllers, but too expensive to optimize directly on hardware. One approach to learn policies in simulation and deploy on hardware is domain randomization Mordatch, Lowrey, and Todorov, 2015. It can be used to learn robust neural network policies in simulation by applying random perturbations to the dynamics and other properties of the simulator. This approach has been applied to manipulation problems Peng et al., 2017, as well as quadrupedal locomotion problems Tan et al., 2018. However, typical domain randomization can lead to controllers that perform worse than controllers trained without randomization Tan et al., 2018, as well as make the learning problem much harder OpenAI et al., 2018 taking over 100 years of simulation time to learn successful policies.

#### Deep Reinforcement Learning for locomotion

Peng, Berseth, and Panne, 2016 formulate the problem of learning locomotion gaits as a actor-critic Reinforcement Learning with neural networks as function approximators for policy and value functions. The neural network takes as input terrain and robot states, parametrized leaps or steps as output. The input dimensionality is large (83D robot state and a 200D terrain state) and maps to a 29D control space, that operates at a high level, like leaps and steps for the robot, leading to about 570k parameter large network. The outputs from the policy network is fed to a finite state machine which is hand-designed to achieve the goal dictated by the neural network.

While highly successful at traversing very uneven terrain, this network needs over 10 million data points to train the network.

Heess et al., 2017 use deep reinforcement learning to learn locomotion tasks for a biped, humanoid walker and a quadruped, training the neural network with increasingly difficult terrains. The network takes as input the terrain state and the robot state and directly outputs the torques for each joint. They develop a robust policy gradient method that uses a trust region constraint to restrict the policy update from changing too much, making the policy gradient robust to noise and hyper-parameter selection. This results in highly dynamic and robust gaits in simulation, though it is unclear if such policies can be learned on hardware.

To avoid having to learn such policies on hardware directly, Tan et al., 2018 use domain randomization in simulation to learn robust policies for a quadrupedal robot. They learn two dynamic gaits - trotting and galloping in simulation, and test the trained policies on hardware. The trained policies were able to achieve about the same speed as handcrafted policies, they consumed lesser mechanical power. While controllers trained with domain randomization had a lower expected return in simulation than those trained without, their performance on hardware was much better. This is expected because robust controllers are typically more conservative, but easily generalizable to different systems.

A: Maybe add a section about other sim to real work in deep rl

### Guided policy search and related methods

Guided policy search is a recently popularized method for learning policies for robotic tasks Levine and Koltun, 2013 using neural networks. It has been applied to learning policies from images for complex manipulation tasks, such as peg-in-hole Levine et al., 2016, contact-rich tasks like opening doors Levine, Wagener, and Abbeel, 2015, etc. These networks represent global policies that are initialized by locally optimal policies. On facing new situations, where the local policies fail, a new local policy is initialized and trained to minimize cost and stay close to the global policy. The global policy is now updated to match the local policy. This ensures an increasingly general global policy that stays close to the initial policy, minimizing the “forgetting” factor for neural networks.

While there hasn't been work on locomotion on hardware with guided policy search, initializing the network in simulation over perturbed models and implementing on hardware seems straightforward. To enable fast learning on hardware, it might be beneficial to aid the policy gradients from optimal gradient step-size from simulation. This can be done either using natural gradients Peters and Schaal, 2006 from simulation or a meta-function that predicts gradient step-size Meier, Kappler, and Schaal, 2017. Aiding gradient descent based on information from simulation can help with sample-efficiency on hardware. This was originally proposed in Abbeel, Quigley, and Ng, 2006 where exact evaluations were aided with approximate gradients to suggest local improvements. While the exact value of the value function might be different between simulation and hardware, the gradient direction and step-size might have higher probability of transferring. Since learning rates are sensitive to hyper parameters like step-size, learning these in simulation seems straight-forward and beneficial. This can be done in combination with a mismatch-map which predicts the likelihood of transfer between simulation and hardware. If we expect high mismatch, we can use hardware samples to learn the correct learning rate.



## Chapter 3

# Learning to learn

Learning to learn or meta-learning is growing increasingly popular in machine learning and robotics. It can refer to learning hyper-parameters for learning methods to overcome the need for hand-tuning these, from simulation to hardware or across tasks. In our case, we use simulations to extract information that will enhance the rate of learning on hardware.

In this chapter we describe two ways of adding data from simulation to hardware optimization. We start by describing feature transforms in simulation and using them to speed up learning on hardware. The second approach is to learn a robust policy directly in simulation and implementing it on hardware. The two approaches have different advantages. While learning features lets us use very inaccurate simulations, and still learn on hardware, it needs expert input in designing the controller structure. On the other hand, directly learned policies can have very small amount of expert input and still successfully learn walking controllers. Although, we show that adding structure in the form of expert knowledge can greatly help in the rate of transfer of learned policies between simulation and hardware.

We start by describing a hand-designed locomotion-specific feature transform which is inspired from the Determinants of Gait walking metric (Inman and Eberhart, 1953). Next, we explain an automatic way of learning a feature transform from data using neural networks. Both these approaches aim at collecting data by running a lot of simulations (“Big simulation”) and use it to extract behavioral information about the controller space. This information will later be used for hardware and perturbed-simulation experiments that demonstrate sample-efficiency at learning controllers.

### 3.1 Distance metrics from simulation

In this section, we describe our proposed bipedal locomotion specific feature transform, followed by a more general transform learned from data. Once these feature transforms are collected for a range of controllers in simulation, they are then used in the optimization of controllers on hardware. The general pipeline of this approach is shown in Figure 3.1.

#### 3.1.1 A bipedal locomotion specific transform

The proposed locomotion feature transform is a generalization of the Determinants of Gaits (DoG) used by physiotherapists to evaluate the quality of human walking (Inman and Eberhart, 1953). We modify these features to look at the following aspects of bipedal walking:

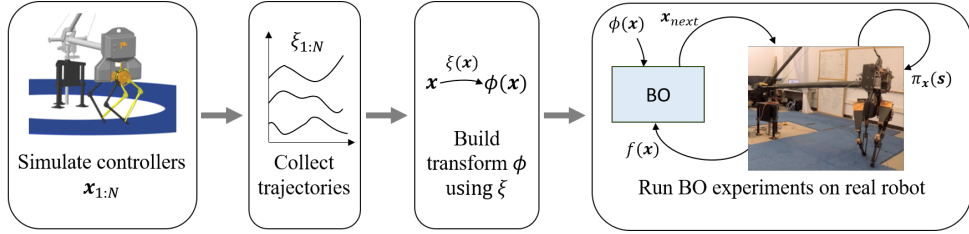


FIGURE 3.1: Overview of our proposed approach. Here,  $\pi_{\mathbf{x}}(\mathbf{s})$  is the policy (described in Section ??);  $\mathbf{x}$  is a vector of controller parameters;  $\mathbf{s}$  is the state of the robot;  $\xi(\mathbf{x})$  is a trajectory observed in simulation for  $\mathbf{x}$ ;  $\phi(\cdot)$  is the transform built using  $\xi(\mathbf{x})$ .  $f(\mathbf{x})$  is the cost of  $\mathbf{x}$  evaluated on hardware. BO uses  $\phi(\mathbf{x})$  and evaluated costs  $f(\mathbf{x})$  to propose next promising controller  $x_{next}$ .

1.  **$M_1$  : Swing leg retraction** – We look at the swing leg trajectory in swing and if the maximum leg retraction is more than a threshold, we set  $M_1 = 1$ . Otherwise,  $M_1 = 0$ . Higher swing leg retraction is better for disturbance rejection in the presence of obstacles, etc. Hence, a controller is less likely to fall if  $M_1 = 1$ .
2.  **$M_2$  : Center of Mass height** – We look at the Center of Mass (CoM) height at the start and end of each step. If the CoM height stays about the same (change is below a threshold), we set  $M_2 = 1$ . Otherwise,  $M_2 = 0$ . This metric checks that the robot is not falling across steps, but allows changes in CoM height within a step. Human-like walking typically exhibits a oscillatory CoM movement within a step, while with a linear inverted pendulum controller, the CoM height stays constant through the step. Thus, looking at just the CoM height at the start and end of a step includes both these situations and makes sure that the controller isn't falling. Thus,  $M_2 = 1$  controllers are likely to walk.
3.  **$M_3$  : Trunk lean** – We compare the mean trunk lean at the start and end of a step, and if the average lean is about the same (change is below a threshold), we set  $M_3 = 1$ . Otherwise,  $M_3 = 0$ . This ensures that the trunk is not changing orientation between steps, but allows the lean to change within a step. Again human-like walking typically exhibits a oscillatory torso movement within a step, while typical walking controllers maintain a constant torso lean. Thus, looking at just the torso lean at the start and end of a step includes both these situations and makes sure that the controller isn't falling. Thus,  $M_3 = 1$  controllers are likely to walk.
4.  **$M_4$  : Average walking speed** – We evaluate the average speed of a controller per step and set  $M_4 = v_{avg}$ . Unlike the other metrics,  $M_4$  is not binary and helps distinguish between controllers that satisfy all conditions of  $M_{1-3}$ . In general, faster walking controllers could be better, though that depends on the desired walking speed.  $M_4$  helps distinguish controllers that score the same of  $M_{1-3}$  but lead to different behaviors in simulation.

The step metrics  $M_{1-4}$  are collected per step  $i$  and summed over the total number of steps  $N$ .

$$\text{score}^i = \sum_{j=1}^4 M_j^i \quad (3.1)$$

$$\text{score}_{DoG} = \sum_i^N \text{score}^i \quad (3.2)$$

In general, a higher score implies better performance of a controller for  $M_{1-3}$ . If  $M_{1-3}$  are 0 for a particular controller, it is likely to fall. On the other hand if  $M_{1-3}$  are 1 for a controller, it is likely to walk. However, the score doesn't have a fixed relationship to a particular cost function. The cost depends on the specific desired behavior/outcome.

Controllers that chatter (step very fast, with step time less than 100ms) can have a large number of steps before falling. Since this could lead to a misleadingly high score, the DoG score is scaled by the fraction of time the simulation walked before falling. If the simulation terminated at time  $t_{sim}$  and the desired time for simulation was  $t_{max}$ , the final DoG score  $\phi$  becomes:

$$\phi = \text{score}_{DoG} \cdot \frac{t_{sim}}{t_{max}} \quad (3.3)$$

$\phi$  defines a reparameterization of a controller from the original space of controller parameters into a 1-dimensional space. We use  $\phi$  to define a 1-dimensional kernel that utilizes the Determinants of Gait scores. The functional form of this kernel is the same as Squared Exponential kernel. However, instead of Euclidean distances of points in the original space, we use distances between the DoG scores of the points:

$$k(\mathbf{x}_i, \mathbf{x}_j) \rightarrow k(\phi(\mathbf{x}_i), \phi(\mathbf{x}_j)) \quad (3.4)$$

$$k_{DoG}(\mathbf{x}_i, \mathbf{x}_j) = \sigma_k^2 \exp\left(-\frac{1}{2l^2}\|\phi(\mathbf{x}_i) - \phi(\mathbf{x}_j)\|^2\right), \quad (3.5)$$

where hyperparameters  $\sigma_k^2$ ,  $l^2$  are signal variance and length scale respectively. We refer to  $k_{DoG}$  as 'DoG-based kernel' in the following sections. To speed up calculation of kernel distances during optimization, we pre-calculate  $\phi$  for a large grid of points in simulation. We run short simulations of each point/controller, evaluate  $\phi$  and store it in a large look-up table.

The DoG score helps cluster controllers based on their behaviour in simulation. The hope is that behavioral cues like the ones described in metrics  $M_{1-4}$  have a higher chance of transferring between simulation and hardware than costs. On hardware, once we have evaluated a controller with a particular value of  $\phi$ , we expect controllers with similar values of  $\phi$  to have a similar cost. This roughly splits the cost function landscape, separating points that can potentially walk, and those that cannot, as shown in Figure 3.2. Suppose we sample an unstable point with a low  $\phi$  score and obtain a high cost on hardware (we can also seed our search with such points). We can then be fairly certain of other unstable points from simulation doing poorly as well. As a result, we can focus on potentially promising points to sample – making the search more sample efficient and biased towards sampling safe points.

Note that in Equation 3.1, metrics  $M_{1-4}$  are weighed equally when summing up. This over-condensed version is very efficient at finding walking controllers as it groups all non-walking controllers as one and separates them from all walking

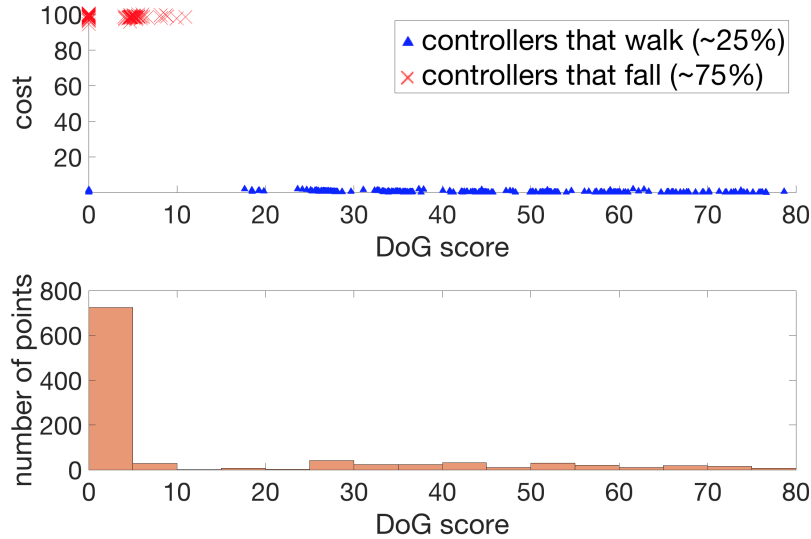


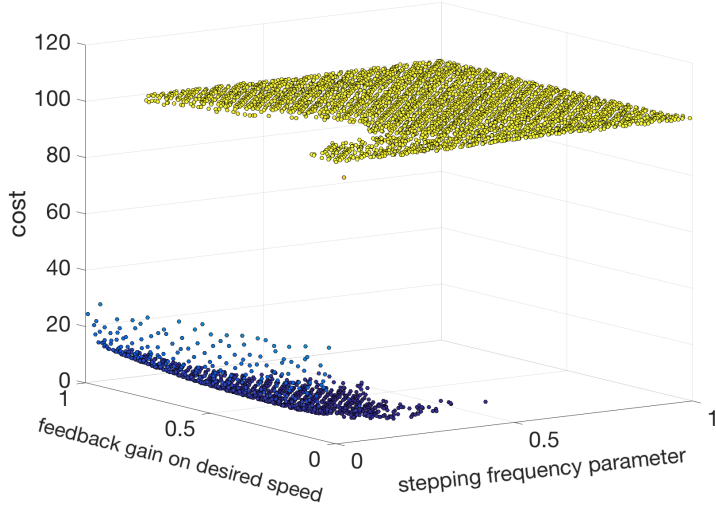
FIGURE 3.2: DoG score vs cost for 1000 randomly selected controller parameters (controller and cost from Sections 4.2.2,5.2.3). Lower DoG scores usually lead to higher costs and falling. A few points that step very fast (chatter) don't fall in simulation, so can have low cost and low DoG score. But such points are very likely to fall on hardware.

controllers. However, it is not good for distinguishing between walking controllers. In other words, if we are only searching for reasonably good walking controllers, and do not care about optimizing the quality of walking of each controllers, the 1 dimensional kernel is ideal for quickly reaching such a controller. However, if we care about the quality of walking, for example, we would like to walk at a particular speed, or minimize metabolic energy, the 1 dimensional kernel isn't ideal for distinguishing between such controllers. A small but useful addition could be to learn the weights for a 4-dimensional feature transform  $[M_1, M_2, M_3, M_4]$  using Automatic Relevance Determination (ARD), described in Rasmussen and Williams, 2005, before summing up. This would enable us to weigh the 4 metrics depending on their importance for a particular task, controller or robot. Another addition would be to use a 4-dimensional kernel, which might be less sample-efficient, but more robust to mismatch between simulation and hardware, as well as help optimize particular cost functions better.

### 3.1.2 A feature transform from data

While hand-designed feature transforms can be very data-efficient, as well as shed light on what the optimization is prioritizing, they are not ideal for situations where such information is not available. In this section, we automatically learn an informed transform for optimizing bipedal locomotion controllers without extensive domain-expertise. We start by running short simulations in a high-fidelity simulator for the locomotion controller of interest. We run simulations for a large grid of parameter sets and record the resulting costs and simulation trajectories. Costs obtained during short simulations serve as approximate indicators of the quality of the controller parameters for longer simulations, though they can diverge later. Our idea is to use the behaviors obtained from simulation to generate an informed distance metric for the Bayesian optimization kernel.

FIGURE 3.3: 2D slice of the cost landscape.



### Regression with Implicitly Asymmetric Loss

We consider a cost function focused on matching the desired walking speed and heavily penalizing falls:

$$cost_{sim} = \begin{cases} 100 - x_{fall}, & \text{if fall} \\ 10 \cdot \|v_{tgt} - \mathbf{v}_{actual}\|^2, & \text{if walk} \end{cases} \quad (3.6)$$

where  $x_{fall}$  is the distance travelled before falling,  $v_{tgt}$  is the target velocity and  $\mathbf{v}_{actual}$  is the vector containing actual velocities of the robot. This kind of cost function is of interest because it helps easily distinguish points that walk from points that fall. Similar costs have been considered in prior work when optimizing locomotion controllers (Song and Geyer, 2015).

Figure 3.3 shows a scatter plot of applying cost from Equation 3.6 to simulations of a 5-dimensional controller for the ATRIAS robot as introduced in Section 4.2.2. For visualization we only vary the 2 most sensitive dimensions, leading to a 2-dimensional subspace of the parameter space. We pick a well-performing set of parameters (in 5D), then vary the first two dimensions - the stepping frequency of the controller and the feedback gain on the desired speed. As seen in the figure, less than a quarter of this subspace contains points corresponding to low-cost simulation results (blue points on the scatter plot).

The challenge comes from the fact that the boundary between the well-performing (blue) and poorly performing (yellow) parameters is discontinuous. This is a typical landscape for bipedal systems, where a controller that makes the robot fall is much worse than one that walks, and the boundary is extremely sharp. While there can be variations to how costs are structured among stable walking points – efficiency vs speed vs distance covered, parameters that fall are much worse than those who don't. Fitting such cost function with regression can be difficult. Learning to reconstruct the boundary exactly using the training set might result in overfitting and poor performance on the test set. Trying to fix this by applying regularization is likely to result in high loss and uncertainty about the points close to the boundary. This is particularly problematic if poorly performing points lie close to some of the most promising regions of the parameter space, which is the case for the setting we

consider. We propose to use a transformation of the cost as the target for the supervised learning. Our approach is to train a deep neural network to reconstruct a reflected shifted softplus function of the cost:

$$score_{NN} = \zeta(cost_{walk} - cost_{sim}(\mathbf{x})) \quad (3.7)$$

Here  $\zeta$  is a softplus function:  $\zeta(a) = \ln(1 + e^a)$ ,  $cost_{walk}$  is the average cost for the parameter sets that walk during short simulations,  $cost_{sim}(\mathbf{x})$  is the cost computed by the simulator for vector  $\mathbf{x}$  of controller parameter values (Eq. 3.6). Using this transformation yields a “score” function such that parameter sets which produce poor results in simulation are mapped to values close to zero. With this, the differences in scores of the poorly performing parameter sets become small or zero. In contrast, the differences in scores of the parameter sets yielding potentially promising results remain proportional to the difference in the corresponding costs.

Cost transformation in Equation 3.7 serves to essentially create an asymmetric loss for neural network training. This asymmetric loss is minimized when the promising (low-cost, high-score) points are reconstructed correctly. For the poorly performing (high-cost, low-score) points, it only matters that the output of the neural network is close to zero. Such asymmetric loss can be interpreted as implementing a hybrid of regression and “soft” classification. The regression aspect aims to fit the promising points which correspond to parameters yielding walking behaviors. The “soft” classification causes an increase in the loss only if a poorly performing point is “mis-classified” as well-performing (output of the neural network is not close to zero). As a result, while the network still tries to perfectly fit the well performing points, it only needs to classify poorly performing points as poor.

The asymmetry in the loss is essential for training to reconstruct noisy costs with sharp discontinuities. Such cost functions are frequently used in optimization of locomotion controllers, with the aim to sharply penalize falling. This challenge is further addressed by learning to reconstruct the transformation of the cost (as discussed above) in combination with using a L1 loss, instead of the usual L2 loss when training the neural network. With this, errors in reconstructing points on the boundary contribute only linearly to the overall loss. This helps achieve a better fit of the stable parts of the parameter space, instead of focusing on the boundary.

The resultant transform  $\phi(\mathbf{x})$  from this cost based transform is the output of the neural network:

$$\phi(\mathbf{x}) = score_{NN}(\mathbf{x}) \quad (3.8)$$

We utilize the reconstructed transformed costs to define *asymNN* kernel for Bayesian Optimization:

$$k(\mathbf{x}_i, \mathbf{x}_j) \rightarrow k(\phi(\mathbf{x}_i), \phi(\mathbf{x}_j)) \quad (3.9)$$

$$k_{asymNN}(\mathbf{x}_i, \mathbf{x}_j) = \sigma_k^2 \exp\left(-\frac{1}{2l^2} \|\phi(\mathbf{x}_i) - \phi(\mathbf{x}_j)\|^2\right), \quad (3.10)$$

with hyperparameters  $\sigma_k, l$ . The proposed approach is able to clearly separate the unpromising part of the parameter space. Under the resulting distance metric poorly performing sets of parameters are close together and far from well-performing ones. A smaller priority is given to high-precision reconstruction of the poorly performing region of the parameter space. This is desirable, since it has been observed that usually simulators are optimistic compared to the real world (Cutler, Walsh, and How, 2015). This is indeed the case with the locomotion simulators we consider: if a set of controller parameters causes falling or instability in simulation, it is very unlikely

that the same controller parameters would result in successful walking when applied to real hardware. With that, distinguishing all the various ways in which poorly performing points fail is not useful. Using *asymNN* kernel helps rapidly separate bad regions of the parameter space from the regions that might contain promising points.

### Reconstructing Cost-agnostic Trajectory Summaries

While learning a distance metric from the cost could be effective for a wide variety of problems, frequently there is a need for a cost-agnostic approach. Such cases arise when the data from the simulator is computationally expensive to collect and we need to change the cost function. Different tasks might call for slightly different cost functions. For example, high energy consumption could be penalized if energy use needs to be restricted; robustness of the walk could be emphasized if only stable walking is acceptable; if achieving the desired speed is the most important factor – then the cost might instead only reflect how well the desired speed is maintained. For such cases we propose to train a neural network to reconstruct summaries of trajectories that are cost-agnostic, then utilize these trajectory summaries for constructing kernel distance metric.

In most cases, a summary of trajectory information contains all the pertinent information. Hence, we focus on collecting the following aspects of the simulated trajectories: walking time (time before falling), energy used during walking, position of the torso, angle of the torso, coordinates of the center of mass at the end of the short simulation runs. These summaries of simulated trajectories are collected for a range of controller parameters and comprise the training set for the neural network to fit (input:  $\mathbf{x}$  – a set of control parameters; output:  $\widehat{\mathbf{traj}}_{\mathbf{x}}$  – the corresponding trajectory summary obtained from simulation). The outputs of the (trained) neural network offer the reconstructed/approximate trajectory summaries:

$$score_{trajNN}(\mathbf{x}) = \widehat{\mathbf{traj}}_{\mathbf{x}} \quad (3.11)$$

where  $\mathbf{x}$  is the input controller parameters, and  $\widehat{\mathbf{traj}}_{\mathbf{x}}$  is the corresponding reconstructed trajectory summary. These are then used to define a distance metric for the kernel for Bayesian Optimization:

$$\phi(\mathbf{x}) = score_{trajNN}(\mathbf{x}) \quad (3.12)$$

$$k_{trajNN}(\mathbf{x}_i, \mathbf{x}_j) = \sigma_k^2 \exp \left( -\frac{1}{2l^2} \|\phi(\mathbf{x}_i) - \phi(\mathbf{x}_j)\|^2 \right) \quad (3.13)$$

with hyperparameters  $\sigma_k, l$ .

The general concept of utilizing trajectory data to improve sample efficiency of BO has been proposed before, for example in Wilson, Fern, and Tadepalli, 2014. However, prior work assumed obtaining trajectory data is possible every time kernel values  $k(\mathbf{x}_i, \mathbf{x}_j)$  need to be evaluated. This is not the case in our setting, as each controller has to be evaluated to obtain the simulation trajectory. To overcome this, we obtain trajectory summaries via costly high-fidelity simulations. To avoid having to run simulations while performing BO on hardware, we train a neural network to learn reconstructing trajectory summaries first. Running a forward pass of the neural network is a relatively inexpensive operation, hence reconstructed/approximate trajectory summaries can be quickly obtained during BO whenever  $k_{trajNN}(\mathbf{x}_i, \mathbf{x}_j)$  needs to be computed. Note that the trajectory information we extract is generic and

can be applied to other problems without requiring in-depth domain knowledge. When applying this approach to a new domain, the strategy would be to include trajectory information used to compute cost functions that are of interest/relevance in the domain. For example, for a manipulator, the coordinates of end-effector(s) could be recorded at relevant points. In contrast, information extracted in Antonova, Rai, and Atkeson, 2016; Cully et al., 2015 are more domain specific.

In addition to offering a cost-agnostic approach, our trajectory-based kernel retains more information about important aspects of simulated trajectories than a cost-based kernel. We observe that this re-parameterization could be more effective than a cost-based kernel in cases when the kernel does not retain enough information to effectively optimize the acquisition function used in Bayesian Optimization, due to over-condensing the characteristics of the simulation. In particular, cost-based kernel offers most sample-efficient results in the case of using lower-dimensional controller and the case of using a smooth cost with a higher-dimensional controller - basically easier to optimize problems. On more challenging discontinuous costs and high-dimensional controllers, trajectory-based kernel outperforms cost-based kernel. The trajectory-based kernel also significantly outperforms standard Bayesian Optimization, even when the optimization uses challenging discontinuous costs.

## 3.2 Modelling mismatch between simulation and hardware

While all the generalized transform  $\phi$  proposed in the previous section can successfully characterize the quality of a gait, large mismatch between a simulator and real-world hardware could still present a challenge. Some controller parameters could yield good gait characteristics in a short simulation, but perform poorly during a longer trial on hardware or simulation. While this issue did not arise during our hardware experiments with the controller described in Section 4.2.2, this could be an issue with a different and higher-dimensional controller and inaccurate simulator. Hence, it is important to study how the performance worsens as the fidelity of the simulator decreases and how the kernel can be adjusted to compensate for this mismatch.

In Rai et al., 2018, we proposed a way to incorporate information about simulation-hardware mismatch into the kernel from the samples evaluated so far. We augment the simulation-based kernel to include this additional information about mismatch, by expanding the original kernel by an extra dimension that contains the predicted mismatch for each controller  $\mathbf{x}$ .

A separate Gaussian process is used to model the mismatch experienced on hardware, starting from an initial prior mismatch of 0:  $g(\mathbf{x}) \sim \mathcal{GP}(0, k_{SE}(\mathbf{x}_i, \mathbf{x}_j))$ . For any evaluated controller  $\mathbf{x}_i$ , we can compute the difference between  $\phi(\mathbf{x}_i)$  in simulation and on hardware:

$$d_{\mathbf{x}_i} = \phi^{sim}(\mathbf{x}_i) - \phi^{hw}(\mathbf{x}_i) \quad (3.14)$$

We can now use mismatch data  $\{d_{\mathbf{x}_i} | i = 1 \dots n\}$  to construct a model for the expected mismatch:  $\bar{g}(\mathbf{x})$ . In the case of using a GP-based model,  $\bar{g}(\cdot)$  would denote the posterior estimate of expected mismatch. With this, we can predict simulation-hardware mismatch in the original space of controller parameters for unevaluated

controllers. Combining this with kernel  $k_\phi$  we obtain an adjusted kernel:

$$\begin{aligned}\boldsymbol{\phi}_{\mathbf{x}}^{adj} &= \begin{bmatrix} \phi^{sim}(\mathbf{x}) \\ \bar{g}(\mathbf{x}) \end{bmatrix}, & \mathbf{t}_{ij}^{adj} &= \boldsymbol{\phi}_{\mathbf{x}_i}^{adj} - \boldsymbol{\phi}_{\mathbf{x}_j}^{adj} \\ k_{\phi_{adj}}(\mathbf{x}_i, \mathbf{x}_j) &= \sigma_k^2 \exp \left( -\frac{1}{2} (\mathbf{t}_{ij}^{adj})^T \left( \begin{bmatrix} \boldsymbol{\ell}_1 \\ \boldsymbol{\ell}_2 \end{bmatrix} \right)^{-2} \mathbf{t}_{ij}^{adj} \right)\end{aligned}\quad (3.15)$$

The similarity between points  $\mathbf{x}_i, \mathbf{x}_j$  is now dictated by two components: representation in  $\phi$  space and expected mismatch. This construction has an intuitive explanation: Suppose controller  $\mathbf{x}_i$  results in walking when simulated, but falls during hardware evaluation.  $k_{\phi_{adj}}$  would register a high mismatch for  $\mathbf{x}_i$ . Controllers would be deemed similar to  $\mathbf{x}_i$  only if they have both similar simulation-based  $\phi(\cdot)$  and similar estimated mismatch  $\bar{g}(\cdot)$ . Points with similar simulation-based  $\phi(\cdot)$  and low predicted mismatch would still be ‘far away’ from the failed  $\mathbf{x}_i$ . This would help BO sample points that still have high chances of walking in simulation, but are in a different region of the original parameter space than  $\mathbf{x}_i$ . In the next section, we present a more mathematically rigorous interpretation for  $k_{\phi_{adj}}$ .

We will call this adjusted kernel with hardware and simulation mismatch the adjusted DoG-based kernel in the future. This formulation is similar in spirit to other approaches, such as Marco et al., 2017b. However, while previous work “mistrusts” all simulation data, our formulation lets us fit a dynamic mismatch function from data. This lets us trust the simulation in some regions, while mistrust it in others.

There are several approaches in literature that attempt to model the difference between simulation and hardware. Wilson, Fern, and Tadepalli, 2014 propose modelling the mismatch between a learned model and the real system by a second “residual” GP. They predict the expected cost at a new point using a convex combination of two GPs:

$$J(\mathbf{x}) = (1 - \beta) J_{sim}(\mathbf{x}) + \beta J_{err}(\mathbf{x}) \quad (3.16)$$

$$J_{err}(\mathbf{x}) \sim \mathcal{GP}(0, k(\mathbf{x}, \mathbf{x}')) \quad (3.17)$$

$$J_{sim}(\mathbf{x}) \sim \mathcal{GP}(m_{sim}(\mathbf{x}, \mathbf{x}_i, \dots, \mathbf{x}_n), k(\mathbf{x}, \mathbf{x}')) \quad (3.18)$$

$\beta$  can be learned from data.  $J_{err}$  models the residual between the simulation model and the actual data, initialized with a 0 prior.  $J_{sim}$  is a cost model learned over simulation points  $m_{sim}(\mathbf{x}, \mathbf{x}_i, \dots, \mathbf{x}_n)$ , which are be an inaccurate representation of the actual system. The resultant GP has a mean which is a convex combination of the two GP means, and the same variance as the chosen  $k$ . While this approach can be very powerful when the simulation is close to hardware, with significant mismatch the bias of simulation can be hard to overcome.

In contrast, our approach puts majority of the information from simulation into the kernel, which is an easier to overcome biased prior information. We present a more mathematical foundation for our mismatch model in the next section. Results comparing our approach to other approaches from literature are in Section ??

Multiple sources of information can also be added to Gaussian Processes (Poloczek, Wang, and Frazier, 2016). For example, let the true cost be a combination of cost in simulation and a residual error - each with a separate kernel:

$$J(\mathbf{x}) = J_{sim}(\mathbf{x}) + J_{err}(\mathbf{x}) \quad (3.19)$$

where

$$J_{err}(\mathbf{x}) \sim \mathcal{GP}(0, k_{err}(\mathbf{x}, \mathbf{x}')) \quad (3.20)$$

$$J_{sim}(\mathbf{x}) \sim \mathcal{GP}(\mu_{sim}(\mathbf{x}), k_{sim}(\mathbf{x}, \mathbf{x}')) \quad (3.21)$$

Here  $J(\mathbf{x})$  is the true cost of the controller on hardware,  $J_{sim}(\mathbf{x})$  is a measurement from simulation, and  $J_{err}(\mathbf{x})$  is the noise distribution, which is the mismatch between simulation and hardware. Points sampled from hardware do not have this mismatch, and hence are samples from the true GP  $J(\mathbf{x})$ . However points from simulation are samples from  $J_{sim}(\mathbf{x})$  and their corresponding residual  $J_{err}$  needs to be estimated.

Poloczek, Wang, and Frazier, 2016 extend the kernel by an additional binary variable  $\delta$ , which indicates whether the cost is evaluated in simulation ( $\delta = 0$ ) or on the physical system ( $\delta = 1$ ). Based on the extended parameter  $a = (\mathbf{x}, \delta)$ , we can model the cost by adapting the kernel of  $J$  to

$$k(\mathbf{x}, \mathbf{x}') = k_{sim}(\mathbf{x}, \mathbf{x}') + \delta\delta'k_{err}(\mathbf{x}, \mathbf{x}') \quad (3.22)$$

Marco et al., 2017b develop an automatic way of trading off data from simulation and hardware based on the expected improvement of each source, normalized by the time cost of sampling simulation vs hardware.

For high dimensional controllers, these error maps can need a lot of data to accurately model the inaccuracy of simulation, especially for rapidly changing discontinuous costs. To overcome this problem, it is worth exploring if characteristics of simulation can be used to create a prior mismatch. For example, controllers with higher impacts might have a high chance of failing on hardware even if they walk in simulation. Similarly, controllers that venture close to joint limits might be likely to fail on hardware, even if successful in simulation.

In comparison, building a mismatch map for the reduced dimensional DoG-space can be very data efficient. This allows us to compensate for the mismatch between simulation and hardware and propagate this information back to update the features collected in simulation. This leads to a novel way of updating models from hardware data in a transformed space with very few data points. Moreover, if the simulation is close to hardware in some regions, the learned mismatch is close to 0 and higher in other regions where the simulation is different from the hardware.

### 3.2.1 Interpretation of Kernel with Mismatch Modeling

In this section we give a more mathematically sound interpretation the mismatch adjusted kernel described in the previous section.

Let us consider a controller  $\mathbf{x}_i$  evaluated on hardware. The difference between simulation-based and hardware-based feature transform for  $\mathbf{x}_i$  is  $d_{\mathbf{x}_i} = \phi^{sim}(\mathbf{x}_i) - \phi^{hw}(\mathbf{x}_i)$ . The ‘true’ hardware feature transform for  $\mathbf{x}_i$  is  $\phi^{hw}(\mathbf{x}_i) = \phi^{sim}(\mathbf{x}_i) - d_{\mathbf{x}_i}$ . After  $n$  evaluations on hardware,  $\{d_{\mathbf{x}_i} | i = 1 \dots n\}$  can serve as data for modeling simulation-hardware mismatch. In principle, any data-efficient model  $g(\cdot)$  can be used, such as GP (a multi-output GP in case  $\phi(\cdot) > 1D$ ). With this, we can obtain an adjusted transform:  $\hat{\phi}^{hw}(\mathbf{x}) = \phi^{sim}(\mathbf{x}) - \bar{g}(\mathbf{x})$ , where  $\bar{g}(\cdot)$  is the output of the model fitted using  $\{d_{\mathbf{x}_i} | i = 1 \dots n\}$ .

Suppose  $\mathbf{x}_{new}$  has not been evaluated on hardware. We can use  $\hat{\phi}^{hw}(\mathbf{x}_{new}) = \phi^{sim}(\mathbf{x}_{new}) - \bar{g}(\mathbf{x}_{new})$  as the adjusted estimate of what the output of  $\phi$  should be, taking into account what we have learned so far about simulation-hardware mismatch.

Let's construct kernel  $k_{\phi_{adj}}^{v_2}(\mathbf{x}_i, \mathbf{x}_j)$  that uses these hardware-adjusted estimates directly:

$$\begin{aligned}\mathbf{q}_{ij}^{adj} &= \hat{\phi}^{hw}(\mathbf{x}_i) - \hat{\phi}^{hw}(\mathbf{x}_j) \\ &= (\phi^{sim}(\mathbf{x}_i) - \bar{g}(\mathbf{x}_i)) - (\phi^{sim}(\mathbf{x}_j) - \bar{g}(\mathbf{x}_j)) \\ &= \underbrace{(\phi^{sim}(\mathbf{x}_i) - \phi^{sim}(\mathbf{x}_j))}_{\mathbf{v}_\phi} + \underbrace{(\bar{g}(\mathbf{x}_j) - \bar{g}(\mathbf{x}_i))}_{\mathbf{v}_g}\end{aligned}$$

$$\begin{aligned}k_{\phi_{adj}}^{v_2}(\mathbf{x}_i, \mathbf{x}_j) &= \sigma_{k_{v_0}}^2 \exp\left(-\frac{1}{2}(\mathbf{q}_{ij}^{adj})^T(\boldsymbol{\ell})^{-2}\mathbf{q}_{ij}^{adj}\right) \\ &= \sigma^2 \exp\left(-\frac{1}{2}[(\mathbf{v}_\phi + \mathbf{v}_g)^T(\boldsymbol{\ell})^{-2}(\mathbf{v}_\phi + \mathbf{v}_g)]\right) \\ &= \sigma^2 \exp\left(-\frac{1}{2}[\mathbf{v}_\phi^T(\boldsymbol{\ell})^{-2}\mathbf{v}_\phi + \mathbf{v}_g^T(\boldsymbol{\ell})^{-2}\mathbf{v}_g + prod_{ij}]\right) \\ &\quad \text{where } prod_{ij} = 2\mathbf{v}_\phi^T(\boldsymbol{\ell})^{-2}\mathbf{v}_g\end{aligned}$$

Using  $\exp(a + b + c) = \exp(c) \cdot \exp(a + b)$ , we have:

$$k_{\phi_{adj}}^{v_2}(\mathbf{x}_i, \mathbf{x}_j) = \sigma^2 \exp(-prod_{ij}) \exp\left(-\frac{1}{2}[\mathbf{v}_\phi^T(\boldsymbol{\ell})^{-2}\mathbf{v}_\phi + \mathbf{v}_g^T(\boldsymbol{\ell})^{-2}\mathbf{v}_g]\right)$$

If we now observe that  $\mathbf{v}_g^T(\boldsymbol{\ell})^{-2}\mathbf{v}_g = (-\mathbf{v}_g)^T(\boldsymbol{\ell})^{-2}(-\mathbf{v}_g)$  we get:

$$\begin{aligned}k_{\phi_{adj}}^{v_2}(\mathbf{x}_i, \mathbf{x}_j) &= \sigma^2 \exp(-prod_{ij}) \exp\left(-\frac{1}{2}(\mathbf{t}_{ij}^{adj})^T\left(\begin{bmatrix} \boldsymbol{\ell} \\ \boldsymbol{\ell} \end{bmatrix}\right)^{-2}\mathbf{t}_{ij}^{adj}\right) \\ \mathbf{t}_{ij}^{adj} &= \begin{bmatrix} \phi^{sim}(\mathbf{x}_i) - \phi^{sim}(\mathbf{x}_j) \\ \bar{g}(\mathbf{x}_i) - \bar{g}(\mathbf{x}_j) \end{bmatrix} \text{ (from Equation 3.15)}\end{aligned}$$

Compare this to  $k_{\phi_{adj}}$  from Equation 3.15:

$$k_{\phi_{adj}}(\mathbf{x}_i, \mathbf{x}_j) = \sigma_k^2 \exp\left(-\frac{1}{2}(\mathbf{t}_{ij}^{adj})^T\left(\begin{bmatrix} \boldsymbol{\ell}_1 \\ \boldsymbol{\ell}_2 \end{bmatrix}\right)^{-2}\mathbf{t}_{ij}^{adj}\right) \quad (3.23)$$

Now we see that  $k_{\phi_{adj}}^{v_2}$  and  $k_{\phi_{adj}}$  have a similar form. Hyperparameters  $\boldsymbol{\ell}_1, \boldsymbol{\ell}_2$  provide flexibility in  $k_{\phi_{adj}}$  as compared to having only vector  $\boldsymbol{\ell}$  in  $k_{\phi_{adj}}^{v_2}$ . They can be adjusted manually or with Automatic Relevance Determination (Rasmussen and Williams, 2005). For  $k_{\phi_{adj}}^{v_2}$ , the role of signal variance is captured by  $\sigma^2 \exp(-prod_{ij})$ . This makes the kernel nonstationary in the transformed  $\phi$  space. Since  $k_{\phi_{adj}}$  is already non-stationary in  $\mathbf{x}$ , it is unclear whether non-stationarity of  $k_{\phi_{adj}}^{v_2}$  in the transformed  $\phi$  space has any advantages.

The above discussion shows that  $k_{\phi_{adj}}$  proposed in Rai et al., 2018 is motivated both intuitively and mathematically. It aims to use a transform that accounts for the hardware mismatch, without adding extra non-stationarity in the transformed space. It also helps propagate data seen on hardware back to simulation, thus updating simulation models in a sample-efficient manner. If one has intuitions about the mismatch in the space of controllers, they could be used in the prior of the mismatch kernel to improve sample-efficiency further.

### 3.3 Transfer learning with contextual Bayesian optimization

It is possible to transfer knowledge between tasks using Bayesian optimization by adding context to the learning. Contexts can include specific features of the experiment such as target speed of walking, or the incline of the ground. In such cases, the cost observed on hardware is a function of not just the controller parameters  $\mathbf{x}$ , but also the context  $c$ , leading to a cost of the form  $f(\mathbf{x}, c)$ . Since the context is an observed variable, and not an optimized variable, Bayesian optimization is done on the parameters  $\mathbf{x}$ , which conditioning the posterior of the GP on the observed  $c$ .

$$f(\mathbf{x}, c) \sim \mathcal{GP}(\mu(\mathbf{x}, c), k((\mathbf{x}, c), (\mathbf{x}', c'))) \quad (3.24)$$

$$\mathbf{x}_{t+1} = \arg \max EI(f(\mathbf{x}, c) | c = c_{\text{observed}}) \quad (3.25)$$

Additionally, the feature transform in simulation can be a function of  $c$ , as well as the updates learned on hardware. The features observed on hardware  $\phi^w(\mathbf{x}, c)$  depend on both the controller as well as context. Hence the mismatch GP is also a function of both as  $d_{\mathbf{x}_i, c} = \phi^{\text{sim}}(\mathbf{x}_i, c) - \phi^{\text{hw}}(\mathbf{x}_i, c)$ . Even if we do not know the contexts when calculating simulation features, the mismatch update gives us a way of building a context-dependant feature transform from data. Figure 3.4 shows an example where BO was conducted on 6 different target speeds for a 50-dimensional neuromuscular controller on the ATRIAS biped.

The target speeds were  $[0.5, 1.0, 1.5, 0.75, 1.25, 0.25, 1.75] \text{ m/s}$ . Initial speeds of  $[0.5, 1.0, 1.5] \text{ m/s}$  were simulated for 10 trials while latter speeds were simulated for 5. As shown in the figure, fewer trials are needed to reliably reach walking controllers as more data is added to the GP. This shows that learning on other target speeds indeed speeds up the learning for future targets, even when extrapolating. Target speeds of  $[0.75, 1.25, 0.25, 1.75] \text{ m/s}$  reach a mean cost of 11.96 after 5 trials, as compared to a mean cost of 19.61 for the initial target speeds.

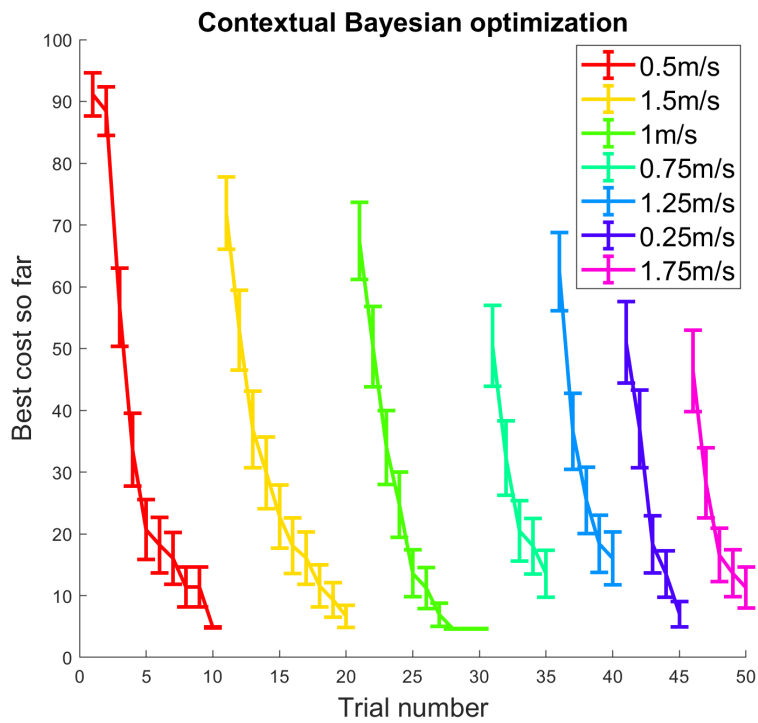


FIGURE 3.4: Transfer learning with contextuan bayesian optimization can be used to transfer knowledge between different target speeds. Initial speeds of  $[0.5, 1.0, 1.5]m/s$  were simulated for 10 trials while latter speeds of  $[0.75, 1.25, 0.25, 1.75]m/s$  were simulated for 5 trials. The latter speeds reach a mean cost of 11.96 after 5 trials, as compared to a mean cost of 19.61 for the initial target speeds.



## Chapter 4

# Robots and controllers evaluated

In this chapter, we describe the experiments conducted to validate our approach. Since this thesis is focused on using simulation to speed up hardware experiments, robot experiments form an important part of this work. Our hardware experiments are done on the ATRIAS robot on a boom. We present results on a feedback based reactively stepping controller, optimizing 5 and 9 parameters in 2 sets of experiments on hardware.

Our simulation experiments are conducted on two different robot morphologies – a planar 7-link biped model, and an ATRIAS simulation on the boom. We present two neuromuscular walking controllers – on a 7-link biped optimizing 16 parameters, and then on an ATRIAS simulation optimizing 50 parameters.

In addition, we present experiments on learning neural network policies using deep reinforcement learning. These policies are learned in simulation and deployed on the ATRIAS biped.

We detail our robots in the next section, followed by the controllers.

## 4.1 Robot morphologies tested

### 4.1.1 The ATRIAS Robot

Our test platform is CMU’s ATRIAS robot (Figure 1.1), a human sized bipedal robot Hubicki et al., 2016a. The ATRIAS robot was designed so that the inertial properties of the Center of Mass of ATRIAS matched that of humans. The robot weights about 64kg, with most of its mass concentrated around the trunk. The torso is located about 0.19m above the pelvis, and its rotational inertia is about  $2.2\text{kgm}^2$ . The legs are 4-segment carbon-fiber linkages driven with a point foot, making the legs very light and enabling fast swing movements. The legs are actuated by 2 Series Elastic Actuators (SEAs) in the sagittal plane and a DC motor in the lateral plane. The SEAs consist of a fiberglass leaf spring attached to a geared DC motor on one end and the leg load on the other. Each spring is equipped with a load-side and motor-side encoder, which given the spring stiffness, can be used to estimate joint torques on each joint. Although ATRIAS is capable of 3D walking, in this work, we focus on planar movements around a boom.

### 4.1.2 A 7-link biped model

We also experiment with a 7-link planar human-like robot model as shown in Figure 4.1. It has two legs - composed of foot, shin and thigh and a hip. There are 6 actuators at the ankle, knee and hip joints in each leg with infinite allowed torque. This model is used as a simple 2-dimensional approximation to complex humanoid robots like Sarcos.

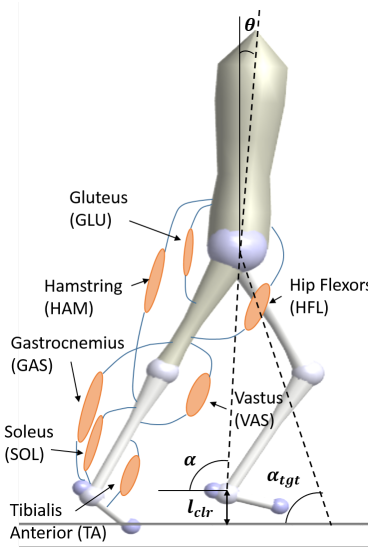


FIGURE 4.1: The neuromuscular model. The muscles and swing parameters are highlighted.

## 4.2 Controllers tested

### 4.2.1 Neuromuscular model for humanoid robots

We use neuromuscular model policies, as introduced in Geyer and Herr, 2010, as our controller for a 7-link planar human-like model. These policies use approximate models of muscle dynamics and human-inspired reflex pathways to generate joint torques, producing gaits that are similar to human walking in stance. Desai and Geyer, 2012 designed reflex laws for swing that enable target foot-placement and leg clearance, by analyzing the double pendulum dynamics of the human leg. Integrating this swing control with the previous reflex control enables the model to overcome disturbances in the range of up to  $\pm 10\text{cm}$ , as described in Song and Geyer, 2015. We next describe this control in some detail.

#### Neuromuscular Stance Control

In stance of the neuromuscular controller, each leg is actuated by 7 Hill-type muscles Morrison, 1970, consisting of the soleus (SOL), gastrocnemius (GAS), vastus (VAS), hamstring (HAM), tibialis anterior (TA), hip flexors (HFL) and gluteus (GLU), illustrated in Figure 4.1. Together, these muscles produce torques about the hip, knee and ankle. The muscle force  $F$  is a non-linear function of the muscle state  $s^m$  and stimulus  $S^m$ , which when multiplied by the moment arm  $r(\theta_i)$  gives the resultant torque on joint  $i$ :

$$\tau_i^m = F(S^m, s^m)r(\theta_i),$$

where  $\tau_i^m$  is the torque applied by muscle  $m$  on joint  $i$  and  $\theta_i$  is the joint angle.

Most of the muscle reflexes in stance are positive length or force feedback on the muscle stimulus. In general, the stimulus  $S^m(t)$  for muscle  $m$  is a function of the time delayed length or force signal  $P^m$  times a feedback gain  $K^m$ :

$$S^m(t) = S_0^m + K^m \cdot P^m(t - \Delta t),$$

where  $S_0^m$  is the pre-stimulus,  $K^m$  is the feedback gain and  $P^m$  is the time-delayed feedback signal of length or force. Some muscles can be co-activated and have multiple feedback signals from more than one muscle. The feedback gains  $K^m$  described above are a subset of the parameters that we aim to tune in our optimization. The details of these feedback pathways can be found in Song and Geyer, 2015.

This feedback structure generates compliant leg behaviour and prevents the knee from overextending in stance. To balance the trunk, feedback on the torso angle is added to the GLU stimulus:

$$S_{torso}^{GLU}(t) = K_p^{stance}(\theta_{des} - \theta) - K_d^{stance}\dot{\theta},$$

where  $K_p^{stance}$  is the position gain on the torso angle  $\theta$  and  $\theta_{des}$  is the desired angle.  $K_d^{stance}$  is the velocity gain and  $\dot{\theta}$  is the angular velocity. Specifically, here are the stance parameters we optimize over, and their roles in the neuromuscular model:

- $K^{GAS}$  : Positive force feedback gain on GAS
- $K^{GLU}$  : Positive force feedback gain on GLU
- $K^{HAM}$  : Positive force feedback gain on HAM
- $K^{SOL}$  : Positive force feedback gain on SOL
- $K_{SOL}^{TA}$  : Negative force feedback from SOL on TA
- $K^{TA}$  : Positive length feedback on TA
- $K^{VAS}$  : Positive force feedback on VAS
- $K_p^{stance}$  : Position gain on feedback on torso angle
- $K_d^{stance}$  : Velocity gain on feedback on torso velocity
- $K_{mix}^{GLU}$  : Gain for mixing force feedback and feedback on angle for GLU

### Swing Leg Placement Control

The swing control is controlled by three main components – target leg angle, leg clearance and hip control. Target leg angle is a direct result of the foot placement strategy which is a function of the velocity of the center of mass (CoM)  $v$ , and the as distance between the stance leg the CoM, and presented in Yin, Loken, and Panne, 2007:

$$\alpha_{tgt} = \alpha_0 + C_d d + C_v v,$$

where  $\alpha_{tgt}$  is the target leg angle,  $\alpha_0$  is the nominal leg angle,  $C_d$  and  $C_v$  are parameters optimized by our control.

Leg clearance is a function of the desired leg retraction during swing. The knee is actively flexed until the leg reaches the desired leg clearance height,  $l_{clr}$  and then held at this height, until the leg reaches a threshold leg angle. At this point, the knee is extended and allowed to reach the target leg angle  $\alpha_{tgt}$ . Details of this control can be found in Desai and Geyer, 2012. As was noted in Song and Geyer, 2015, and observed in our experiments, the control is relatively insensitive to the individual gains of the set-up in swing. It is sufficient to control the higher level parameters such as the desired leg clearance and target leg angle.

The third part of the control involves maintaining the desired leg angle  $\alpha_{tgt}$  by applying a hip torque  $\tau_{hip}^\alpha$ :

$$\tau_{hip}^\alpha = K_p^{swing}(\alpha_{tgt} - \alpha) - K_d^{swing}(\dot{\alpha}),$$

where  $K_p^{swing}$  is the position gain on the leg angle,  $K_d^{swing}$  is the velocity gain,  $\alpha$  is the leg angle and  $\dot{\alpha}$  is the leg angular velocity (see Figure 4.1).

More concisely, the swing parameters that we focus on in our optimization are the following:

1.  $K_p^{swing}$  : Position gain on feedback on leg angle
2.  $K_d^{swing}$  : Velocity gain on feedback on leg velocity
3.  $\alpha_0$  : Nominal leg angle
4.  $C_d$  : Gain on the horizontal distance between the stance foot and CoM
5.  $C_v$  : Gain on the horizontal velocity of the CoM
6.  $l_{clr}$  : Desired leg clearance

Though originally developed for explaining human neural control pathways, these controllers have recently been applied to robots and prosthetics, for example in Thatte and Geyer, 2016 and Noot, Ijspeert, and Ronsse, 2015. As demonstrated in Song and Geyer, 2015, these models are indeed capable of generating a variety of locomotion behaviours for a humanoid model - for example, walking on flat, rough ground, turning, running, walking upstairs and on ramps. However, a full study of using these models to control biped robots still needs to be done. Whether these models will transfer well to robots with significantly different dynamics and inertial properties than humans needs to be explored. It is difficult to transfer these models to robots because of a large number of interdependent gains that need to be tuned. Typically, this is done using Covariance Matrix Adaptation Evolutionary Strategy (CMA-ES) (Hansen, 2006), an evolutionary algorithm for difficult non-linear non-convex black-box optimization problems. Even though CMA-ES is useful for optimizing non-convex problems in high dimensions, it is not sample efficient and depends on the initial starting point. An optimization for 16 neuromuscular parameters takes 400 generations, around a day on a standard i7 processor and about 5,000 trials, as reported in Song and Geyer, 2015.

The large number of trials make it impossible to implement CMA-ES on a real robot. This is a shortcoming because often we find that after training the policies in simulation, they do not transfer well to the real robot, due to differences between simulation and real hardware. We aim to overcome this problem by using Bayesian Optimization with informed feature transforms for optimizing controllers.

The neuromuscular controller is a model-free controller. It does not need the exact dynamics of the robot to generate torques. The dynamics are inherently embedded in the learned parameters of the controller. As a result, the same controller can be used on very different robots without any modification to the policy structure.

We next describe a model-based reactively stepping controller. This controller uses the dynamics models of the robot to generate torques. Hence, to transfer to new systems, the dynamics need to be updated.

#### 4.2.2 Feedback based reactive stepping policy

We design a parametric controller for controlling the CoM height, torso angle and the swing leg by commanding desired ground reaction forces and swing foot landing location.

$$F_x = K_{pt}(\theta_{des} - \theta) + K_{dt}(\dot{\theta}_{des} - \dot{\theta}) \quad (4.1)$$

$$F_z = K_{pz}(z_{des} - z) + K_{dz}(\dot{z}_{des} - \dot{z}) \quad (4.2)$$

$$x_p = k(v - v_{tgt}) + C \cdot d + 0.5 \cdot v \cdot T \quad (4.3)$$

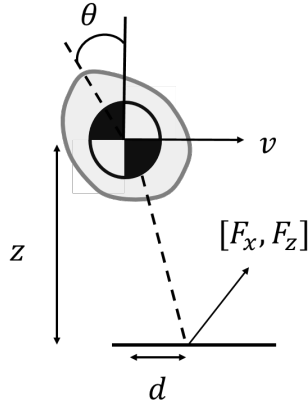


FIGURE 4.2: Illustration of the Center of Mass model and variables used for the feedback-based stepping policy.

Here,  $F_x$  is the desired horizontal ground reaction force (GRF),  $K_{pt}$  is the proportional gain on the torso angle  $\theta$  and  $K_{dt}$  is the derivative gain on the torso angular velocity  $\dot{\theta}$ .  $\theta_{des}$  and  $\dot{\theta}_{des}$  are the desired torso lean and desired torso angular velocity.  $F_z$  is the desired vertical GRF,  $K_{pz}$  is the proportional gain on the CoM height  $z$  and  $K_{dz}$  is the derivative gain on the CoM vertical velocity  $\dot{z}$ .  $z_{des}$  and  $\dot{z}_{des}$  are the desired CoM height and desired CoM vertical velocity. Both  $\dot{\theta}_{des}$  and  $\dot{z}_{des}$  are always set to 0.  $x_p$  is the desired foot landing location for the end of swing;  $v$  is the horizontal CoM velocity,  $k$  is the feedback gain that regulates  $v$  towards the target velocity  $v_{tgt}$ . These quantities are highlighted in Figure 4.2.  $C$  is a constant and  $d$  is the distance between the stance leg and the CoM;  $T$  is the swing time and the term  $0.5 \cdot v \cdot T$  is a feedforward term similar to a Raibert hopping policy, described in Raibert, 1986.

This parametrization results in desired ground reaction forces (GRFs) in stance and a desired foot landing position in swing. Note that there is no desired CoM trajectory in this controller. We only command a desired CoM velocity, regulated through the swing foot placement. In stance, the desired GRFs regulate a desired CoM height and torso angle. These are then sent to the ATRIAS inverse dynamics model that generates desired motor torques ( $\tau_f, \tau_b$ ) that realize the GRFs.

$$M\ddot{q} + h = S\tau + J^T F \quad (4.4)$$

where  $M$  is the mass matrix,  $\ddot{q}$  are the joint accelerations,  $h$  are the gravitational terms,  $S$  is a selection matrix,  $\tau$  are resultant joint torques,  $J$  is the contact Jacobian and  $F = [F_x, F_z]$  are the desired forces generated in 4.1. There are no Coriolis terms due to the assumption of massless legs. Details can be found in Wu and Geyer, 2014. These desired motor torques are then sent to a low level motor velocity-based feedback loop that generates the desired torques in the robot SEAs.

In swing, we continually re-generate a 5th order spline that starts from the current position and velocity of the swing leg,  $x_{sw}$  and  $\dot{x}_{sw}$  and terminates at the desired foot position  $x_{fp}$ , with ground speed matching (swing leg is at rest with respect to the ground). The desired initial and final point of this spline is continually regenerated based on the current estimate of the swing foot position and velocity, as well as the desired footstep and CoM velocity. This trajectory gives the next desired position and velocity of the swing leg,  $x_{sw}^*, \dot{x}_{sw}^*$ , which is translated to desired joint positions and velocities using the robot kinematics. These are then position-controlled by sending a velocity command to the robot SEAs.

This controller assumes no double-stance, swing leg takes off as soon as stance

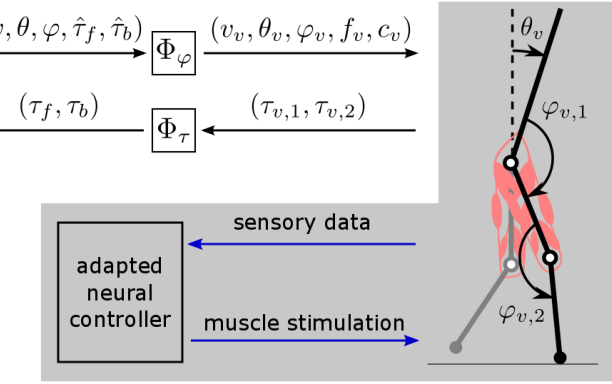


FIGURE 4.3: Virtual neuromuscular control. VNMC maps the robot's state,  $(v, \theta, \varphi, \hat{\tau}_f, \hat{\tau}_b)$ , to virtual measurements required to emulate a neuromuscular model,  $(v_v, \theta_v, \varphi_v, f_v, c_v)$ , where  $\varphi$  are joint angles, and  $f_v$  and  $c_v$  are force and contact data of the virtual leg. The virtual neuromuscular model (in the gray box) outputs virtual joint torques,  $(\tau_{v,1}, \tau_{v,2})$ , that are mapped to desired robot joint torques,  $(\tau_f, \tau_b)$ , which are tracked by the SEA controller.

is detected. This leads to a highly dynamic gait, as the contact polygon for ATRIAS in single stance is a point. It should be possible to extend this walking controller to include a double stance phase, but we leave that to future work.

The controller also depends on the desired speed of walking (as this determines the next stepping location). This means that the "stability" of the controller depends not only on the parameters chosen, but also the desired target speed. We assume that the target speed is provided by the user and is constant in our experiments. It is possible to add the desired speed as an extra dimension to the controller and optimize controllers conditioned on this. But we leave that for future work.

1. 5 dimensional walking controller : In our first set of experiments, we optimized 5 parameters from the above described controller. These were  $[K_{pt}, K_{dt}, k, C, T]$ . The desired positions and velocities were hand tuned, and so was the feedback on  $z$ .
2. 9 dimensional walking controller : In our second set of experiments, we optimized 9 parameters of the above described controller. They were :  
 $[K_{pt}, K_{dt}, \theta_{des}, K_{pz}, K_{dz}, z_{des}, k, C, T]$

#### 4.2.3 Virtual Neuromuscular Controller for ATRIAS

We adapt a previously proposed virtual neuromuscular controller (VNMC) Batts, Song, and Geyer, 2015 adapted for ATRIAS. VNMC maps a neuromuscular model to the robot's topology and emulates it to generate desired motor torques, which is sent to the SEA controller (Figure 4.3). The emulated neuromuscular model, which is originally developed to study human locomotion, consists of primarily spinal reflexes, and with appropriate sets of control parameters, it generates diverse human locomotion behaviors Song and Geyer, 2015, such as walk, run, turn, walk up stairs, etc. The VNMC control consists of 6 muscles on each leg - the hip flexors (HFL), the glutei (GLU), the hamstrings (HAM), the rectus femoris (RF), the vastii (VAS) and the biceps femoris (BFSH). Since ATRIAS doesn't have any ankles, these muscles are removed from the model. The feedbacks are similar to the ones described in 4.2.1, and details can be found in Song and Geyer, 2015.

For this study, we adapt the previous VNMC Batts, Song, and Geyer, 2015 by removing some unnecessary biological components while preserving its basic functionalities. First, the new VNMC directly uses joint angular and angular velocity data instead of estimating it from physiologically plausible sensory data, such as muscle fiber states, when applicable. Second, most of the neural transmission delays are removed, except the ones utilized by the controller.

The adapted VNMC consists of 50 control parameters including feedback gains for each muscle feedback in swing and stance, pre-stimulations for each muscle in swing and stance, high level leg placement gains and desired trunk inclination. When optimized using covariance matrix adaptation evolution strategy Hansen, 2006, it can control ATRIAS to walk on rough terrains with height changes of  $\pm 20$  cm in planar simulation. The original VNMC in Batts, Song, and Geyer, 2015 doesn't start from rest, which is impossible to achieve on a robot. To overcome this problem, for now, we start with a 5-dimensional walking controller that can start from rest. Once a desired speed is reached, we switch to the virtual neuromuscular control.

## 4.3 Inaccurate simulations for constructing kernels

To compare the performance of different methods that can be used to transfer information from simulation to hardware, we create a series of increasingly approximate simulators. These simulators emulate increasing mismatch between simulation and hardware and its effect on the information transfer. Commonly seen discrepancies between simulation and hardware can be classified into three categories: incorrect dynamics parameters, incorrect dynamics models and incorrect environment/task. Incorrect dynamics parameters include discrepancies such as wrong mass, inertia, CoM location of links of the robot. Incorrect models on the other hand are more systematic errors, such as incorrect friction models, actuator dynamics and unmodeled parts of the robot. The third type of discrepancy occurs when simulation is modelling a task different from what is seen on hardware, for example walking on flat ground vs climbing stairs. We perturb our simulation to create discrepancies of the first two kinds described above, and test the performance of BO at optimizing a 5, 9 and 50 dimensional controller. This allows us to study the effect of increasing mismatch between simulation and hardware on the performance of our proposed approach.

### 4.3.1 Incorrect dynamics parameters

Our first set of experiments create a "*simulated hardware*" that is increasingly different from the simulation, in which the DoG features were collected. This is done by changing the mass, inertia, center of mass location of each link of the by up to  $\pm x\%$  ( $x = 20, 40, 60$ ) of its original value. This perturbed simulation now serves as a test hardware for features calculated in the unperturbed simulator. The friction coefficient of the ground contact models, ground stiffness and actuator delay is also changed by the same amount. Unlike domain-randomization, from Mordatch, Lowrey, and Todorov, 2015, instead of training on perturbations, we test on these perturbations. This setup is designed to test whether our approach can be used even when the scale of mismatch between simulation and hardware is unknown a-priori.

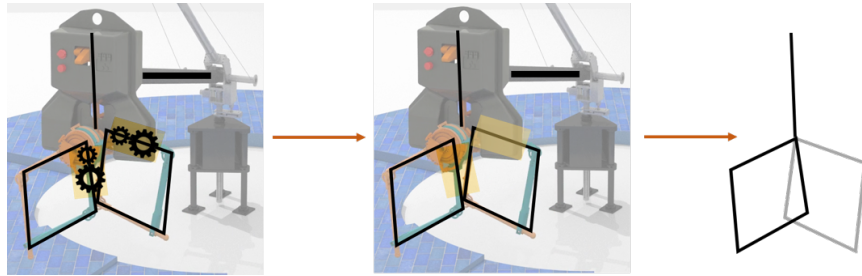


FIGURE 4.4: Different fidelity simulators for ATRIAS. The original simulator (left) is very high-fidelity with complex gear and boom dynamics. The second simulator (middle) has an approximate gear dynamics model and the third simulator (right) simulates a 2-dimensional robot without boom or gear dynamics.

### 4.3.2 Incorrect dynamics models

In this setting, the high-fidelity ATRIAS simulator (Martin, Wu, and Geyer, 2015), is the *simulated “hardware”*. We make dynamics approximations to the original simulator, which are used commonly in simulators to decrease fidelity and increase simulation speed. For example, the complex dynamics of harmonic drives are approximated as a torque multiplication, and the boom is removed from the simulation, leading to a two-dimensional simulator. These approximate simulators now become the *simulated “simulators”*. As the approximations in these simulators are increased, we expect the performance of methods that utilize simulation for optimization on hardware to deteriorate.

The details of the approximate simulators are described below:

- 1. Simulation with simplified gear dynamics :** The ATRIAS robot has geared DC motors attached to leaf springs on the legs. Their high gear ratio of 50 is achieved through a harmonic drive. In the original simulator, this drive is modelled using gear constraints in MATLAB SimScape Multibody simulation environment. These require significant computation time as the constraint equations have to be solved at every time instant, but lead to a very good match between the robot and simulation. We replace this model with a commonly used approximation for geared systems – multiplying the rotor torque by the gear ratio. This reduces the simulation time to about a third of the original simulator, but leads to an approximate gear dynamics model.
- 2. Simulation with no boom and simplified gear dynamics :** The ATRIAS robot walks on a boom in our hardware experiments. The boom leads to lateral torques on the robot, which have vertical and horizontal force components that need to be considered in a realistic simulation of the robot. In our second approximation, we remove the boom from the original simulator and constrain the motion of the robot to a 2-dimensional plane, making a truly two-dimensional simulation of ATRIAS. This is a common approximation for two-dimensional robots. Since this approximation has both simplified gear dynamics and no boom, it is further from the original simulator than the first approximation.

A visual illustration of these approximations is shown in Figure 4.4. The advantage of such an arrangement is that we can extensively test the effect of unmodelled and wrongly modelled dynamics on information transfer between simulation and hardware. Even in our high-fidelity original simulator, there are several

un-modelled components of the actual hardware. For example, the non-rigidness of the robot parts, misaligned motors and relative play between joints. In our experiments, we find that the 50-dimensional VNMC is a sensitive controller, with little hope of directly transferring from simulation to hardware. Anticipating this, we can now test several methods of compensating for this mismatch using our increasingly approximate simulators. In the future, we would like to take this approximations further and study when there is useful information even in over-simplified simulations of legged systems.

## 4.4 Neural network policies on the ATRIAS biped

Another way of transferring information between simulation and hardware is to directly learn a robust policy in simulation and deploy it on hardware. We train a deep neural network policy for controlling ATRIAS in simulation with ground height disturbance and test it on hardware. We experiment with different neural network controller structures, and study their effect on transfer from simulation to hardware, without any domain randomization. We show that structured neural network controllers have a fast training rate in simulation as well as higher rate of transfer to hardware. The structure also gives the user the power to modify the controller, if required, without having to re-train the neural network from scratch.

Deep reinforcement learning from scratch proved to be very challenging for a high-fidelity simulation of a bipedal robot. Deep RL methods depend on randomly exploring the space to get a notion of gradient of the cost. However, for underactuated bipedal robots most regions of space have very low reward, and hence no clear gradient. Stable walking regions in the controller space can be very narrow, making it unlikely to reach a promising controller by merely random sampling. To overcome this, we used behavior cloning to initialize our actor policy using the expert feedback-based reactive controller described in Section 4.2.2. Behavior cloning learns a policy over state-action pairs from expert trajectory by finding the policy parameters  $\theta$  that solve the following maximum-likelihood optimization problem, as described in Rajeswaran et al., 2017a:

$$\text{maximize}_{\theta} \sum_{(s, a^*) \in \rho_D} \ln \pi_{\theta}(a^* | s) \quad (4.5)$$

where  $\rho_D$  indicates the expert's trajectory distribution, with  $a^*$  is actions that expert took, and  $s$  are the states visited.

Similarly, rewards accumulated during the expert's demonstrations can be used to pre-train a Q-function by minimizing TD error (Sendonaris and Dulac-Arnold, 2017). As the Q-function provides the guidance for policy update, a well pre-trained Q-function benefits actor training as well.

In practice, imitation learning does not guarantee that the cloned policy can work as well as the expert due to compounding error caused by distributional shift in states seen during training and testing, as described in Ross and Bagnell, 2010. Moreover, the expert controller might not perform sufficiently well in settings where it is difficult to design a controller. For example, while our expert controller is very stable on flat ground walking, rough ground seems to present a challenge. This means that the learned policy actually has to be updated to perform well in this situation, even in simulation. Nevertheless, the expert is a good initialization for the policy and makes the learning process much faster, by overcoming the need to randomly

sample. We discuss two different types of neural network controllers that can be trained to obtain a better and more robust policy.

#### 4.4.1 Neural Network Policy

In our first setting, we create a general neural network policy without a lot of structure. Similar to the expert controller, we design the action space of the neural network to be horizontal and vertical ground reaction forces (GRFs)  $F_z, F_x$  and the swing leg foot place location  $x_p$ . The input space is the state of the CoM:  $(x, v_{act}, z, \dot{z}, \theta, \dot{\theta})$ . This means that the structure of the neural network policy becomes:

$$\pi(x, v_{act}, z, \dot{z}, \theta, \dot{\theta})_{NN} \rightarrow (F_z, F_x, x_p) \quad (4.6)$$

The stance and swing control pipeline is similar to the expert and shown in Figure 4.5.

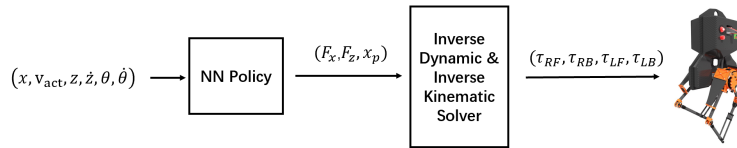


FIGURE 4.5: Pipeline of our first neural network policy for controlling ATRIAS. Here  $\tau_{RF}, \tau_{RB}, \tau_{LF}, \tau_{LB}$  are torques in the right leg's front and back and left leg's front and back motors.

While this policy still has the information about dynamics constraints of the robot through the inverse dynamics and inverse kinematics blocks, it loses the well-defined structure of the expert. This means that the output of the neural network is unpredictable, and the user does not have a lot of control over the behavior of the robot. Roboticists typically prefer controllers that can be understood and predictable, as well as can be modified if needed. In our second controller, we try to emulate this shared autonomy, which lets the user control the overall behavior of the robot, and the neural network helps improve the user-designed policy through deep RL.

#### 4.4.2 Neural Network in the Heuristic Policy

In our second setting, instead of directly predicting the vertical and horizontal ground reaction force ( $F_z, F_x, x_p$ ) as well as desired swing leg foot place location  $x_p$ , we use a neural network as part of the feedback based reactive stepping policy, described in Section 4.2.2. While the original policy has a fixed desired torso lean  $\theta_{des}$ , desired CoM height  $z_{des}$  and fixed structure for  $x_p$ , we learn these as a function of the state of the CoM using a neural network. The neural network now takes the state of the CoM as input, and predicts the desired torso pitch, CoM height and an offset on the footstep location.

$$\pi(x, v_{act}, z, \dot{z}, \theta, \dot{\theta})_{HP} \rightarrow (\theta_{NN}, z_{NN}, x_{NN}) \quad (4.7)$$

When inserted into the expert controller, this gives a structured neural network policy, where neural network outputs are used as part of a heuristic policy. It is worth noting that this policy is capable of generating the same outputs as the general

neural network policy. For example, for any desired  $F_x$  profile, it is always possible to find a  $\theta_{NN}$  given  $K_{pt}$ ,  $K_{dt}$ ,  $\theta$  and  $\dot{\theta}$ . The pipeline is illustrated in Figure 4.6.

$$F_x = K_{pt}(\theta_{NN} - \theta) + K_{dt}(-\dot{\theta}) \quad (4.8)$$

$$F_z = K_{pz}(z_{NN} - z) + K_{dz}(-\dot{z}) \quad (4.9)$$

$$x_p = k(v_{act} - v_{tgt}) + 0.5 \cdot v \cdot T + x_{NN} \quad (4.10)$$

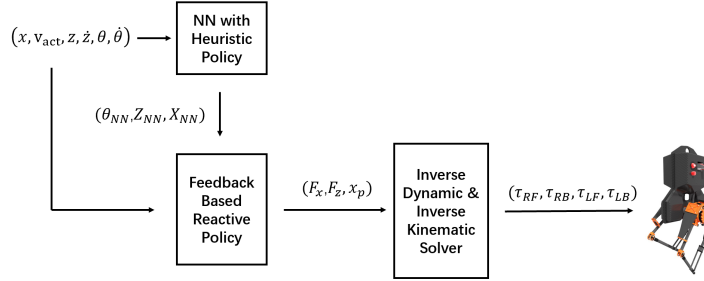


FIGURE 4.6: Pipeline of our second neural network controller using a heuristic structure and neural network outputs for controlling ATRIAS.

There are several benefits to having such structure in our policies. First and foremost, the user can predict the behavior and understand the outputs of this policy. This is important for policies implemented on robots to ensure safety of the robot and its environment. Moreover, if the user wants to test a slightly different setting than the simulation, she can easily tune other parameters of this policy, keeping the neural network fixed. Lastly, if the policy fails on hardware, it is easy for the user to understand why that might be, and even possible to fix other parts of the controller without re-training the neural network.



## Chapter 5

# Results and evaluation

We now present our experiments to evaluate the different ways of transferring information from simulation to hardware described in the previous sections. We start by describing hardware experiments with feature transforms, followed by simulation experiments that study the effect of inaccurate simulations. Finally, we present some experiments on a deep neural network policy learned in simulation and deployed on hardware.

## 5.1 Completed Experiments

We start by highlighting our completed experiments for the domain-specific feature transform and the data-driven feature transform in simulation and on the ATRIAS robot. We also include experiments on a 7-link biped in simulation. This is followed by our experiments using deep reinforcement learning.

The experiments shown in this work are:

- Hardware experiments learning parameters of a feedback-based reactively stepping controller - optimizing 5 and 9 parameters
- Simulation experiments on a neuromuscular controller for humanoid robots - optimizing 16 parameters of the controller
- Simulation experiments with a 50-dimensional virtual neuromuscular controller for the ATRIAS robot - studying the effect of deteriorating simulation on performance
- Hardware experiments with a neural network policy learned in simulation - studying the effect of structure on policy transfer

## 5.2 Experiments with the DoG Transform

### 5.2.1 Hardware experiments with the 5-dimensional controller

The first set of hardware experiments were conducted on a 5-dimensional controller, described in Section 4.2.2 on the ATRIAS robot. The target speed profile for these experiments was  $0.4m/s$  (15 steps) –  $1.0m/s$  (15 steps) –  $0.2m/s$  (15 steps) –  $0m/s$  (5 steps). The total number of steps before the controller shut off were 50. The cost function that was optimized was:

$$cost = \begin{cases} 100 - x_{fall}, & \text{if fall} \\ ||v_{avg} - v_{tgt}||, & \text{if walk} \end{cases} \quad (5.1)$$

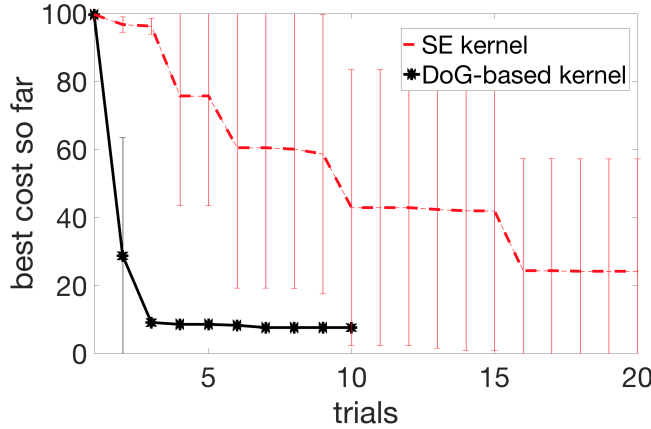


FIGURE 5.1: BO for 5 dimensional controller on ATRIAS robot hardware. BO with SE finds walking points in 4/5 runs in 20 trials. BO with DoG-based kernel finds walking points in 5/5 runs in 3 trials.

where  $x_{fall}$  is the distance in meters covered before falling,  $v_{avg}$  is the average speed per step and  $v_{tgt}$  is the target velocity profile in  $m/s$ .

Random sampling is an effective way of determining how difficult or easy a particular problem is. If random sampling can easily stumble upon successful solutions, the optimization has to be very sample-efficient and reliable to justify the added computational cost. As noted in Calandra et al., 2016b, random sampling often performs better than optimization methods like gradient descent in higher dimensions.

We sampled 100 random 5-dimensional controllers on hardware and 10 of them walked for this target speed profile. This means that random sampling has a 1/10 chance of sampling a good point. In simulation, 276 points out of 1000 randomly sampled points walked, implying a 1/4 success rate. This highlights the difference between hardware and simulation, making this a tougher problem on hardware.

On hardware, we conducted 5 runs of each – BO with DoG-based kernel and BO with SE, 10 trials for DoG-based kernel per run, and 20 for SE kernel. In total, this led to 150 experiments on the robot (excluding the 100 random samples). We also experimented with using fixed vs automatically learned hyperparameters for both kernels. A simple choice of fixed hyperparameters worked well for DoG-based kernel, while for SE kernel it was better to learn these automatically. DoG scores were calculated on 20,000 points in simulation, by running 3.5s long simulations with target speed of  $0.5m/s$ .

BO with DoG-based kernel found walking points in 3 trials in 5/5 runs. BO with SE found walking points in 10 trials in 3/5 runs, and in 4/5 runs in 20 trials. These results can be seen in Figure 5.1.

A: Add a speed profile? And hardware data?

### 5.2.2 Hardware experiments with the 9 dimensional controller

The second set of hardware experiments were conducted on a 9-dimensional controller, described in Section 4.2.2 on the ATRIAS robot. The target speed profile for these experiments was  $0.4m/s$  (30 steps). The total number of steps before the controller shut off was 30. The cost optimized was the same cost as in Equation 5.1.

Again, we sampled 100 random points on hardware and 3 of them walked for this speed profile. This means that random sampling has a 1/33 chance of sampling

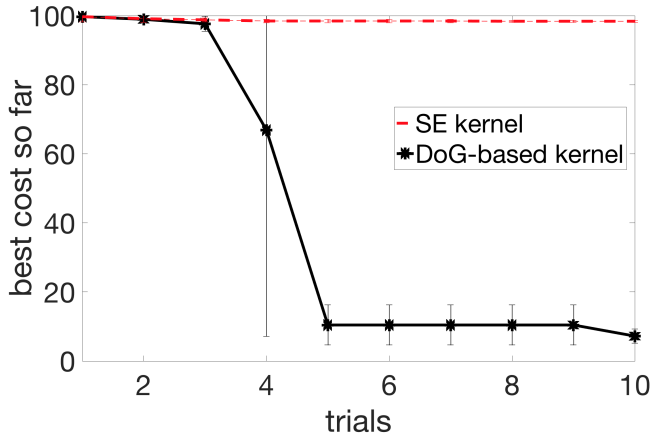


FIGURE 5.2: BO for 9 dimensional controller on ATRIAS robot hardware. BO with SE doesn't sample any walking points in 3 runs. BO with DoG-based kernel finds walking points in 5 trials in 3/3 runs.



FIGURE 5.3: A time lapse of ATRIAS walking around the boom during a run of DoG-based kernel.

a good point. On the variable speed profile from Section 5.2.1, the number of successful points out of 100 were 0, implying a less than 1% success rate. To keep the problem at hand reasonable, we used the simpler target speed profile. In comparison, the success rate in simulation is 8% for the tougher profile, implying a greater mismatch between hardware and simulation than the 5-dimensional controller.

For this setting, we conducted 3 runs of each BO with DoG-based kernel and BO with SE, 10 trials for DoG-based kernel per run, and 10 for SE. In total, this led to 60 experiments on the hardware (excluding the random sampling).

BO with DoG-based kernel found walking points in 5 trials in 3/3 runs. BO with SE did not find any walking points in 10 trials in all 3 runs. These results can be seen in Figure 5.2.

Based on these results, we concluded that BO with DoG-based kernel was indeed able to extract useful information from simulation and speed up learning on hardware. However, it took slightly longer to find points for the 9-dimensional controller and the quality of solution might have improved further if we continued the optimization. This is all as per expectation, as a higher dimensional controller should take longer to optimize, but eventually lead to a better or as good a solution as a smaller dimensional controller.

### 5.2.3 Simulation experiments with the 9-dimensional controller

To facilitate further experiments we used the ATRIAS simulator from Martin, Wu, and Geyer, 2015 with modeling disturbances and a variable target speed profile of  $0.4m/s$  (15 steps) –  $0.6m/s$  (15 steps) –  $1.0m/s$  (15 steps) –  $0.6m/s$  (15 steps) –  $0.2m/s$  (5 steps).

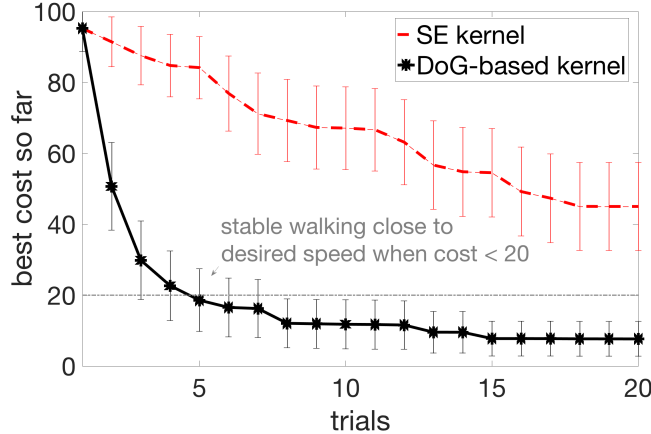


FIGURE 5.4: Further experiments using ATRIAS simulator: BO for “speed-up-down” target speed profile on robot model with mass and inertia differences (mean over 50 runs; 95% confidence intervals).

For these experiments, we use the 9-dimensional controller described in 4.2.2 as this proved to be a more challenging setting for the ATRIAS hardware. Masses of the robot torso, legs, the boom, as well as inertia of the torso were perturbed randomly by up to 15% of their original values during optimization. This ensured a mismatch between the setting used to generate the kernel and the experimental setting for evaluating its performance, aimed at capturing the discrepancy between hardware and simulation. Note that the kernel was generated on the unperturbed setting, with parameters as described in Section 4.1.1 for a target speed of 0.5m/s. The grid size for DoG scores was 100,000 points, and simulations were run for 5s.

The cost used for these experiments was

$$cost = \begin{cases} 100 - x_{fall}, \text{if fall} \\ ||v_{avg} - v_{tgt}|| + c_{tr}, \text{if walk} \end{cases} \quad (5.2)$$

where  $x_{fall}$  is the distance covered before falling in meters,  $v_{avg}$  is the average speed per step,  $v_{tgt}$  is the target velocity for that step in m/s, and  $c_{tr}$  captures the cost of transport - calculated by taking a sum of motor torques and normalizing them by a constant. Simulations for evaluating the cost were run for 30s. Note the addition of the cost of transport in this cost, as compared to 5.1.  $c_{tr}$  needs more than 10 trials to be optimized significantly, and the current low-level motor controllers in Section 4.2.2 are not designed to reduce  $c_{tr}$ . Hence, it's not considered in the hardware experiments.

Figure 5.4 illustrates BO on a simulated model with mass and inertia disturbances. The target was to start walking at 0.4m/s, then speed up to 0.6m/s, then 1.0m/s, slow down to 0.6m/s, then walk at 0.2m/s. DoG-based kernel was collected using an unperturbed model with a target speed of 0.5m/s, and yet it performed very well on this more challenging setting, with the top speed two times of the speed on which the kernel was collected. After 20 trials, 96% of BO runs using the DoG-based kernel found a stable walking solution, compared to 56% of the runs using an SE kernel. The average cost of the walking solutions was also improved: lower by  $\approx 30\%$  when using DoG vs SE kernel.

These experiments suggest that DoG-based kernel is able to offer improvement for the settings different from the one used to generate it. This improvement is robust to both the deviations of the robot model/hardware parameters as well as desired

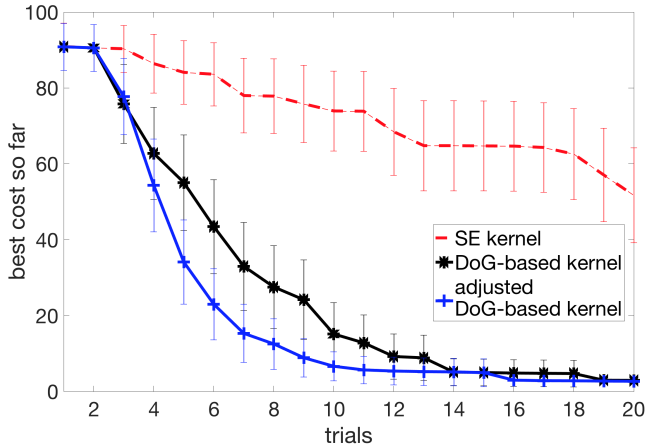


FIGURE 5.5: BO with 50-dimensional Virtual Neuromuscular Controller on the ATRIAS simulation.

walking speed profiles.

#### 5.2.4 Simulation experiments with the 50-dimensional controller

Next set of experiments were using the VNMC 50-dimensional controller, as described in Section 4.2.3 on the ATRIAS simulation.

VNMC does not start from rest, and needs an initial velocity. In previous work this has been emulated by either giving simulations initial speeds, or by giving a push. These are either un-realizable or unreliable on hardware. To overcome this problem, we start the VNMC with a 5-dimensional walking controller (described in Section 4.2.2, parameters hand-tuned and fixed). Once the robot has taken 10 steps with this controller, the control is switched to VNMC.

To construct DoG-based kernel for this controller we collected 250,000 points from 7-second simulations. The DoG scores were computed after switching to the VNMC (so after first 10 steps). Searching in 50 dimensional space could be completely intractable if the search region is too large. Usually enough domain knowledge is available to confine the search to a reasonably manageable region. We tried to hand-tune an initial point that walked 3-4 steps before falling in simulation (this point still had a very high cost of  $\approx 93$ ). This point became the “center” of our search space, and we searched in a hyper-cube of size  $[0.75, 1.25]$  in each dimension around this point. So, with initial point  $x_0$ , the search space was  $[0.75 \cdot x_0, 1.25 \cdot x_0]$ . With these boundaries, 4% of points sampled randomly in simulation were walking.

Figure 5.5 shows results of Bayesian Optimization with SE, DoG-based kernel and adjusted DoG-based kernel with mismatch information. During optimization simulations were run for 30 seconds. We used the same cost function as described in the previous section (equation 5.2).

In 50-dimensional control, the mismatch between long and short simulations becomes apparent. This raises concerns for how useful DoG-based kernel would be on hardware, since it tries to infer the quality of the controller parameters from short simulations. For the 5-dimensional and 9-dimensional controllers, the performance during short simulations usually predicted whether 30s simulations would be successful. That is, points that walk for 5s would usually walk for 30s. However, this is not true for the 50-dimensional controller. Since this controller is capable of much richer behaviors, if a point is not in a limit cycle before the end of a short simulation, it can lead to a range of behaviours later. As a result, we noticed an improvement

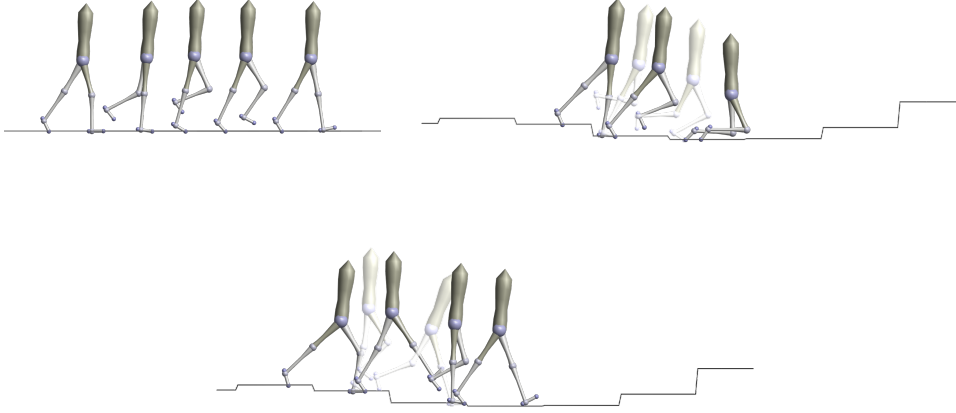


FIGURE 5.6: Top row: a policy that generates successful walking on flat ground could fail on rough ground. Bottom row: optimization on rough ground finds policies that walk, even though pre-computation for DoG kernel is done using unperturbed model on flat ground.

when using adjusted DoG-based kernel described in Section 3.2. While DoG is still very competitive and finds walking points in 100% of the runs by 20 trials, the adjusted DoG with mismatch has an advantage. It reaches the same performance as DoG-based kernel, but faster.

To anticipate potential mismatch between simulation and hardware, we tested it on slightly perturbed initial conditions for the VNMC. The different conditions were aimed to replicate issues likely to be seen on hardware. The starting states for VNMC would differ slightly each time, since they would depend on the state of the robot after the 5-dimensional initiating controller has finished. Both DoG and adjusted DoG were robust to slight changes in initial condition.

It would be interesting to study the effect of a mismatch map on performance on hardware. While essentially a mismatch map adds more parameters to learn, which would result in a slower optimization, if initialized properly with domain knowledge, it might help. The DoG-based kernel samples a few unstable points in the start of the 50-dimensional optimization, as these have high DoG scores on short simulations, but still might fall in longer simulations under disturbances. Since a lot of the 50-dimensional space is clustered around each DoG score, its an over-condensation of the space. A lot of potentially good points get rejected because one of the points falls. If we detect a mismatch at the high DoG point that fell, and effectively increase its distance to other high DoG points, we will help speed up the optimization.

### 5.2.5 Simulation experiments on a 16-dimensional controller

To make sure that our feature transform generalizes to multiple robot morphologies, we also did experiments on the 7-link biped, described in Section ??.

We conduct our experiments on models with mass and inertial disturbances and on different ground profiles. After collecting the DoG scores, we perturb the mass of each link, inertia and center of mass location randomly by up to 15% of the original value. For mass/inertia we randomly pick a variable from a uniform distribution

between  $[-0.15, 0.15] \cdot M$ , where  $M$  is the original mass/inertia of the segment. Similarly we change the location of the center of mass by  $[-0.15, 0.15] \cdot L/2$ , where  $L$  is the length of the link. These disturbances are different for each run of our algorithm, hence we test a wide range of possible modelling disturbances. For the ground profiles, we generate random ground height disturbances of upto  $\pm 8\text{cm}$  per step.

To ensure that our approach can perform well across various cost functions, we conduct experiments on two different costs, constructed such that parameter sets achieving low cost also achieve stable and robust walking gaits. The first cost function varies smoothly over the parameter space:

$$\text{cost} = \frac{1}{1+t} + \frac{0.3}{1+d} + 0.01(v - v_{tgt}), \quad (5.3)$$

where  $t$  is seconds walked,  $d$  is the final CoM position,  $v$  is mean velocity and  $v_{tgt}$  is the desired walking velocity (from human data). This cost encourages walking further and for longer through the first two terms, and penalizes deviating from the target velocity with the last.

The second cost function is a slightly modified version of the cost used in Song and Geyer, 2015 for experiments with CMA-ES, also similar to the cost described in previous sections. It penalizes policies that lead to falls in a non-smooth manner:

$$\text{cost}_{\text{CMA}} = \begin{cases} 300 - x_{fall}, & \text{if fall} \\ 100||v_{avg} - v_{tgt}|| + c_{tr}, & \text{if walk} \end{cases} \quad (5.4)$$

Here  $x_{fall}$  is the distance travelled before falling,  $v_{avg}$  is the average speed in simulation,  $v_{tgt}$  is the target speed and  $c_{tr}$  is the cost of transport calculated using muscle activations. The first term directly penalizes policies that result in a fall, inversely to the distance walked. If the model walks for the whole simulation time, the cost is lower, ensured by the constants, and encourages policies that result in lower cost of transport and walk at target velocity. Since we have the same set of gains for left and right legs, the steadiness cost of the original cost Song and Geyer, 2015 was unimportant. So, we removed that term and focused on the first and second conditions in the optimization.

In the following sections we compare the performance of several baseline and state-of-the-art optimization algorithms in simulation. Motivated by the discussion in Calandra et al., 2016b, we include the baseline of uniform random search. While this search is uninformed and not sample-efficient, it could (perhaps surprisingly) serve as a competitive baseline in non-convex high-dimensional optimization problems.

We also provide comparisons with CMA-ES Hansen, 2006 and Bayesian Optimization with a Squared Exponential kernel (basic BO). Since we were optimizing a non-convex function in a 16D space, it was not feasible to calculate the global minimum exactly. To estimate the global minimum for the costs we used, we ran CMA-ES (until convergence) and BO with our domain kernel (for 100 trials) for 50 runs without model disturbances on flat ground. When reporting results, we plot the best results found in this easier setting as the estimated optimum for comparison.

All the experiments described below are done for 50 independent runs, each with a unique set of modeling disturbances and a different ground profile for rough ground walking. Each run consists of 100 trials or cost function evaluations, in which the optimization algorithm evaluates a parameter set for 100 seconds of simulation.

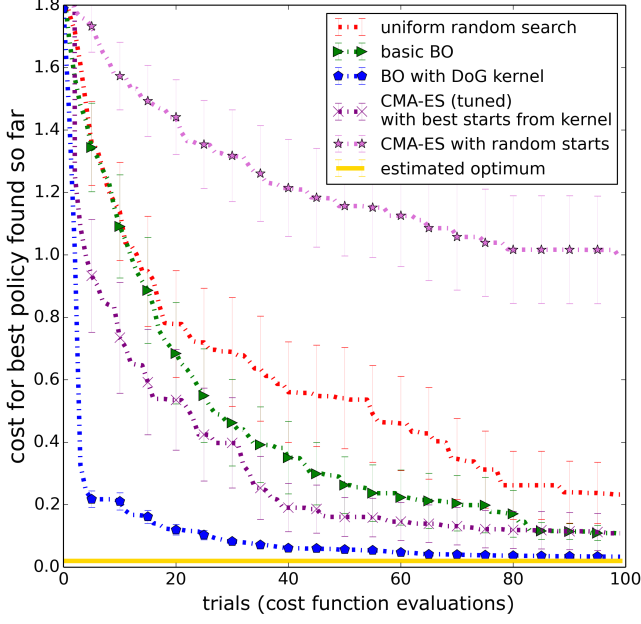


FIGURE 5.7: Experiments using DoG kernel on rough ground with model disturbances on the smooth cost over 50 runs. Basic BO line (green triangles) was obtained using BO with a Euclidean distance kernel. Estimated optimum (yellow line) was obtained on the unperturbed setting. BO with DoG-based kernel kernel (blue pentagons) used the DoG feature transform and was substantially more sample-efficient than the alternative approaches.

Note that the disturbances and ground profiles remain constant across each run (100 trials).

### Experiments on the smooth cost function

Figure 5.7 shows results of our experiments using the DoG-based kernel kernel on the smooth cost. Policies with costs of less than  $\approx 0.15$  corresponded to robot model walking on rough ground with  $\pm 8\text{cm}$  disturbance. For BO with DoG-based kernel kernel, 25-30 cost function evaluations were sufficient to find points that corresponded to robot model walking on a randomly generated rough ground. This is in contrast to basic BO that did not find such results in under 100 trials.

To let CMA-ES also benefit from the kernel, we started each run from one of the best 100 points for the DoG-based kernel kernel. After tuning the  $\sigma$  parameter of CMA-ES to make it exploit more around the starting point, we were able to find policies that resulted in walking on rough ground after 65-70 cost function evaluations on most runs. On the other hand, CMA-ES starting from a random initial point was not able to find walking policies in 100 evaluations.

These results suggest that DoG scores successfully captured useful information about the parameter space and were able to effectively focus BO and CMA-ES on the promising regions of the policy search space.

### Experiments with the non-smooth cost

We observed good performance on the non-smooth cost function (Figure 5.8), though it was not as remarkable as the smooth cost. BO with kernel still outperformed all other methods by a margin, but this different cost seems to hurt BO and CMA-ES

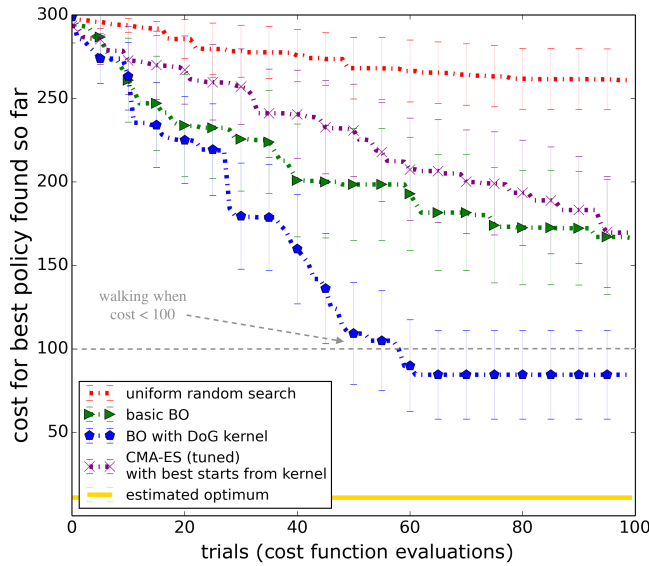


FIGURE 5.8: Experiments using DoG-based kernel kernel on rough ground with model disturbances on the non-smooth cost over 50 runs. Policies with costs below 100 generate walking behaviour for 100 seconds in simulation. None of the optimization methods find optimal policies in all the runs and hence the mean cost is higher than the estimated optimum.

alike. Since this cost is discontinuous, there is a huge discrepancy between costs for parameters that walk and those that don't. If no walking policies are sampled, BO learns little about the domain and samples randomly, which makes it difficult to find good parameters. Hence not all runs find a walking solution. BO was able to find successful walking in 74% of cases on rough ground with  $\pm 6\text{cm}$  disturbance in less than 60 trials/evaluations. CMA-ES starting from a good kernel point was able to do it in 40% of runs.

This showed that our kernel was indeed independent of the cost function to an extent, and worked well on two very different costs. We believe that the slightly worse performance on the second cost is because of the cost structure, rather than a kernel limitation, as it still finds walking solutions for a significant portion of runs.

### Experiments on different terrains

We also optimized on ramps – sloping upwards, as well as downwards, with the kernel generated on flat ground. The ramp up and down ground slopes were gradually increased every 20m, until the maximum slope was reached. The maximum slopes for going down and going up were 20% ( $\tan(\theta) = 0.2, \theta = 11.31 \text{ deg}$ ). BO with DoG kernel was able to find parameters that walked for 100 seconds in 50% of cases in ramp up and 90% in ramp down. Example optimized policies walking up and down slope are shown in Figure 5.9.

We believe the reason we could not find walking policies on ramps in all runs, was that we are not optimizing the hip lean, which was noted to be crucial for this profile in Song and Geyer, 2015. Since we did not consider this variable when generating our 16 dimensional kernel, it was not trivial to optimize over it without re-generating the grid. Similarly, we found that we could not find any policies that climbed up stairs. Perhaps this could be achieved when optimizing over a much larger set of parameters, as in Song and Geyer, 2015.

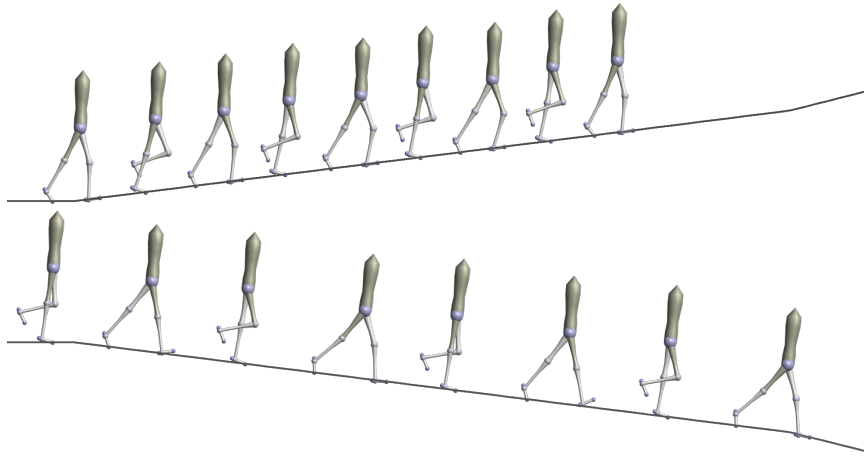


FIGURE 5.9: Optimized policies walking up and down a 12.5% ramp.

To test if the hip lean indeed helps climb up a ramp, we hand-tuned the hip lean to be  $15^{\text{deg}}$ , instead of the original angle of  $6^{\text{deg}}$  for which the kernel was generated. Indeed, our rate of success on walking on ramp up ground profile increased from 50% to 65%. This shows that the hip lean indeed helped walking on these terrains, and ideally we would like to optimize it along with the other parameters. Also, it shows that the DoG-based kernel is robust to changes in parameters that were used to generate it. This is an important property, as parameters in the neuromuscular model are changed slightly for different experiments, for example the ground stiffness, initial conditions of the model, etc. If the kernel results hold across a variety of such conditions, we don't need to regenerate it.

### 5.2.6 Summary of experiments with the DoG transform

A: Add a table summarizing results from previous section

## 5.3 Experiments with the NN transform

In this section we describe our experiments with cost-based and trajectory-based neural network kernels, described in Section ???. We first consider the setting of optimizing a 5-dimensional controller for the ATRIAS robot from Section 4.2.2. We show that the cost-based kernel is able to improve sample efficiency over standard Bayesian Optimization. We present hardware experiments to demonstrate that our kernel allows obtaining a set of parameters close to optimal on the second trial for a constant target speed. With a variable target speed, it can find walking controllers reliably in 5 trials.

Next, we discuss simulation experiments with a 16 dimensional controller that utilizes a Neuromuscular model from Section ?? on a 7-link biped. These experiments show that our trajectory-based kernel is able to significantly outperform standard Bayesian optimization for a higher-dimensional controller even when a sharply discontinuous cost is used during optimization.

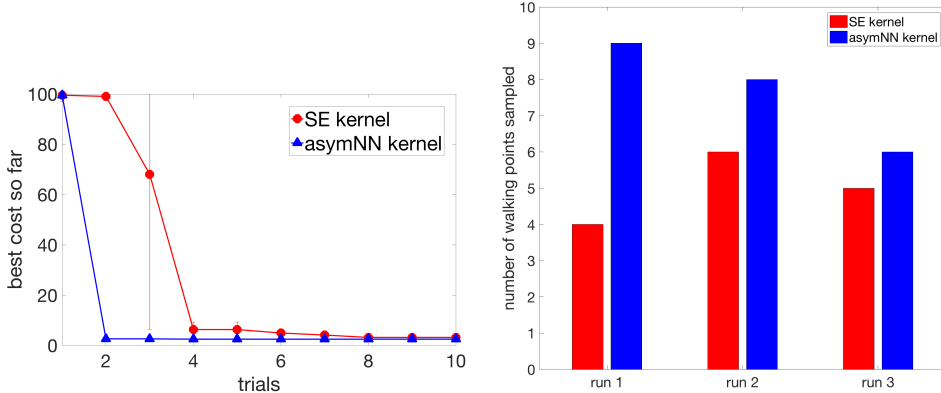


FIGURE 5.10: (left) Best cost so far during BO (mean over 3 runs) for a target speed of  $0.4\text{m/s}$ . (right) Number of walking points sampled in each of the 3 runs.

### 5.3.1 Hardware experiments with a 5-dimensional controller

For our experiments on the ATRIAS robot we used a high-fidelity ATRIAS simulator from Martin, Wu, and Geyer, 2015 to generate the data for learning the network. We constructed a distance metric for a kernel used in Bayesian Optimization by training a neural network to reconstruct cost obtained from short simulations. We created a sobol grid on the input parameter space with 20000 points and ran short 3.5 second simulations on each of the corresponding 20000 parameter sets to compute the costs. We then used a fully connected network with 4 hidden layers (128, 64, 16, 4 units) with L1 loss to reconstruct the transformation of the cost described in section 3.1.2.

We sampled 100 random controllers with a target speed of  $0.4\text{m/s}$  on hardware, and 16 controllers walked. A lower target speed meant that  $\frac{1}{6}$  of the controller space was stable walking controllers. We completed 6 sets of runs of BO: 3 using *asymNN* kernel and 3 using a standard *SE* kernel with 10 trials each, leading to a total of 60 hardware experiments. Figure 5.10 shows the performance of BO with *SE* versus *asymNN* kernel. *SE* obtains a stable walking solution on the 3rd trial in one run, and on the 4th trial in the two other runs. *asymNN* kernel is able to find the best-performing set of parameters on the second trial in each of the 3 runs. This confirms that using *asymNN* kernel offers an improvement over using *SE* kernel in this setting. We suggest that *asymNN* reliably selects an excellent point on the 2nd trial because such points lie far from poorly performing subspace of parameters (under the distance metric constructed with *asymNN*).

While both *SE* kernel and *asymNN* kernels perform very well in this setting, the *asymNN* kernel is more biased towards sampling stable points than the *SE* kernel, as shown in Figure 5.10. In the three runs, *asymNN* kernel samples 23 stable controllers out of 30, while *SE* kernel samples 15 stable controllers. This implies that the search for optimal controllers is biased towards safety in the case of *asymNN* kernel. This is desirable as stable points are less likely to break the robot.

On a more challenging, variable target speed profile of  $0.4\text{m/s}$  (15 steps) –  $1.0\text{m/s}$

$$(15 \text{ steps}) - 0.2\text{m/s} (15 \text{ steps}) - 0\text{m/s} (5 \text{ steps})$$

, the performance of the *asymNN* kernel is slightly worse than the DoG-based kernel, though still better than *SE* kernel. Figure ?? shows BO with *asymNN* kernel, *SE* kernel and DoG-based kernel for the variable speed profile. DoG-based kernel can

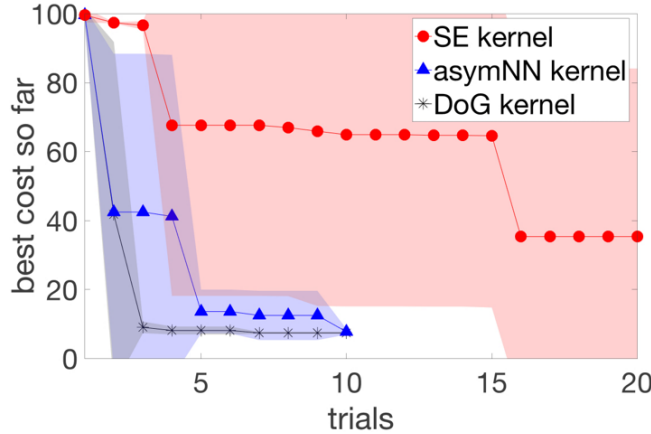


FIGURE 5.11: Bayesian optimization for a 5-dimensional controller with a variable target speed profile.

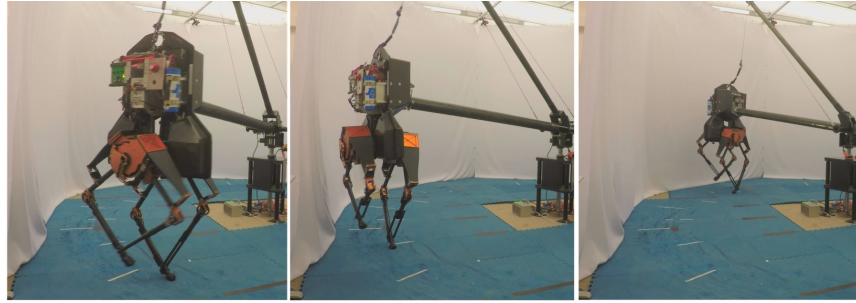


FIGURE 5.12: ATRIAS during BO with *asymNN* kernel.

find walking controllers in 2 trials in all 3 runs, while it takes *asymNN* kernel 5 trials. On the other hand, SE kernel fails to reliably find controllers even after 20 trials.

While in our hardware setup most methods are likely to sample walking points within 10 trials, we believe our experimentation is an important step towards optimizing locomotion policies for complex humanoid robots. Bayesian Optimization studies in the past have also used real robot hardware, for example, Calandra et al., 2016a, Cully et al., 2015 and Tesch, Schneider, and Choset, 2011. However, Tesch, Schneider, and Choset, 2011; Lizotte et al., 2007; Cully et al., 2015 used robots which are statically stable for significant parts of their gait, making discontinuities in the cost function landscape less likely and in turn making the optimization easier. On the other hand, ATRIAS is a complex bipedal system which is likely to fall with unstable controllers due to point feet. Calandra et al., 2016a use a walking robot similar to ours. However, their controller parametrization is very different, and not widely used, unlike our inverse dynamics and force-based controller which is more modern and state-of-the-art Kuindersma et al., 2016, Herzog et al., 2016, Feng et al., 2015.

Hence, even if our policy parametrization was chosen so that steady walking points could be found in a few trials, our testbed is fairly complex and our problem formulation is widely applicable.

### 5.3.2 Hardware experiments with a 9-dimensional controller

In the next set of experiments, we evaluated performance of the NN-based kernel described in Section ???. We optimize the 9-dimensional controller from Section ??.

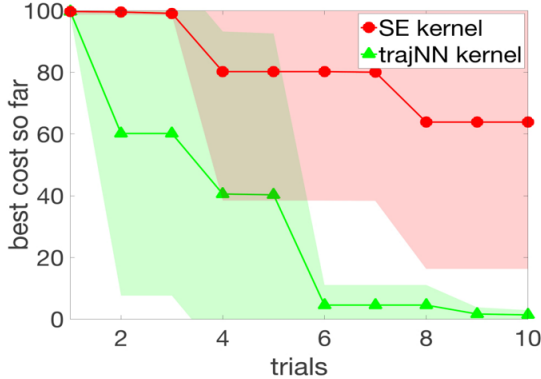


FIGURE 5.13: Bayesian optimization of a 9-dimensional kernel with the NN-based kernel.

The target of hardware experiments was to walk for 30 steps at  $0.4m/s$ , similar to Section ???. We observed that the SE performance was slightly better as compared to the old experiments, even though starting from the same random samples, hyper-parameter setting and speed profile. We attribute this change to a better estimation and control of the CoM vertical height, owing to a new IMU on the robot.

Figure 5.13 shows comparison of BO with NN-based kernel and SE kernels. We conducted 5 runs of both algorithms with 10 trials in each run, leading to a total of 100 robot trials. BO with the NN-based kernel found walking points in all 5 runs within 6 trials, while BO with SE kernel only found walking points in 2 of 5 runs in 10 trials. Hence, even without explicit hand-designed domain knowledge, like the DoG-based kernel kernel, the NN-based kernel is able to extract useful information from simulation and successfully guide hardware experiments.

### 5.3.3 Simulation experiments with the 16-dimensional controller

In section 3.1.2 we introduced a cost-agnostic approach for constructing an informed kernel from simulations. Our approach is to train a neural network to reconstruct trajectory information. In this Section, we describe our experiments with 16-dimensional controller of the Neuromuscular model on a 7-link biped. We created a grid of 100K points in the input parameter space and ran short 5 second simulations on each of the corresponding 100K parameter sets to collect the trajectory summaries. We then used a fully connected network with 4 hidden layers (512, 128, 32 units) with L1 loss to reconstruct the summaries of the trajectories (as described in section 3.1.2). This transformation induced by the neural network was used as a re-parameterization from the input space of 16-dimensional controller parameters to 8-dimensional space of trajectory summaries. These 8-dimensional outputs of the neural network define kernel distances in the informed kernel (*trajNN*). All experiments were conducted on perturbed models, as described in Section 5.2.5.

Figures 5.14, 5.15 illustrate our experiments comparing using *trajNN* versus using Squared Exponential (SE) kernel for BO. To analyze the performance of *trajNN* on different cost functions we conducted experiments on two different costs suggested in prior literature. The first cost promotes walking further and longer before falling, while penalizing deviations from the target speed (Antonova, Rai, and Atkeson, 2016):

$$\text{cost}_{\text{smooth}} = 1/(1+t) + 0.3/(1+d) + 0.01(v - v_{tgt}), \quad (5.5)$$

FIGURE 5.14: Optimizing smooth cost from Equation 5.5 over 50 runs.

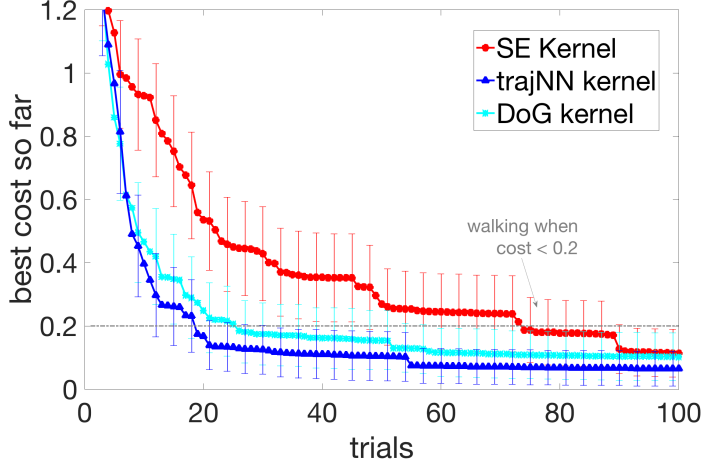
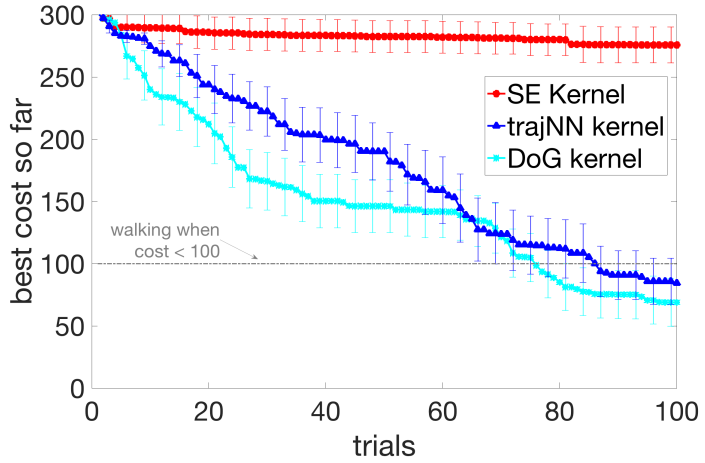


FIGURE 5.15: Optimizing non-smooth cost from Equation 5.6 over 50 runs.



where  $t$  is seconds walked,  $d$  is the final hip position,  $v$  is mean velocity and  $v_{tgt}$  is the desired walking velocity ( $1.3m/s$  in our case). The second cost function is a simplified version of the cost used in Song and Geyer, 2015, penalizes falls explicitly, and encourages walking at desired speed and with lower cost of transport:

$$cost_{non-smooth} = \begin{cases} 300 - x_{fall}, & \text{if fall} \\ 100||v_{avg} - v_{tgt}|| + c_{tr}, & \text{if walk} \end{cases} \quad (5.6)$$

where  $x_{fall}$  is the distance covered before falling,  $v_{avg}$  is the average speed of walking,  $v_{tgt}$  is the target velocity, and  $c_{tr}$  captures the cost of transport.

Figure 5.14 shows that *trajNN* offers a significant improvement in sample efficiency when using  $cost_{smooth}$  during optimization. Points with cost less than 0.15 correspond to robust walking behavior. With *trajNN*, more than 90% of runs obtain walking solutions after only 25 trials. In contrast, using *SE* requires more than 90 trials for such success rate. The performance of *trajNN* matches that of a DoG-based kernel kernel. This is notable, since *trajNN* is learned automatically, whereas DoG-based kernel kernel is constructed using domain expertise.

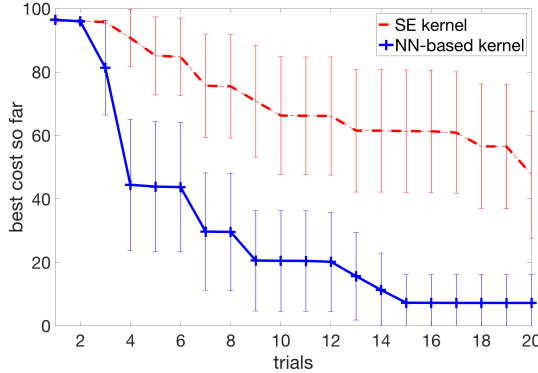


FIGURE 5.16: 50-dimensional controller with a *trajNN* kernel in simulation.

Figure 5.15 shows that *trajNN* also provides a significant improvement when using the second cost. Points with cost less than 100 correspond to walking. With *trajNN*, 70% of the runs find walking solutions after 100 trials. In contrast, optimizing non-smooth cost is very challenging for BO with *SE* kernel: a walking solution is found only in 1 out of 50 runs after 100 trials.

The difference in performance on the two costs is due to the nature of the two costs. If a point walks some distance  $d$ , Equation 5.5 penalizes points according to  $1/d$  and Equation 5.6 penalizes them according to  $-d$ . This results in a much steeper fall in cost with the first cost, and BO starts to exploit around points that walk some distance, quickly finding points that walk forever. However, with the second cost, BO continues to explore, and sometimes does not find walking points even in 100 trials. Exploitative methods might be better suited for higher dimensional problems, as compared to exploratory methods, in our experience.

*trajNN* kernel might be preferable to a cost-based kernel not only for settings with multiple costs. For some higher dimensional problems reduction to a 1-dimensional space in the kernel could be undesirable. So, while 1-dimensional cost-based kernel could yield highly sample-efficient optimization for lower dimensional problems, a higher-dimensional kernel like *trajNN* could provide more flexibility without compromising sample-efficiency for higher dimensional problems.

### 5.3.4 Simulation experiments with 50-dimensional controller

Our last set of simulation experiments were on the 50-dimensional controller, with the same experimental setting as Section ???. The neural network kernel was trained to reconstruct the summaries of simulation trajectories over 200,000 simulation controllers. As can be seen in Figure 5.16, BO with NN-based kernel was able to find walking controllers in 20 trials in 95% of the runs. This performance is similar to DoG-based kernel which can find walking controllers in 20 trials for 100% of the runs.

These results show that while the NN-based kernel uses lesser domain specific information than DoG-based kernel, its performance in simulation and hardware is very comparable to DoG-based kernel. As an additional advantage, the weights of the NN-based kernel can be learned from data experienced on hardware, by continuing to do gradient descent. This leads to a simple and straight-forward way of updating the kernel from hardware experiments.

A summary of results and experimental settings described in the previous section is below:

Kernel type	Controller dimension	Number of sim points	Sim duration	Kernel dim	Features in kernel
$k_{DoG}$	5	20K	3.5s	1	$score_{DoG}$
	9	100K	5s	1	$score_{DoG}$
	50	200K	5s	1	$score_{DoG}$
$k_{trajNN}$	9	100K	5s	4	$t_{walk}, x_{end}, \theta_{avg}, v_{x,avg}$
	16	100K	5s	8	$t_{walk}, x_{end}, \theta_{end}, v_{x,end}$
	50	200K	5s	13	$c_\tau, y_{end}, v_{y,end}, \dot{\theta}_{end}$ $t_{walk}, x_{end}, c_\tau, traj_x, traj_\theta$

TABLE 5.1: Simulation Data Collection Details.  $score_{DoG}$  was described in Section ???. For  $k_{trajNN}$ :  $t_{walk}$  is time walked in simulation before falling,  $x_{end}$  and  $y_{end}$  are the  $x$  and  $y$  positions of Center of Mass (CoM) at the end of the short simulation,  $\theta$  is the torso angle,  $\dot{\theta}$  is the torso velocity,  $v$  is the CoM speed ( $v_x$  is the horizontal and  $v_y$  is the vertical component),  $c_\tau$  is the squared sum of torques applied;  $traj_x, traj_\theta$  denote vectors with mean CoM and  $\theta$  measurements every second.

A: Add an overview table from experiments in this section.

## 5.4 Effect of inaccurate simulations on the performance

In this section, we describe our experiments with increasing simulation-hardware mismatch and its effect on approaches that use information from simulation during hardware optimization. The quality of information transfer between simulation and hardware depends not only on the mismatch between the two, but also on the controller used. For a robust controller, small dynamics errors would not cause a significant deterioration in performance, while for a sensitive controller this might be much more detrimental. There is still an advantage to studying such a sensitive controller, as it might be much more energy efficient and versatile. In our experiments, the 50-dimensional VNMC described in Section ?? is capable of generating very efficient gaits but is sensitive to modelling errors. Figure 5.5 shows the performance of the DoG-based and adjusted DoG-based kernel on the original high-fidelity simulator. While both methods find walking points in 20 trials, adjusted-DoG performs better. There is mismatch even between short 5s and long 30s simulations for this controller. This mismatch is compensated by the adjusted-DoG kernel.

In the rest of this section, we provide experimental analysis of settings with increasing simulated mismatch and their effect on optimization of the 50-dimensional VNMC. We compare several approaches that improve sample-efficiency of BO and investigate if the improvement they offer is robust to mismatch between the simulated setting used for constructing kernel/prior and the setting on which BO is run.

### 5.4.1 Incorrect dynamics models

First, we examine the performance of our proposed approaches with informed kernels:  $k_{DoG}$ ,  $k_{trajNN}$  and  $k_{DoG_{adj}}$ . Figure 5.17a shows the case when informed kernels are generated using inaccurate dynamics models, as described in Section ???. The first

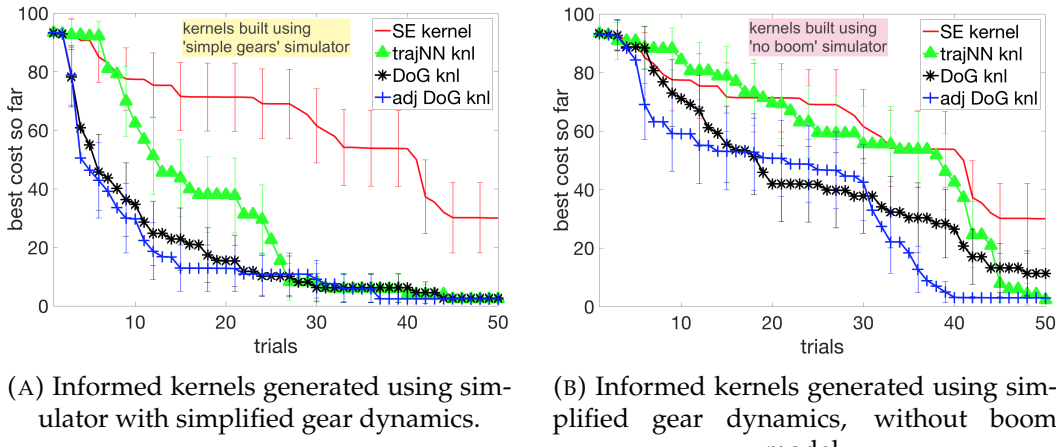


FIGURE 5.17: BO is run on the original simulator. Informed kernels perform well despite significant mismatch, when kernels are generated using simulator with simplified gear dynamics (left). In the case of severe mismatch, when the boom model is also removed, informed kernels still improve over baseline SE (right). Plots show best cost for mean over 50 runs for each algorithm, 95% CIs.

approximate simulator has simplified gear dynamics while BO is run on the original simulator. The second approximation removes the boom of the robot and simulates a purely 2-dimensional robot.

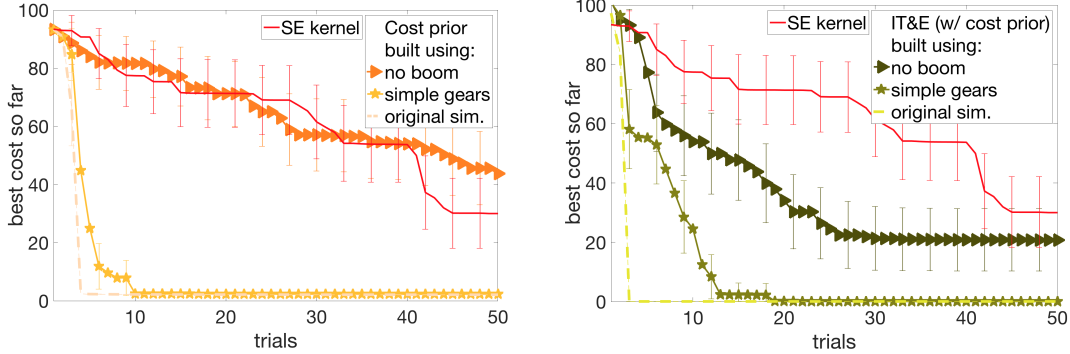
When kernel is generated in simulator with approximate gear dynamics, all runs with informed kernels find walking solutions in 50 trials, while for SE only 70% of the runs have walking solutions.

Next, Figure 5.17b shows performance of  $k_{DoG}$ ,  $k_{\text{trajNN}}$  and  $k_{DoG_{adj}}$  when the kernels are constructed using a simulator with simplified dynamics and without a the boom. In this case the mismatch with the original simulator is larger than before and we see the advantage of using adjustment for DoG-based kernel:  $k_{DoG_{adj}}$  finds walking points in all runs after 35 trials.  $k_{\text{trajNN}}$  also achieves this, but after 50 trials.  $k_{DoG}$  finds walking points in  $\approx 90\%$  of the runs after 50 trials. The performance of SE stays the same, as it uses no prior information from any simulator.

This illustrates that while the original DoG-based kernel can recover from slight simulation-hardware mismatch, the adjusted DoG-kernel is required if one expects higher mismatch.  $k_{\text{trajNN}}$  seems to recover from the mismatch, but might benefit from an adjusted version. We leave this to future work.

### Comparisons of Prior-based and Kernel-based Approaches

We will classify approaches that use simulation information in hardware optimization as prior-based or kernel-based. Prior-based approaches use costs from the simulation in the prior of the GP used in the BO. This can help BO a lot if the costs between simulation and hardware transfer, and the cost function is fixed. However, in the presence of large mismatch, points that perform well in simulation might fail on hardware. A prior-based method can be biased towards sampling promising points from simulation, resulting in an even poorer performance than methods with no prior. Kernel-based approaches consist of methods that incorporate the information from simulation into the kernel of the GP. These can be sample-inefficient as compared to prior-based method, but less likely to be biased towards unpromising regions in the presence of mismatch. They also easily generalize to multiple costs, so



(A) BO with cost prior: straightforward approach useful for low-to-medium mismatch; but no improvement if mismatch is severe.

(B) Performance of IT&E algorithm (our implementation of Cully et al. (2015), adapted to bipedal locomotion).

FIGURE 5.18: BO using prior-based approaches. Mean over 50 runs for each algorithm, 95% CIs.

that there is no additional computation if the cost is changed. This is important because a lot of these approaches can take several days of computation to generate the informed kernel. For example, Cully et al., 2015 report taking 2 weeks on a 16-core computer to generate their map.

It is possible to also combine both prior-based and kernel-based methods, as in Cully et al., 2015. We will classify these as ‘prior-based’ methods, since in our experiments prior outweighs the kernel effects for such cases. In our comparison with Cully et al., 2015, we will implement a version with and without the prior points. We do not add a cost prior to BO using DoG-based kernel, as this limits us to a particular cost, and high-fidelity simulators. Since both of these can be major obstacles in real robot experiments, we refrain from doing so.

Figure 5.18a shows the performance when using simulation cost in the prior during BO, and learning a model for the difference between simulation and hardware costs (Wilson, Fern, and Tadepalli, 2014). BO with a cost prior created using the original version of the simulator illustrates what would happen in the best case scenario, as optimization is merely a look-up here. When the simulator with simplified gear dynamics is used for constructing the prior, we observe significant improvements over uninformed BO prior. However, when the prior is constructed from simplified gear dynamics and no boom setting, the approach performs slightly worse than uninformed BO. This shows that while an informed prior can be very helpful when created from a simulator close to hardware, it can hurt performance if simulator is significantly different from hardware.

Next, we discuss experiments with our implementation of Intelligent Trial and Error (IT&E) algorithm from Cully et al. (2015). This algorithm combines adding a cost prior from simulated evaluations with adding simulation information into the kernel. IT&E defines a behavior metric and tabulates best performing points from simulation on their corresponding behavior score. The behavior metric used in our experiments is duty-factor of each leg, which can go from 0 to 1.0. We discretize the duty factor into 21 cells of 0.05 increments, leading to a  $21 \times 21$  grid. We collect the 5 highest performing controllers for each square in the behavior grid, creating a  $21 \times 21 \times 5$  grid. Next, we generate 50 random combinations of a  $21 \times 21$  grid, selecting 1 out of the 5 best controllers per grid cell. Care was taken to ensure that all 5 controllers had comparable costs in the simulator used for creating the map.

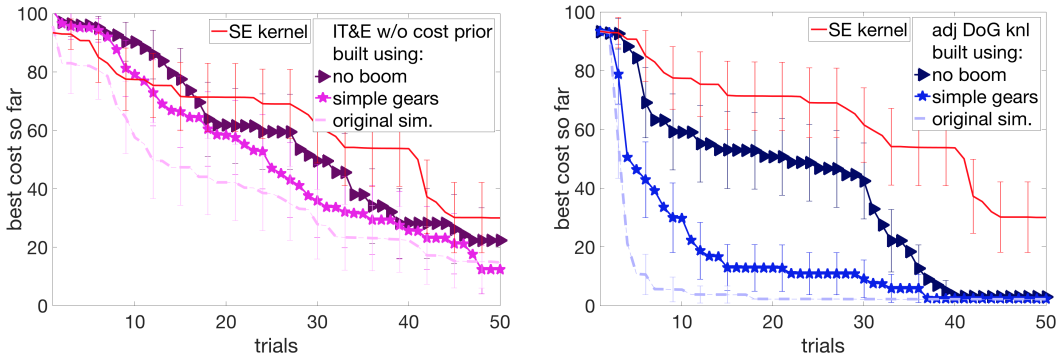


FIGURE 5.19: BO using kernel-based approaches. Mean over 50 runs for each algorithm, 95% CIs.

Cost of each selected controller is added to the prior and BO was performed in the behavior space, like in Cully et al., 2015.

Figure 5.18b shows BO with IT&E constructed using different versions of the simulator. IT&E constructed using simplified gear dynamics simulator is slightly less sample-efficient than the straightforward ‘cost prior’ approach. When constructed with the simulator with no boom, IT&E is able to improve over uninformed BO. However, it only finds walking points in 77% of the runs in 50 trials in this case, as some of the generated maps contained no controllers that could walk on the ‘hardware’. This is a shortcoming of the IT&E algorithm, as it eliminates a very large part of the search space and if the pre-selected space does not contain a walking point, no walking controllers can be sampled with BO. This problem could possibly be avoided by using a finer grid, or a different behavior metric. However tuning such hyper-parameters can turn out to be expensive, in computation and hardware experiment time.

To separate the effects of using simulation information in prior mean vs kernel, we evaluated a kernel-only version of IT&E algorithm. Figure 5.19a shows these results. It shows that the cost prior is crucial for the success of IT&E and performance deteriorates without it. Hence, it is not practical to use IT&E on a cost different than what it was generated for.

Nonetheless, Figure 5.17 showed that BO with adjusted DoG kernel is able to handle both moderate and severe mismatch with kernel-only information, collected in Figure 5.19b.

In summary, we created two simulators with increasing modelling approximations, and studied the effect of using these to aid optimization on the original simulator. We found that while methods that use cost in the prior of BO can be very sample-efficient in low mismatch, their performance worsens as mismatch increases. IT&E introduced in Cully et al., 2015 uses simulation information in both prior mean and kernel, and is very sample-efficient in cases of low mismatch. Even with high mismatch, it performs better than just prior-based BO but doesn’t find walking controllers reliably. In comparison, adjusted DoG-based kernel performed well in all the tested scenarios. All of this shows that the adjusted DoG-based kernel can reliably improve sample-efficiency of BO even when the mismatch between simulation and hardware is high. We would like to continue working in this direction and explore the usefulness of even simpler simulators in the future.

A: Add note about smooth cost and performance

### 5.4.2 Incorrect dynamics parameters

Our next set of experiments create “simulated hardware” that is increasingly different from the simulation, in which the DoG features were collected. This is done by changing the mass, inertia, center of mass location, friction coefficient of the ground contact models, ground stiffness and actuator delay, as described in Section ??.

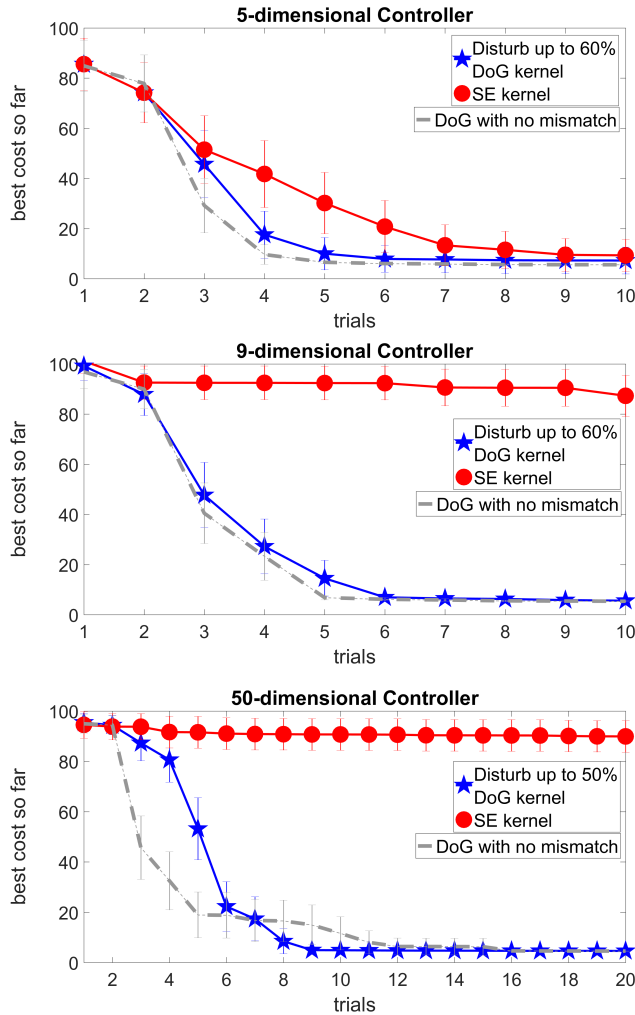


FIGURE 5.20: Performance of DoG and SE kernel with disturbance for 5-dimensional (top), 9-dimensional (middle) and 50-dimensional (bottom) controllers over 50 runs. DoG with no simulation-hardware mismatch is also shown. DoG performs better than SE even on maximum disturbance, and performance does not deteriorate as disturbance increases.

As shown in Figure 5.20, adjusted-DoG kernel obtains walking controllers in less than 10 trials for 5 and 9-dimensional controllers with up to  $\pm 60\%$  perturbation of dynamics parameters. In comparison, while for the 5-dimensional controller BO with SE finds walking controllers in less than 10 trials, its performance deteriorates for the 9-dimensional controller. Our approach can scale well even to 50 dimensions,

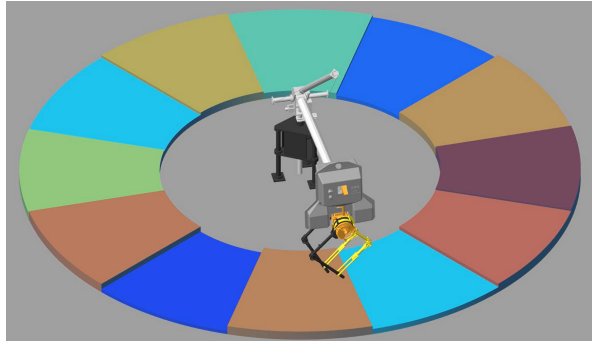


FIGURE 5.21: Simulation of ATRIAS with ground height disturbance. Different colors indicate different ground height disturbances. Maximum ground height disturbance is  $\pm 10$  cm.

learning walking VNMC controllers reliably in less than 20 trials, with up to  $\pm 50\%$  perturbation of dynamics parameters.

A: Add a summary of experiments in this section

## 5.5 Deep reinforcement learning for learning high level policies

In this section we describe our experiments with deep reinforcement learning for bipedal robots. Our experiments compare a general neural network policy with a more structured policy, where the neural network helps modulate an expert controller. We compare both policies in simulation and hardware.

### 5.5.1 Simulation Experiments

We trained our neural network controllers in simulation before implementing on hardware. This is because we use Proximal Policy Optimization (PPO) as our learning algorithm. PPO needs to collect a large amount of data points at each iteration. When our current policy is not good enough, we would not be able to collect much data since the robot might fall at the very beginning of experiment. In order to collect enough number of data points, we need to do a large number of trials, making it near impossible to train on hardware. However, since we train our policies in simulation, the resulting controllers might work well in simulation environment but when implemented on hardware, they might fall. In order to overcome this issue, we add ground height disturbances to learn robust controllers in simulation.

The reward function is defined focusing on matching the desired walking speed and preventing large angular velocity of the torso. We also add a large penalty if the controller falls:

$$reward_t = \begin{cases} -C_1 \cdot (v_{act,t} - v_{tgt})^2 - C_2 \cdot (\dot{\theta}_t)^2 + 1, & \text{if walk} \\ -C_3 * T_{sim}, & \text{if fall} \end{cases} \quad (5.7)$$

where  $v_{act,t}$  is the vector is the actual forward velocity of the robot at time  $t$ ,  $v_{tgt}$  is the target velocity,  $\dot{\theta}_t$  is the angular velocity of torso pitch,  $T_{sim}$  is the simulation time,  $C_1, C_2, C_3$  are positive fixed parameters. This kind of cost function is similar to prior work on optimizing locomotion controllers, and it can easily distinguish points that walk from points that fall. The longer the controller can survive, the closer to

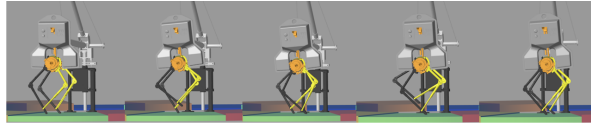


FIGURE 5.22: Sequence of frames from a single walking cycle (left to right).

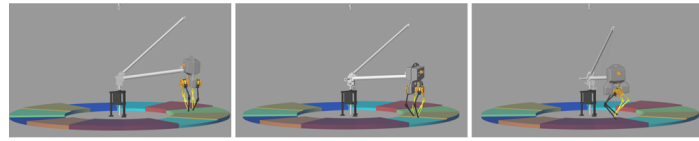


FIGURE 5.23: A time lapse of Neural Network Policy walking around the boom with ground height disturbance in simulation.

the target speed, the less torso pitch the higher total reward the controller can get. In this setting,  $C_1 = 1$ ,  $C_2 = 0.3$ ,  $C_3 = 0.01$ . In our observation, often the highest scoring controllers in simulation tend to exploit simulation inaccuracies. For example, some controllers tend to jerk the torso to achieve speeds closer to the target speed. While these perform well in simulation, they tend to fail on hardware.

### Neural Network Policy

The first set of simulation experiments were with the Neural Network Policy (NN Policy), described in Section 4.4.1. The first step for Neural Network Policy was behavior cloning. After initialization, our NN policy could walk on flat ground, but it had difficulties with ground height disturbances. This was unsurprising because the 'expert controller' also cannot walk on ground with ground height disturbance. Hence, we had to train the policy further to achieve acceptable performance.

We trained 10 different NN policies, the rewards for which are shown on Figure 5.24. The rewards shown is the averaged reward of one iteration which consisted on 30,000 data points. As shown in the plot, the reward keeps growing as training goes on, starting from the average cost of the expert. This shows that PPO achieves a very stable training with little to no forgetting of the initial expert.

The NN policy achieved good reward improvement compared to the initialization. After training, the NN policy could walk with ground height disturbance with a reasonable success rate. Figure 5.22 and Figure 5.23 shows the NN policy walking with ground height disturbance.

### Neural network with heuristic policy

The second set of simulation experiment uses a neural network in a heuristic policy, described in section 4.4.2. By initializing this policy to the target values of the 'expert controller', the initial policy was able to walk on flat ground but cannot walk on rough ground.

The training plot of Heuristic Policy is shown on Figure 5.24. As shown on the plot, the Heuristic Policy reward improves faster than the NN policy but reaches its peak in very few iterations. It then remains at that reward for the rest of iterations. The initial fast improvement is expected because as the heuristic policy uses the structure of the feedback-based reactive stepping policy, the search for reasonable parameters is simple. Hence, walking controllers are found much faster. However, the same structure also imposes a strong bias on the search, and as a result, it is hard

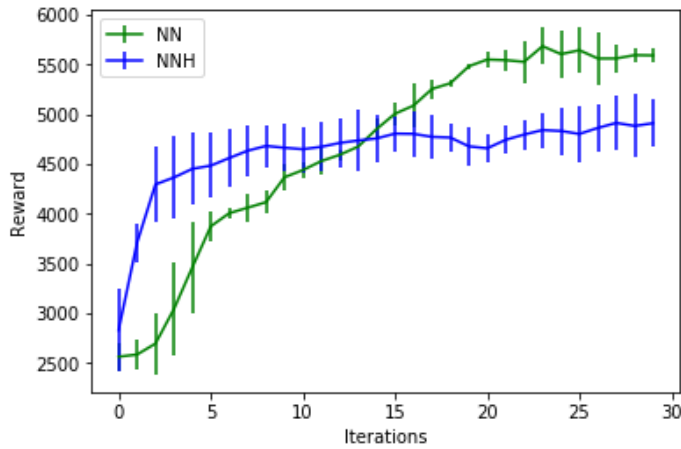


FIGURE 5.24: Training plot of Neural Network Policy (green) and Neural Network with Heuristic Policy (blue). Each of them is averaged of 5 trials data. In our training, we collected 30000 data in one iteration. For each simulation episode, we simulated 10 seconds if the controller keeps walking, and in simulation our time step was 0.001s. Thus, we could collect no more than 10000 data in a single episode, which also means in one iteration we needed data at least from 3 different episodes. By collecting data from more than one episodes, we could average the total rewards to determine the performance of the controller, also eliminating 'lucky' runs.

to find controllers that can perform as well as the pure NN controller in simulation. However, as we describe later, even though the best reward achieved by Heuristic controllers is lower, the rate of transfer to hardware is much higher than the NN policy.

### 5.5.2 Hardware Experiments

We tested 5 NN policies and 5 heuristic policies in our first set of hardware experiment, with the reward function described in Function 5.7.

There is a large mismatch between simulation and hardware starting conditions for our system. Starting from rest is a significant challenge for bipedal robots, especially underactuated robots like ATRIAS. ATRIAS is incapable of balancing by standing in place, and needs to continue stepping to stay upright. Typically, a start-up routine is designed for these robots to reach some initial walking gait, and then the controller to be tested is initiated. For example Hubicki et al., 2016a start by executing a stepping motion in air, and a human holds on to the robot as its lowered onto the ground. We train our controllers to start from rest in both simulation and hardware, to avoid having to design a start-up routine. However, our simulation leg is not initially loaded, so the simulation has to make an initial push to keep the CoM from going too low. On the other hand, on hardware the robot starts in position control in the air and then is lowered. So as stance starts, there is already sufficient force in the leg, and the initial push (from simulation) makes the robot leave ground. Such a controller falls on hardware. This behavior is illustrated in Figure 5.25 where the first two steps on hardware experience higher leg forces than the rest of the steps.

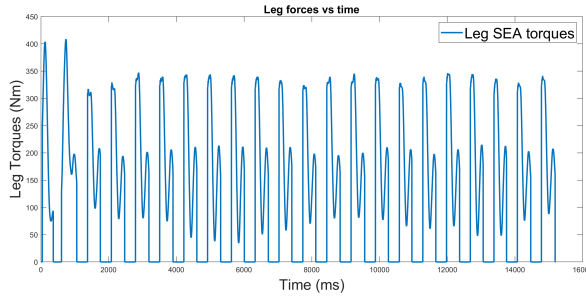


FIGURE 5.25: A plot of the stance leg SEA torques measured during one run of the NN policy on hardware. The torques are 0 during swing and follow a double hump pattern in stance. Note the high initial torques in the first two steps as compared to the rest of the walking cycle.

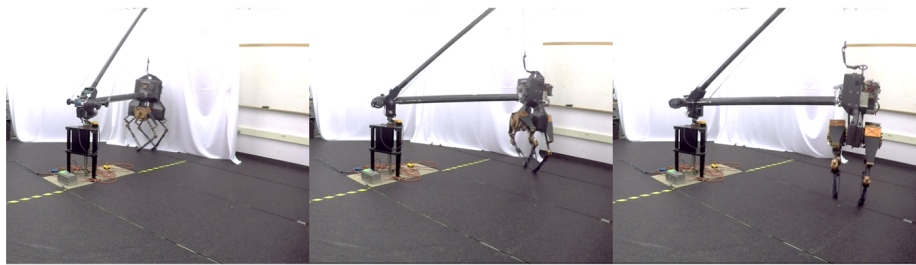


FIGURE 5.26: A time lapse of ATRIAS walking around the boom during a run of a NN with heuristic policy.

### Neural network policy

2 out of 5 of the NN policy could walk on hardware. But all of the NN policies shared the same issue that at the beginning of walking they would jump up. This behavior can also be seen in our simulation. The initializing 'expert controller' has a jump up behavior at the beginning of walking, and our NN policy also inherits this behavior. In simulation, this behavior would not lead to falling, but on hardware, ATRIAS would fall as soon as it tries to start walking because of the initial jump. On hardware, 2 out of 5 controllers could overcome the initial disturbance and then started normal walking pattern. 3 out 5 controllers, however could not recover from this disturbance. This led to a 40% rate of transfer of learned policies between simulation and hardware.

### Neural network with heuristic policy

4 out 5 controllers trained with neural network as part of the heuristic structure were able to walk on hardware. There are a few reasons for the success of the NN with heuristic structure policy, over the pure NN policy. Firstly, the initial discrepancy between simulation and hardware leg force is already compensated for by the heuristic structure. In the simulation, the NN predicts a desired height, and the feedback on this desired height results in a high leg force, as the actual height of the robot is lower. On hardware, the actual height of the robot is close to this desired height, so it automatically reduces the initial leg force. Unlike pure NN policy, where the forces were high on both simulation and hardware, now the initial forces are only high when the actual state of the robot is different from the desired. This structure

in our policy, hence, makes the generalization from simulation to hardware very simple and intuitive.

Secondly, since the structure of the policy is readable by an expert, the expert can still edit the policy after being trained in simulation. For example, if the NN was trained on a lower velocity but the expert wanted to run the robot on a higher velocity, the heuristic structure allows to directly edit this target. Similarly, we observed that some of our controllers were falling because of speeding, and we increased the feedback gain  $k$  on velocity feedback, described in Equation 4.10. This modification significantly improved the success rate of policies learned in simulation on hardware.

These experiments highlight the advantages of structure in learned policies. While the NN helped us improve our heuristic policy, as shown in Figure 5.24, by learning a state-dependant desired height, pitch and footstep location, it also kept the intuitive structure of the heuristic. So, it was able to better reject disturbances between simulation and hardware, as well as be modified for slightly different test situations, without needing re-learning. This allowed a 80% rate of transfer of learned policies between simulation and hardware.



## Chapter 6

# Conclusion

In this thesis, we presented different ways of adding simulation information to hardware experiments, with the aim of speeding up learning on hardware. We started with a global black-box optimizer like Bayesian Optimization, and added model-based information into it with the help of feature transforms. We studied different ways of designing these feature transforms, and compared their performance in simulation and hardware. Our results show that our approach can learn controllers on hardware much faster than traditional optimization approaches like BO with SE kernel and CMA-ES on multiple robot morphologies and costs.

Using simulation for hardware experiments raises the question of the effect of inaccuracies in simulation on the performance of the proposed approaches. To address this, we proposed a way of updating simulation models in a sample-efficient way in the space of features learned in the previous step. We then compared our approach and to approaches from literature on a series of increasingly inaccurate simulators – with both inaccurate modelling parameters, as well as inaccurate dynamic models. Our experiments showed that while other approaches from literature might be able to learn faster with accurate simulators, our approach is very robust to simulation inaccuracies.

Lastly, we studied ways of training neural network policies in simulation and deploying them on hardware. While domain randomization is a popular approach for learning robust policies in simulation, it can lead to very conservative and low performing controllers. We experimented with the effect of structure in neural network policies learned in simulation on the rate of transfer to hardware. We trained two neural network policies on a simulation with ground height disturbances. The first policy was a general neural network with no expert-designed structure, while the second policy was part of an expert policy. Our experiments show that structures NN policies can enhance the rate of transfer between simulation and hardware, as well as give the expert user control the behavior to an extent. We think that this shared autonomy between the neural network and expert is highly desirable, as the NN improves the expert policy while benefiting from the knowledge of the expert.

In this chapter, we discuss each section of this thesis in some detail, provide some limitations and future directions. We finish by discussing some open questions in learning for robotics, and the application of the work done in this thesis to such questions.

### 6.1 Discussion

This thesis covered three main ideas : (1) Incorporating simulation information in hardware experiments with the help of feature transforms. (2) Updating simulation transforms from hardware data to account for simulation inaccuracies. (3) Effect of

structure on high-dimensional neural network policies learned in simulation. We discuss each of these ideas in some detail next.

### 6.1.1 Feature transforms from simulation in hardware experiments

Adding simulation information to hardware experiments is well explored in literature. For example, Endo et al., 2008 learn a policy in simulation and then continue gradient descent on hardware to further optimize the policy. It is also common to hand-tune controllers learned in simulation by an expert. Abbeel, Quigley, and Ng, 2006 use learn an inaccurate model of the dynamics from simulation, and continue to improve it from data on hardware. While these approaches are promising when we expect our simulation to be close to hardware, they can be very expensive in terms of number of samples if the simulation is very inaccurate. The bias from simulation can get local optimizers stuck in a bad local minimum, and it might be difficult or impossible to recover.

We design a way of incorporating simulation information in a global sample-efficient optimizer on hardware. Instead of adding simulation information in the form of cost, we add information about simulation trajectories. This means that hardware experiments are now guided by the controller behavior recorded in simulation. This transforms the original controller space into a lower dimensional, easier to learn space, where controllers likely to perform well on hardware are close together, and far away from those that are likely to perform poorly.

This lower-dimensional feature space can be hand-designed, in cases where expert knowledge about the task is available. For bipedal locomotion, we describe such features in Section ???. On the other hand, raw trajectories, or trajectory summaries from simulation can also be used to create a higher-dimensional but informed feature space. We do this by training a neural network to predict simulation trajectories, as described in Section 3.1.2. Our hardware experiments on ATRIAS show that both these approaches are able to learn walking controllers very sample-efficiently. They significantly outperform uninformed BO and random sampling. Simulation experiments on a 7-link-biped in Section ?? show that these generalize to multiple robot morphologies and controller types.

These experiments showed that features learned in a high-fidelity simulation were able to help improve sample-efficiency of Bayesian optimization during hardware experiments. While domain-informed kernels performed slightly better than the neural network kernels, both could optimize a 9-dimensional controller in less than 10 trials. For a 50-dimensional controller, we could show improvement in simulation. These controllers are still low dimensional as compared to high-dimensional controllers like neural networks. In the future, we would like to study if such features can be developed for such very high-dimensional policies, possibly enabling these to be directly learned on hardware.

### 6.1.2 Accounting for simulation inaccuracies

An important question that arises when simulation for learning on hardware is : how does performance deteriorate if the simulator is bad? While there are a lot of ways of incorporating simulation information in hardware experiments, there is not a lot of research on studying the effect of inaccurate simulations on these approaches. We develop a systematic way of studying the effect of increasing inaccuracies on the performance of our proposed approach, and compare it to other approaches in literature.

We first study the effect of inaccurate modelling parameters, such as mass, inertia, length and center of mass of each link. These parameters can also be typically identified with system-identification approaches like described in An, Atkeson, and Hollerbach, 1988. However, parameters like friction coefficients and actuator delay can be variable over experiments, and would need to be re-identified continually. Thus, some amount of robustness to changes in these parameters is ideal. We collect features in an unperturbed simulation, and study optimization performance in *simulated hardware* with up to  $\pm 50\%$  perturbed inertial parameters. Next, we studied the effect of incorrectly modelled dynamics, such as simplified actuator dynamics and incorrect boom model on the performance of different approaches that transfer information from simulation to hardware. Unmodelled dynamics form a major part of real robot simulators and can be challenging to overcome. In our setting, the high-fidelity original simulator serves as a *simulated hardware* and low-fidelity simulators serve as *simulated simulators*.

To account for the mismatch between simulation and hardware, we measure the difference between simulation and hardware features, and build a mismatch model from this data. This model lets up update the simulation features in a sample-efficient manner, helping build a better representation of the hardware. Our experiments show that disturbances due to incorrect inertial parameters are in fact easy to overcome with such an update scheme. Features from perturbed simulations find walking controllers in less than 10 trials. On the other hand, inaccurate dynamics models are much harder to compensate for, taking up to 50 trials to learn walking controllers reliably. While other approaches from literature, like Cully et al., 2015 can do well when the simulation is close to hardware, they fail to find walking controllers reliably in the presence of large mismatch between simulation and hardware. On the other hand adjusted DoG-based kernel can learn to walk even with large simulation inaccuracies, though it might be less sample-efficient when simulation is close to hardware.

Our experiments demonstrated the advantages and disadvantages of using simulation information during hardware experiments. While most approaches from literature are highly sample-efficient when simulation is close to hardware, they suffer when the two are significantly different. This is expected, as the information from simulation is not accurate anymore and the performance of simulation-informed BO can be worse than uninformed BO. On the other hand, adjusted DoG-based kernel is able to recover from the simulation inaccuracy and guide the search to a region reliable on hardware. On the other hand, the adjusted DoG-based kernel is also less sample-efficient than other approaches when simulation is very close to hardware, as it spends some samples trying to learn about the function and mismatch landscape.

While our evaluations focused on locomotion, the need for incorporating simulation robustly is profound in other of parts robotics, particularly manipulation. Successful modeling of contact dynamics in manipulation is challenging, even for known object/surface types. Utilizing simulation for complex and dynamic manipulation tasks can be useful, since such simulation could be informative in some parts of optimization space, but incorrect in other parts. We hope that our experimental setup can be used for analyzing the effectiveness of methods at handling simulation-hardware mismatch in domains other than locomotion, and approaches we evaluate can be adapted to work in other parts of robotics.

### 6.1.3 Effect of structure on high-dimensional neural network policies

Recently, there has been a lot of interest in learning very high-dimensional neural network policies in simulation using deep reinforcement learning, for example Rajeswaran et al., 2017b, Peng et al., 2017, etc. To transfer these policies to hardware, a common approach is to learn robust policies with the help of domain randomization, as in Mordatch, Lowrey, and Todorov, 2015, Tan et al., 2018. These works aim to learn robust policies by considering distribution of model parameters in simulations, which includes the real model of the robot. While this is a very effective way of learning policies that transfer between simulation and hardware, the performance of learned policies is typically poorer than policies learned with domain randomization (Tan et al., 2018). In our work, we take a different approach to transferability of controllers. Instead of using domain randomization, we study of structured controllers can eliminate the need to use domain randomization, and lead to a high rate of transfer of policies between simulation and hardware.

We train two neural network policies in simulation - a general NN policy that directly predicts desired forces, and a structured NN policy that predicts set points of a expert-designed policy. Both NN policies are capable of generating arbitrary forces, so there is no loss in generalization with the structure. Our experiments suggest that the structured policy has a much higher rate of transfer between simulation and hardware. Additionally, the structure of the policy lets the user edit the policy for a new, but related, task without retraining the network. This enables a shared autonomy between the NN and the expert, where each benefit from the other.

Peng and Panne, 2017 have shown that even in simulation the choice of action space affects the rate of learning as well as disturbance rejection. Building on this, we study the effect of action space, and in particular, the structure of the NN policy on transfer between simulation and hardware. Unsurprisingly, NN policies with an expert-designed structure are able to generalize to unseen state distributions better than a general NN policy without any structure. For example, in most bipedal robots, the initial conditions between simulation and hardware are quite different. The structured NN policy was able to overcome this disturbance and continue walking at the desired speed. On the other hand, the NN policy without structure was not able to generalize to this setting reliably, and failed to walk. Our experiments show that it is indeed possible to learn high-performing policies in simulation that can transfer to hardware without using domain randomization. Expert-designed structured policies are beneficial for two reasons. The NN helps improve the performance of hand-designed heuristics. And the structure enables the user to predict and change the behavior of the NN policy without retraining.

## 6.2 Future work and open questions

There are several extensions to the current work, as well as unanswered questions about learning for robotics that we would like to talk about now.

### 6.2.1 Learning general features from data

We presented two sets of feature transforms for adding simulation information to hardware experiments. So far, the features were either hand-designed or needed expert input in the relevant simulation trajectories. Very often, there were iterations needed where the right features were not selected, or too many features were selected, bringing down the sample-efficiency. Thus, it is important to study if such

features can be learned directly from data, and important characteristics dynamically added or removed based on the problem at hand.

Features should also include feedback from the environment, for example contact forces. Other than just the end-effector trajectory, the instantaneous forces can also be indicative of the success or failure of particular controllers. Learning low-dimensional representations of these feedback trajectories is an interesting direction for future work.

Adapting features across multiple tasks and changing lower dimensional representations with context, can be useful for transferring data between different tasks and robots. This requires a sample-efficient way of updating features based on newly observed hardware samples, along with automatically determining the relative importance of features. All of these can together be used to build task-specific lower-dimensional representations that can be learned dynamically, and used to transfer information across multiple tasks.

### 6.2.2 Safe exploration and learning

A major concern with learning for robots is the safety of the robot. Exploration often involves sampling controllers that could potentially be unstable and damage our robots. Even worse, robots can damage their surroundings, including people and objects that they interact with. Taking safety of a robot and its environment into account is important when using approaches like Bayesian optimization and reinforcement learning.

Berkenkamp et al., 2017 develop guarantees for model-based reinforcement learning when the dynamics are approximated as a Gaussian process. The policies sampled are guaranteed to be in the region of attraction of an initial stable policy. This is an important work in the direction of building guarantees about safety, but stable initial policies can be hard to find in high-dimensional systems. Building dynamics models might also be prohibitively expensive, and nearly impossible to make them accurate. In such cases, detecting failure or a mismatch between expectation and measurement becomes important.

We think that starting from conservative policies learned in simulation and slowly building dynamics models, and exploring using these is an interesting direction to explore in the future. Exploration while learning dynamics can be done with the help of conservative models and controllers, that build failure maps from expected and measured sensor feedback. All of this together can bring us closer to truly autonomous robots that learn to accomplish goals, starting from inaccurate models and conservative controllers, and slowly learning better controllers along with the dynamics.

### 6.2.3 Transfer learning between controllers and robots

Given how expensive reinforcement learning typically is, it is important to learn systems that can share information and data. Transfer learning is a popular research direction, with works like Finn et al., 2017 trying to identify task-parameters and learn networks that generalize across multiple tasks. While this is promising, compelling hardware demonstrations of these approaches are few. We believe that automatic relevance determination between task-specific features can be an important step towards transfer learning and data sharing. Different tasks can have different important features, and a correspondingly different cost function. But data from the

old task can be included as if from a different source, as in Poloczek, Wang, and Frazier, 2016.

In addition, learning problem representations that can generalize across multiple robots can allow for data transfer across multiple robots. Sharing data in this manner can be extremely helpful in learning to do new tasks sample-efficiently.

### **6.3 Closing remarks**

This thesis tried to address the problem of fast learning on highly dynamic systems, with the help of simulation. We found that even when the simulator is inaccurate, information from simulation can guide hardware experiments to improve sample-efficiency. We also showed that learning lower-dimensional representations of the controller space in simulation not only helps learn faster on hardware, but also enables us to update the simulation in the same space.

All of this points towards the advantages of learning representations for optimization and learning. We believe that there are additional advantages to learning representations, like failure detection, safety and transfer learning. We would like to continue exploring these directions in the future.

# Bibliography

- Abbeel, Pieter, Morgan Quigley, and Andrew Y Ng (2006). "Using inaccurate models in reinforcement learning". In: *Proceedings of the 23rd international conference on Machine learning*. ACM, pp. 1–8.
- Akrour, Riad et al. (2017). "Local Bayesian Optimization of Motor Skills". In: *Proceedings of the 34th International Conference on Machine Learning, ICML 2017, Sydney, NSW, Australia, 6-11 August 2017*, pp. 41–50.
- An, Chae H., Christopher G. Atkeson, and John M. Hollerbach (1988). *Model-based Control of a Robot Manipulator*. Cambridge, MA, USA: MIT Press. ISBN: 0-262-01102-6.
- Antonova, Rika, Akshara Rai, and Christopher G Atkeson (2016). "Sample efficient optimization for learning controllers for bipedal locomotion". In: *Humanoid Robots (Humanoids), 2016 IEEE-RAS 16th International Conference on*. IEEE, pp. 22–28.
- Atkeson, Christopher G (2007). "Randomly sampling actions in dynamic programming". In: *Approximate Dynamic Programming and Reinforcement Learning, 2007. ADPRL 2007. IEEE International Symposium on*. IEEE, pp. 185–192.
- Batts, Zachary, Seungmoon Song, and Hartmut Geyer (2015). "Toward a virtual neuromuscular control for robust walking in bipedal robots". In: *Intelligent Robots and Systems (IROS), 2015 IEEE/RSJ International Conference on*. IEEE, pp. 6318–6323.
- Benbrahim, Hamid and Judy A Franklin (1997). "Biped dynamic walking using reinforcement learning". In: *Robotics and Autonomous Systems* 22.3-4, pp. 283–302.
- Berkenkamp, Felix et al. (2017). "Safe model-based reinforcement learning with stability guarantees". In: *Advances in Neural Information Processing Systems*, pp. 908–918.
- Bertsekas, Dimitri P and John N Tsitsiklis (1995). "Neuro-dynamic programming: an overview". In: *Decision and Control, 1995., Proceedings of the 34th IEEE Conference on*. Vol. 1. IEEE, pp. 560–564.
- Brochu, Eric, Vlad M Cora, and Nando De Freitas (2010). "A Tutorial on Bayesian Optimization of Expensive Cost Functions, with Application to Active User Modeling and Hierarchical Reinforcement Learning". In: *arXiv preprint arXiv:1012.2599*.
- Busoniu, Lucian et al. (2010). *Reinforcement learning and dynamic programming using function approximators*. Vol. 39. CRC press.
- Calandra, Roberto (2017). "Bayesian Modeling for Optimization and Control in Robotics". PhD thesis. Darmstadt University of Technology, Germany. URL: <http://tuprints.ulb.tu-darmstadt.de/5878/>.
- Calandra, Roberto et al. (2016a). "Bayesian Optimization for Learning Gaits under Uncertainty". In: *Annals of Mathematics and Artificial Intelligence (AMAI)* 76.1, pp. 5–23. ISSN: 1573-7470. DOI: [10.1007/s10472-015-9463-9](https://doi.org/10.1007/s10472-015-9463-9).
- Calandra, Roberto et al. (2016b). "Bayesian Optimization for Learning Gaits Under Uncertainty". In: *Annals of Mathematics and Artificial Intelligence* 76.1-2, pp. 5–23.
- Cully, Antoine et al. (2015). "Robots that can adapt like animals". In: *Nature* 521.7553, pp. 503–507.

- Cutler, Mark, Thomas J Walsh, and Jonathan P How (2015). "Real-world reinforcement learning via multifidelity simulators". In: *IEEE Transactions on Robotics* 31.3, pp. 655–671.
- Desai, Ruta and Hartmut Geyer (2012). "Robust Swing Leg Placement Under Large Disturbances". In: *ROBIO 2012*. IEEE, pp. 265–270.
- Endo, Gen et al. (2008). "Learning CPG-based biped locomotion with a policy gradient method: Application to a humanoid robot". In: *The International Journal of Robotics Research* 27.2, pp. 213–228.
- Englert, Peter and Marc Toussaint (2016). "Combined Optimization and Reinforcement Learning for Manipulation Skills." In: *Robotics: Science and Systems*.
- Feng, Siyuan et al. (2015). "Optimization-based Full Body Control for the DARPA Robotics Challenge". In: *Journal of Field Robotics* 32.2, pp. 293–312.
- Feng, Siyuan et al. (2016). "Robust dynamic walking using online foot step optimization". In: *Intelligent Robots and Systems (IROS), 2016 IEEE/RSJ International Conference on*. IEEE, pp. 5373–5378.
- Finn, Chelsea et al. (2017). "One-shot visual imitation learning via meta-learning". In: *arXiv preprint arXiv:1709.04905*.
- Frean, Marcus and Phillip Boyle (2008). "Using Gaussian processes to optimize expensive functions". In: *Australasian Joint Conference on Artificial Intelligence*. Springer, pp. 258–267.
- Geyer, Hartmut and Hugh Herr (2010). "A Muscle-reflex Model that Encodes Principles of Legged Mechanics Produces Human Walking Dynamics and Muscle Activities". In: *IEEE Transactions on Neural Systems and Rehabilitation Engineering* 18.3, pp. 263–273.
- Ha, Sehoon and Katsu Yamane (2015). "Reducing hardware experiments for model learning and policy optimization". In: *Robotics and Automation (ICRA), 2015 IEEE International Conference on*. IEEE, pp. 2620–2626.
- Hansen, Nikolaus (2006). "The CMA evolution strategy: a comparing review". In: *Towards a new evolutionary computation*. Springer, pp. 75–102.
- Heess, Nicolas et al. (2017). "Emergence of locomotion behaviours in rich environments". In: *arXiv preprint arXiv:1707.02286*.
- Herzog, Alexander et al. (2016). "Momentum control with hierarchical inverse dynamics on a torque-controlled humanoid". In: *Autonomous Robots* 40.3, pp. 473–491.
- Hubicki, Christian et al. (2016a). "ATRIAS: Design and validation of a tether-free 3D-capable spring-mass bipedal robot". In: *The International Journal of Robotics Research* 35.12, pp. 1497–1521.
- Hubicki, Christian et al. (2016b). "Walking and running with passive compliance: Lessons from engineering a live demonstration of the atrias biped". In: *IEEE Robotics and Automation Magazine* 2.4.1, pp. 4–1.
- Inman, Verne T, Howard D Eberhart, et al. (1953). "The major determinants in normal and pathological gait." In: *JBJS* 35.3, pp. 543–558.
- Jones, Donald R, Matthias Schonlau, and William J Welch (1998). "Efficient Global Optimization of Expensive Black-box Functions". In: *Journal of Global optimization* 13.4, pp. 455–492.
- Kormushev, Petar et al. (2011). "Bipedal walking energy minimization by reinforcement learning with evolving policy parameterization". In: *Intelligent Robots and Systems (IROS), 2011 IEEE/RSJ International Conference on*. IEEE, pp. 318–324.
- Kuindersma, Scott et al. (2016). "Optimization-based locomotion planning, estimation, and control design for the atlas humanoid robot". In: *Autonomous Robots* 40.3, pp. 429–455.

- Levine, Sergey and Vladlen Koltun (2013). "Guided policy search". In: *Proceedings of the 30th International Conference on Machine Learning (ICML-13)*, pp. 1–9.
- Levine, Sergey, Nolan Wagener, and Pieter Abbeel (2015). "Learning contact-rich manipulation skills with guided policy search". In: *Robotics and Automation (ICRA), 2015 IEEE International Conference on*. IEEE, pp. 156–163.
- Levine, Sergey et al. (2016). "End-to-end training of deep visuomotor policies". In: *Journal of Machine Learning Research* 17.39, pp. 1–40.
- Lillicrap, Timothy P et al. (2015). "Continuous control with deep reinforcement learning". In: *arXiv preprint arXiv:1509.02971*.
- Lizotte, Daniel J et al. (2007). "Automatic Gait Optimization with Gaussian Process Regression." In: *IJCAI*. Vol. 7, pp. 944–949.
- MacAlpine, Patrick, Elad Lieberman, and Peter Stone (2016). "Adaptation of Surrogate Tasks for Bipedal Walk Optimization". In: *Proceedings of the 2016 on Genetic and Evolutionary Computation Conference Companion*. ACM, pp. 1275–1276.
- Marco, Alonso et al. (2017a). "On the Design of LQR Kernels for Efficient Controller Learning". In: *arXiv preprint arXiv:1709.07089*.
- Marco, Alonso et al. (2017b). "Virtual vs. Real: Trading Off Simulations and Physical Experiments in Reinforcement Learning with Bayesian Optimization". In: *arXiv preprint arXiv:1703.01250*.
- Martin, William C, Albert Wu, and Hartmut Geyer (2015). "Robust spring mass model running for a physical bipedal robot". In: *Robotics and Automation (ICRA), 2015 IEEE International Conference on*. IEEE, pp. 6307–6312.
- Martinez-Cantin, Ruben et al. (2007). "Active Policy Learning for Robot Planning and Exploration under Uncertainty." In: *Robotics: Science and Systems*, pp. 321–328.
- Meier, Franziska, Daniel Kappler, and Stefan Schaal (2017). "Online Learning of a Memory for Learning Rates". In: *arXiv preprint arXiv:1709.06709*.
- Mockus, J, V Tiesis, and A Zilinskas (1978). "Toward Global Optimization, volume 2, chapter Bayesian Methods for Seeking the Extremum". In:
- Mordatch, Igor, Kendall Lowrey, and Emanuel Todorov (2015). "Ensemble-CIO: Full-body dynamic motion planning that transfers to physical humanoids". In: *Intelligent Robots and Systems (IROS), 2015 IEEE/RSJ International Conference on*. IEEE, pp. 5307–5314.
- Morimoto, Jun et al. (2005). "Poincare-map-based reinforcement learning for biped walking". In: *Robotics and Automation, 2005. ICRA 2005. Proceedings of the 2005 IEEE International Conference on*. IEEE, pp. 2381–2386.
- Morrison, JB (1970). "The Mechanics of Muscle Function in Locomotion". In: *Journal of Biomechanics* 3.4, pp. 431–451.
- Nakanishi, Jun et al. (2004). "Learning from demonstration and adaptation of biped locomotion". In: *Robotics and autonomous systems* 47.2, pp. 79–91.
- Noot, Nicolas Van der, Auke J Ijspeert, and Renaud Ronsse (2015). "Biped Gait Controller for Large Speed Variations, Combining Reflexes and a Central Pattern Generator in a Neuromuscular Model". In: *ICRA 2015*. IEEE, pp. 6267–6274.
- OpenAI et al. (2018). "Learning Dexterous In-Hand Manipulation". In: *ArXiv e-prints*. arXiv: [1808.00177](https://arxiv.org/abs/1808.00177).
- Peng, Xue Bin, Glen Berseth, and Michiel van de Panne (2016). "Terrain-adaptive locomotion skills using deep reinforcement learning". In: *ACM Transactions on Graphics (TOG)* 35.4, p. 81.
- Peng, Xue Bin and Michiel van de Panne (2017). "Learning locomotion skills using deeplrl: does the choice of action space matter?" In: *Proceedings of the ACM SIGGRAPH/Eurographics Symposium on Computer Animation*. ACM, p. 12.

- Peng, Xue Bin et al. (2017). "Sim-to-real transfer of robotic control with dynamics randomization". In: *arXiv preprint arXiv:1710.06537*.
- Peters, Jan and Stefan Schaal (2006). "Policy gradient methods for robotics". In: *Intelligent Robots and Systems, 2006 IEEE/RSJ International Conference on*. IEEE, pp. 2219–2225.
- Poloczek, Matthias, Jialei Wang, and Peter I Frazier (2016). "Multi-Information Source Optimization". In: *arXiv preprint arXiv:1603.00389*.
- Rai, Akshara et al. (2018). "Bayesian Optimization Using Domain Knowledge on the ATRIAS Biped". In:
- Raibert, Marc H (1986). *Legged robots that balance*. MIT press.
- Rajeswaran, Aravind et al. (2017a). "Learning complex dexterous manipulation with deep reinforcement learning and demonstrations". In: *arXiv preprint arXiv:1709.10087*.
- Rajeswaran, Aravind et al. (2017b). "Towards generalization and simplicity in continuous control". In: *Advances in Neural Information Processing Systems*, pp. 6550–6561.
- Rasmussen, Carl Edward and Christopher K. I. Williams (2005). *Gaussian Processes for Machine Learning (Adaptive Computation and Machine Learning)*. The MIT Press. ISBN: 026218253X.
- Ross, Stéphane and Drew Bagnell (2010). "Efficient reductions for imitation learning". In: *Proceedings of the thirteenth international conference on artificial intelligence and statistics*, pp. 661–668.
- Rubinstein, Reuven (1999). "The cross-entropy method for combinatorial and continuous optimization". In: *Methodology and computing in applied probability* 1.2, pp. 127–190.
- Schulman, John et al. (2015). "Trust region policy optimization". In: *International Conference on Machine Learning*, pp. 1889–1897.
- Schulman, John et al. (2017). "Proximal policy optimization algorithms". In: *arXiv preprint arXiv:1707.06347*.
- Sendonaris, Andrew and COM Gabriel Dulac-Arnold (2017). "Learning from Demonstrations for Real World Reinforcement Learning". In: *arXiv preprint arXiv:1704.03732*.
- Shahriari, Bobak et al. (2016). "Taking the Human Out of the Loop: A Review of Bayesian Optimization". In: *Proceedings of the IEEE* 104.1, pp. 148–175.
- Silver, David et al. (2016). "Mastering the game of Go with deep neural networks and tree search". In: *nature* 529.7587, p. 484.
- Song, Seungmoon and Hartmut Geyer (2015). "A Neural Circuitry that Emphasizes Spinal Feedback Generates Diverse Behaviours of Human Locomotion". In: *The Journal of Physiology* 593.16, pp. 3493–3511.
- Srinivas, Niranjan et al. (2009). "Gaussian Process Optimization in the Bandit Setting: No Regret and Experimental Design". In: *arXiv preprint arXiv:0912.3995*.
- Stein, Michael L (1999). *Interpolation of Spatial Data: Some Theory for Kriging*. Springer.
- Sutton, Richard S and Andrew G Barto (1998). *Reinforcement learning: An introduction*. Vol. 1. 1. MIT press Cambridge.
- Tan, Jie et al. (2018). "Sim-to-Real: Learning Agile Locomotion For Quadruped Robots". In: *arXiv preprint arXiv:1804.10332*.
- Tedrake, Russ, Teresa Weirui Zhang, and H Sebastian Seung (2004). "Stochastic policy gradient reinforcement learning on a simple 3D biped". In: *Intelligent Robots and Systems, 2004.(IROS 2004). Proceedings. 2004 IEEE/RSJ International Conference on*. Vol. 3. IEEE, pp. 2849–2854.

- Tesch, Matthew, Jeff Schneider, and Howie Choset (2011). "Using response surfaces and expected improvement to optimize snake robot gait parameters". In: *Intelligent Robots and Systems (IROS), 2011 IEEE/RSJ International Conference on*. IEEE, pp. 1069–1074.
- Thatte, Nitish and Hartmut Geyer (2016). "Toward Balance Recovery with Leg Prostheses Using Neuromuscular Model Control". In: *IEEE Transactions on Biomedical Engineering* 63.5, pp. 904–913.
- Todorov, Emanuel, Tom Erez, and Yuval Tassa (2012). "Mujoco: A physics engine for model-based control". In: *Intelligent Robots and Systems (IROS), 2012 IEEE/RSJ International Conference on*. IEEE, pp. 5026–5033.
- Whitman, Eric C and Christopher G Atkeson (2009). "Control of a walking biped using a combination of simple policies". In: *Humanoid Robots, 2009. Humanoids 2009. 9th IEEE-RAS International Conference on*. IEEE, pp. 520–527.
- Wilson, Aaron, Alan Fern, and Prasad Tadepalli (2014). "Using Trajectory Data to Improve Bayesian Optimization for Reinforcement Learning". In: *The Journal of Machine Learning Research* 15.1, pp. 253–282.
- Wu, Albert and Hartmut Geyer (2014). "Highly robust running of articulated bipeds in unobserved terrain". In: *Intelligent Robots and Systems (IROS 2014), 2014 IEEE/RSJ International Conference on*. IEEE, pp. 2558–2565.
- Yin, KangKang, Kevin Loken, and Michiel van de Panne (2007). "Simbicon: Simple Biped Locomotion Control". In: *ACM Transactions on Graphics (TOG)*. Vol. 26. 3. ACM, p. 105.